# LIGHT PROGRAMMABLE COMMUNICATION AND CONSORTIA OF MINIMAL SYNTHETIC CELLS

Dissertation zur Erlangung des Grades

**“Doktor rerum naturalium (Dr. rer. nat.)“**

am Fachbereich

Chemie, Pharmazie und Geowissenschaften (FB 09),

der Johannes Gutenberg-Universität, Mainz

vorgelegt von

**Oya Ilke Sentürk**

geb. in Izmir, Türkei

Mainz, 2020

The thesis was carried out from March 2017 until June 2020 in the department of Prof. Dr. Katharina Landfester in the group of Prof. Dr. Seraphine Wegner at the Max Planck Institute for Polymer Research, Mainz.

Dekan: Prof. Dr. [redacted]

Prodekan: Prof. Dr. [redacted]

Gutachter 1: Prof. Dr. [redacted]

Gutachter 2: Prof Dr. [redacted]

Date of oral examination:

*I hereby declare that I wrote the dissertation submitted without any unauthorized external assistance and used only sources acknowledged in this work. All textual passages which are appropriate verbatim or paraphrased from published and unpublished texts, as well as all information obtained from oral sources, are duly indicated and listed in accordance with bibliographical rules. In carrying out this research, I complied with the rules of standard scientific practice as formulated in the statutes of Johannes Gutenberg-University Mainz to ensure standard scientific practice.*

_____ _____

Oya Ilke Sentürk

## Acknowledgements

First of all, I would like to thank [redacted] for giving me the opportunity to conduct my research in her research group, for her support and supervision through my studies.

Furthermore, I would like to thank [redacted] for welcoming me to her research group, being my direct supervisor, all the guidance and support she has given me for the last three years.

I must express my gratitude to [redacted] for her friendship and support from the first day of our Ph.D. Thanks to [redacted] training me and for our collaboration.

Also special thanks to my office mates [redacted] and [redacted] for all the support they have given me.

I would like to thank [redacted] staying in contract from my internship in Heidelberg to the journey in Mainz and for our collaboration in the lab.

Many thanks to [redacted] group members [redacted] their friendship, for providing a peaceful working environment and all the good times we had.

Thank you to all of the Landfester group for nice events, get-togethers and great times together that I will always cherish.

I would like to thank our external collaboration partners [redacted] and [redacted] for all the valuable discussions and help they have provided, which made it possible for me to complete our project.

I would also like to thank our other external collaboration members Assoc. Prof. [redacted] who have taught me the DNA nanotechnology and shared their expertise for our project. Thank you to Prof. Dr. [redacted] making our collaboration possible, for welcoming me in his lab and sharing the proteinosomes expertise.

Additionally, I want to thank [redacted] for the IT support and for all the figures he has prepared throughout these years.

Thank you to [redacted] helped me with discovering new features of Confocal Microscopy.

My special thanks go to all of my friends for their love, support and encouragement regardless of which section of the world they may be.

Finally, I must express my deepest gratitude to my partner [redacted] always supporting me through all the ups and downs, and to my family, for their unconditional love and guidance, they have given me. Without you none of this would have been possible.

Parts of this work were published in:

Sentürk O.I., Chervyachkova, E., Ji Y., and Wegner, S. V.

**Independent Blue and Red Light Triggered Narcissistic Self-Sorting Self-Assembly of Colloidal Particles**

*Small*, 15, 1901801 (2019)

DOI: 10.1002/smll.201901801

Sentürk O.I., Schauer O., Chen F., Sourjik V., and Wegner, S. V.

**Red/Far-Red Light Switchable Cargo Attachment and Release in Bacteria-Driven Microswimmers**

*Advanced Healthcare Materials*, 9, 1900956 (2020)

DOI: 10.1002/adhm.201900956

## Abstract

The ability of cells to dynamically sense and respond to spatial and temporal changes in their environments is the basis of their remarkable adaptivity. As such, intercellular communication allows cells to regulate their function, and attain collective and multicellular behavior. The cell to cell communication in the form of soluble signals and gradients determines important processes, such as cell differentiation, chemotaxis, and cancer development.

The transfer of these concepts to minimal synthetic cells (protocells) through the precisely and dynamically control of interactions between protocells is a key step towards creating microscale technologies that exhibit the fundamental features of living cells. Regulating the interactions between the protocells with visible light offers dynamic control with high spatiotemporal resolution. In this thesis, these unique features of photoregulation were used to control the communication between protocells through soluble signals, regulate the organization un multicomponent mixtures, and the delivery of colloids using bacteria.

In the first part of this thesis, light controlled adhesive interactions between two different populations of protocells were used to regulate their assembly and, consequently their DNA-based communication. For this purpose, semi-permeable protein-polymer based vesicles, known as proteinosomes, were used as sender and receiver cells and functionalized with the proteins iLID and Nano, respectively. Upon blue light illumination, the binding of iLID and Nano brought sender and receiver cells in proximity and allowed for DNA-based communication. In the dark, the sender and receiver proteinosomes remained dispersed and consequently could not communicate based on the soluble DNA signal. These findings highlight the importance of spatial arrangement of sender and receiver cells in the context of communication through soluble signals.

The second part of this thesis aimed at the orthogonal self-assembly and self-sorting of two different types of micro-meter sized colloids, used as models for minimal synthetic cells. Coating the colloidal particles with different homodimerizing light-responsive proteins, VVDHigh and Chp1, which respond to blue and red light, respectively, made it possible to address each population with a different color of light. Further, in a mixture, these two colloid types self-sorted into separate clusters, a behavior known as narcissistic self-sorting. This concept has the potential for the assembly of addressable and adaptable materials into higher-order tissue-like structures.

The aim of the third part of this thesis was to combine engineered chemotactic bacterial cells with micro-sized colloids, as model cargo in bacteriabots, and

regulate cargo integration and release using red and far-red light. In this study, the bacteria surface was functionalized red-light responsive phytochrome B (PhyB) protein and the cargo particles with its binding partner phytochrome interaction partner (PIF6). As a result of PhyB/PIF6 dimerization upon red light illumination, photoswitchable bacteriabots assembled and could transport the cargo. Moreover, far-red light illumination causes the dissociation of the two proteins and was used to release the cargo on-demand. The photo-regulation of bacteriabots with red/far-red light provides noninvasive remote control high spatiotemporal precision and good tissue penetration, which opens new possibilities in engineering biohybrid systems.

## Zusammenfassung

Zellen können räumliche und zeitliche Veränderungen in ihrer Umgebung dynamisch wahrnehmen und darauf reagieren. Diese Fähigkeit ist die Grundlage ihrer bemerkenswerten Anpassungsfähigkeit. Durch interzelluläre Kommunikation können Zellen ihre Funktion regulieren und kollektives Verhalten ausführen. Die Zell-Zell-Kommunikation in Form von löslichen Signalen und Gradienten reguliert wesentliche Prozesse, z.B. Zelldifferenzierung, Chemotaxis und Krebsentstehung.

Der Transfer dieser Konzepte auf syntheitschen Zellen (Protozellen) durch präzise und dynamische Steuerung der Austauschen zwischen den Protozellen ist ein wichtiger Schritt zur Erstellungen mikroskaliger Technologien. Diese Technologien können grundlegenden Eigenschaften lebender Zellen aufweisen. Die Steuerung des Austausches zwischen den Protozellen mit sichtbarem Licht bietet eine dynamische Steuerung mit hoher räumlicher und zeitlicher Auflösung. In dieser Dissertation wurden diese einzigartigen Eigenschaften der Photoregulation verwendet, um die Kommunikation zwischen Protozellen durch lösliche Signale zu kontrollieren und die Organisation von Multikompartiment-Mischungen und der Transport von Kolloiden mit Hilfe von Bakterien zu regulieren.

Im ersten Teil dieser Dissertation wurden lichtgesteuerte adhäsive Interaktionen zwischen zwei verschiedenen Populationen von Modellprotozellen verwendet, um ihre Selbstorganisation und damit ihre DNA-basierte Kommunikation zu regulieren. Dabei wurden semipermeable Vesikel auf Proteinpolymerbasis, sogenannte. Proteinosomen, als Sender- und Empfängerzellen verwendet und mit den lichtschaltbaren Proteinen, nämlich iLID und Nano, funktionalisiert. Bei der Beleuchtung mit blauem Licht brachte die Bindung von iLID und Nano Sender- und Empfängerzellen in der Nähe und ermöglichte die DNA-basierte Kommunikation. Im Dunkeln konnten dispergierte Sender- und Empfängerproteinosomen durch lösliche DNA-Signale nicht kommunizieren. Diese Ergebnisse betonnen, wie wichtig die räumliche Organisation von Sender- und Empfängerzellen im Kontext der Kommunikation durch lösliche Signale sind.

Im zweiten Teil dieser Dissertation wurde die Selbstorganisation von zwei verschiedenen Arten von Mikrometer-großen-Kolloiden (als Modell minimaler synthetischer Zellen) orthogonal kontrolliert. Die Beschichtung der Kolloide mit verschiedenen homodimerisierenden lichtschaltbaren Proteinen, VVDHigh und Chp1, die auf blaues oder rotes Licht reagieren, ermöglichte es, jede Population mit einer anderen Lichtfarbe kontrollieren. In einem Gemisch ordnen sich diese zwei Arten von Kolloiden selbst in isoliterte Aggregate, dieses Verhalten ist als

narzisstische Selbstsortierung bekannt. Dieses Konzept kann für den Aufbauanpassungsfähiger Materialien zu gewebeartigen Strukturen übergeordnete Organisation verwendet werden.

Im dritten Teil dieser Dissertation wurden konstruierte chemotaktische Bakterienzellen mit Kolloiden als Modell-Cargo (für Bacteriabots) kombiniert und die Integregration des Cargos und Freisetzung des Cargos durch rotes und dunkelrotes Licht reguliert. In dieser Studie wurde das auf Rotlicht reagierende Protein Phytochrom B (PhyB) auf der Oberfläche der Bakterien immobilisiert und sein Bindungspartner Phytochrom-Interaktionspartner (PIF6) wurde auf den Cargo-Partikeln immobilisiert. Bei der Beleuchtung mit rotem Licht binden sich durch die lichtschaltbaren Proteine PhyB / PIF6 die Bakteriabots an ihr Cargo und transportieren das Cargo zum Zielort. Die Stimulation mit dunkelrotem Licht bewirkt die Dissoziation der Proteine, was zur bedarfsgerechten Freisetzung des Cargos führt. Die Regulierung durch das Licht von Bakteriabots mit rotem und dunkelrotem Licht bietet eine nichtinvasive Steuerung mit hoher räumlich und zeitlicher Präzision und erlaubt eine gewisse Gewebedurchdringung, die neue Möglichkeiten bei der Entwicklung von Biohybrid-Systemen eröffnen können.

## List of abbreviations

| | |
|---|---|
| Ag43 | Antigen-43 |
| AMP | Adenosine monophosphate |
| BSA | Bovine serum albumin |
| CFPS | Cell-free protein synthesis |
| Cph1 | Cyanobacterial phytochrome 1 |
| Cy5 | Cyanine 5 dye |
| DNA | Deoxyribonucleic acid |
| DSD | DNA-strand-displacement |
| E. coli | *Escherichia coli* |
| EDTA | Ethylenediaminetetraacetic acid |
| FAD | Flavine adenine dinucleoide |
| FITC | Fluorescein isothiocyanate |
| FMN | Flavin mononucleotide |
| FRET | Förster resonance energy transfer |
| GFP | Green fluorescent protein |
| GUV | Giant Unilamellar Vesicle |
| His6 | Histidine tag |
| iLID | Improved light-inducible dimer |
| IMAC | Immobilized metal affinity chromatography |
| IPTG | Isopropyl-$\beta$-D-thiogalactopyranoside |
| LB medium | Luria-Bertani medium |
| LED | Light-emitting diode |
| LOV | Light-oxygen-voltage |
| NTA | Nitrilotriacetic acid |
| $OD_{600}$ | Optical density at 600 nm |
| PAS | Per-ARNT-Sim domain |
| PCB | Phycocyanobilin |
| PEN toolbox | Polymerase, nicking, and exonuclease toolbox |
| PFA | Paraformaldehyde |
| PIF6 | Phytochrome interacting factor 6 |
| Pfr | Far-red light absorbing phytochrome |

| | |
|---|---|
| Phy | Phytochrome |
| PMSF | Phenylmethylsulfonyl fluoride |
| PNIPAM | Poly(N-isopropylacrylamid) |
| Pr | Red light absorbing phytochrome |
| PURE | Protein synthesis using recombinant elements |
| RFU | Relative fluorescence units |
| rpm | Rotation per minute |
| SDS-PAGE | Sodium dodecyl sulfide-polyacrylamide gel electrophoresis |
| SEM | Standard error |
| siRNA | Small interfering ribonucleic acid |
| ssDNA | Single strand deoxyribonucleic acid |
| SD | Standard deviation |
| TB | Tryptone Broth |
| TetR | Tetracycline repressor |
| TMSD | Toehold-mediated strand displacement |
| TRIS | Tris(hydroxymethyl)aminomethane |
| TRITC | Tetramethylrhodamine |
| TXTL | Cell-free transcription–translation |
| VVD | Vivid |

## List of Figures

# Contents

# Chapter 1: Introduction

## 1.1 Designing minimal cells and protocells in synthetic biology

Life is the most fundamental feature of cells, while the cells are the smallest units displaying this feature.[1] Over the centuries, living cells have been of interest and source of inspiration for scientists. However, the enormous complexity of even the simplest living cells and the fundamental features that constitute life is still afar from our grasp.

The construction of well-defined and controlled minimal cells that can still perform the most basic functions of a living cell is being investigated within the field of synthetic biology, which is an emerging field that lies in the intersection of synthetic chemistry, molecular biology, and biotechnology.[2,3] In other words, through the reduction of complexity and the generation of precise, well-understood and predictable life-like entities, it is endeavored to answer these fundamental questions: what are the requirements of life and how can we achieve living entities. Consequently, there are two distinct approaches in synthetic biology to achieve a functional minimal cell fulfilling the above-given criteria: top-down vs. bottom-up (Figure 1.1.1).[2] In the top-down approach, cells are stripped-down to only essential genes and biological processes. Such minimal cells are also used as the host organism and can be equipped with other biological elements (promoters, gene products, etc.) to generate new functions. Here the starting point is a living cell, which is modified and investigated to understand the limits of a minimal genome that is sufficient to survive as a living

unit. A prominent example of the top-down approach is the construction of a minimal genome based on the *Mycoplasma genitalium*, where through gene knock-outs, the genome was reduced from 525 genes to only 324 genes, which are essential for life.[4] Yet, even in this example, the function of 28% of the protein-coding genes is unknown. Part of the problem arises from the crosstalk between the existing biological components and their not completely understood interactions.[5] Besides, the minimal cells created via the top-down approach are still too complicated to provide a complete understanding and come short in providing methods to build cells from scratch and plausible explanations for the origin-of-life.[2]

Contrarily, the bottom-up approach theoretically offers the path to construct a minimal synthetic cell through the brick-by-brick assembly of individual basic building units such as sugars, lipids, polymers, proteins, and genetic material.[6] The *de novo* assembly of molecular building blocks to attain cellular functions provides a high degree of control over the protocellular designs, and to attain programmable functions such as information processing,[7] protein synthesis,[8] metabolism,[9,10] collective and hierarchical behavior,[11,12] and molecular sensing.[13] Reproducing such complexity and organization as observed in natural cells also with synthetic cells attracts great interest in the context of tissue engineering, fabrication of smart materials, origin-of-life studies, and drug delivery.[2,14–19] For such, minimum functions required for life, also named proliferome, should be fulfilled to design a minimal functional cell: compartmentalization; replication and division; metabolism; signaling and motility; energy supply and homeostasis.[1,2,14]

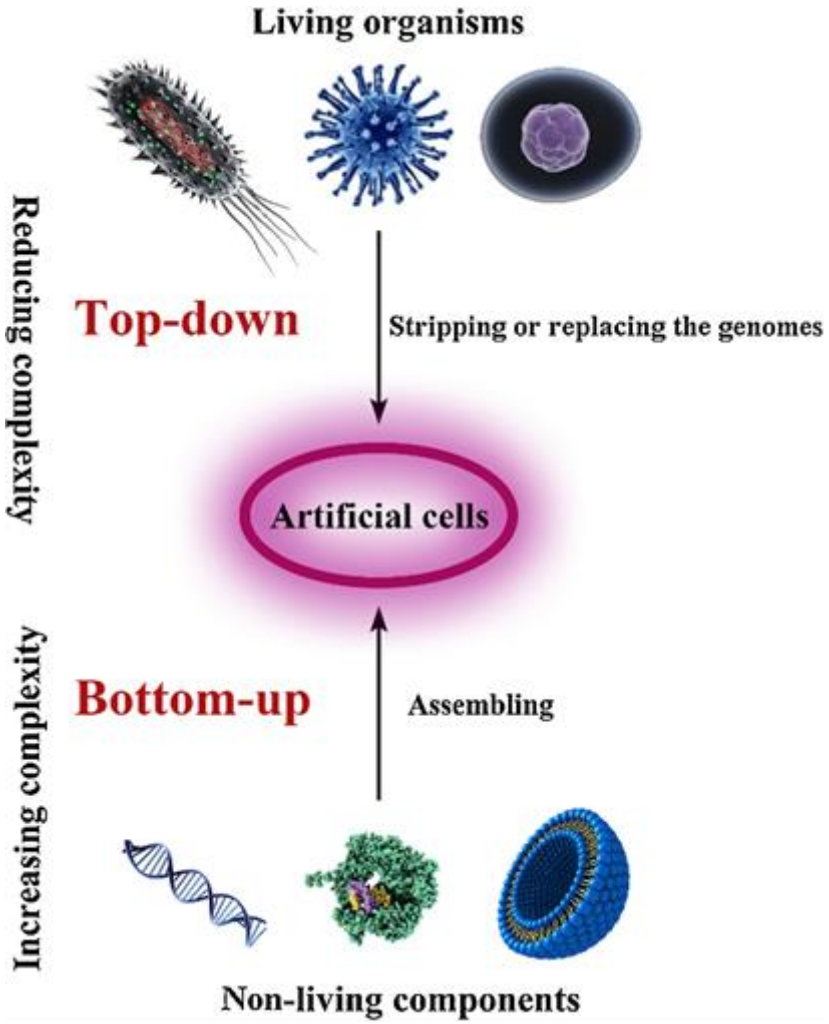


**Figure 1.1.1** Approaches for the design and construction of synthetic cells: In the top-down approach, artificial cells are created by stripping or replacing the genomes of living organisms (cells, bacteria or viruses), reducing their complexity, and only retaining minimum substances to maintain the essential life. In the bottom-up approach, artificial cells are constructed by assembling non-living components to form an integral that can replicate the essential properties of natural cells.[20] Copyright @ 2016, Elsevier. Reprinted with permission from Materials Today.

In summary, the goal of both the top-down and bottom-up approach is to create a minimal cell to understand the fundamentals of living cells, to engineer life covering a wide range of complexity and organization, and to comprehend the basis of the origin-of-life. Although both approaches are valid and complimentary, throughout this thesis, we follow the bottom-up approach

towards a minimal cell since it provides full control over the organization and the interaction of components with high programmability.

## 1.2 Synthetic cell models

One important prerequisite of a cell is compartmentalization, which is the confinement of the interior environment enabling the retention of main elements with an outer membrane. Moreover, the confinement of biochemical reactions in localized volumes of the aqueous cell-like microcompartments allows their out-of-equilibrium operation.[2,14] Only if this is achieved, protocells can function autonomously as a self-maintaining metabolic entity, like a mini-chemical reactor.

Even though there are no limits regarding the choice of membrane molecules or materials for the boundary of cell-like compartments, we should consider certain criteria to ensure the functionality of the protocell model: The membrane should provide mechanical stability and protect the intercellular components. Moreover, the membrane should be semi-permeable and act as a barrier that restricts the accumulation and regulates the transport of the molecules that are essential for the protocell functioning, such as nutrients, and enzymes.[2] Finally, the properties of the membrane define numerous cell processes, including but not limited to adhesion, migration, and communication.[20,21]

In bottom-up Synthetic Biology, numerous types of compartments have been used as the protocell models including polymeric or polypeptide capsules,[22–25] organic and inorganic colloidosomes,[26–30] lipid-based vesicles,[31–35] fatty-acid based vesicles,[36,37] coacervates,[38–43] polymersomes,[44–47] and

proteinosomes.[17,48–50] Due to the particular interest of this thesis proteinosomes as cell-like compartments will be detailed below.

### 1.2.1 Proteinosomes

Proteinosomes are a protocell model with a protein-based membrane developed by Mann and coworkers.[48] Proteinosomes form as a result of the interfacial assembly of protein-polymer nano-conjugates, consisting of a cationized protein with a primary amine group, typically bovine serum albumin (BSA-$NH_2$), and a covalently bound temperature-sensitive polymer, poly(N-isopropylacrylamide)(PNIPAAm).[48] The protein-polymer nano-conjugates, which bare approximately three polymer molecules per protein, localize at a water droplet-oil interface of a Pickering Emulsion (Figure 1.2.1). Subsequently, the closely packed monolayer of the protein-polymer nano-conjugates are crosslinked yielding micron-sized water-filled capsules, which can be transferred into the water without collapsing (Figure 1.2.1).[48] Proteinosomes with specific functions and structures can be generated by changing the chemical structure of the polymer and using different proteins for protein-polymer nano-conjugates.[44,51] An important feature of the proteinosomes membranes is their semi-permeability, which permits the diffusion of molecules with a size-cut of typically 40 kDa.[44] Moreover, the permeability kinetics can be altered by varying the size of the crosslinking agent and the crosslinking density (e.g. shorter crosslinker agent leads to lower permeability).[7] Inside of the capsules, various water-soluble guest molecules that are larger than the size-cut of the membrane,

such as fluorescence proteins, colloidal particles, enzymes, and proteins, can be encapsulated at high efficiency.[7,44,48]

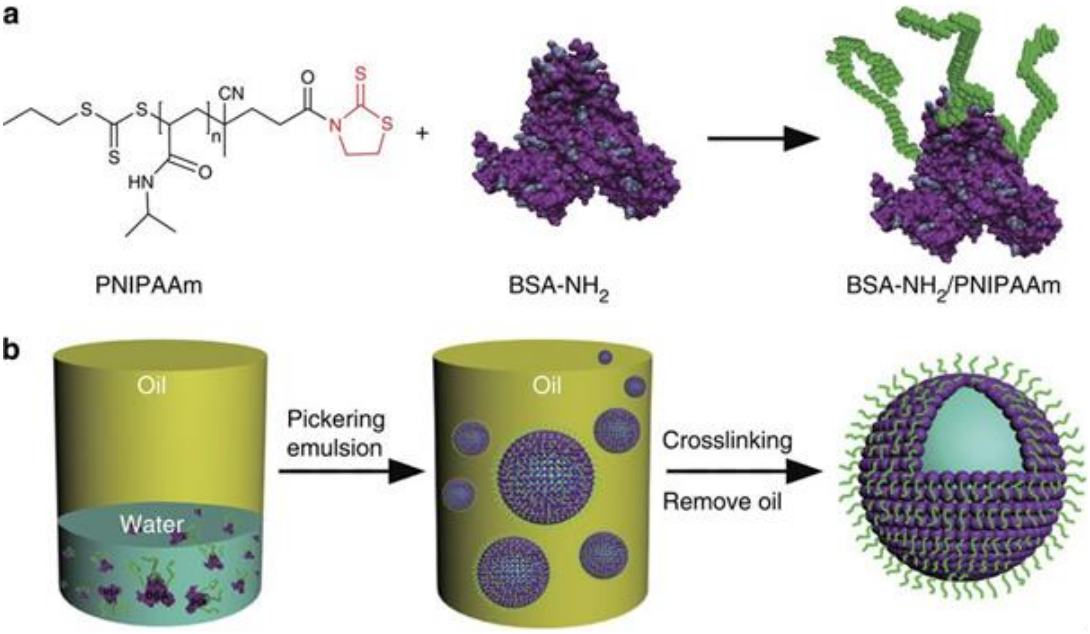


**Figure 1.2.1** Proteinosomes. a) The protein-polymer nano-conjugate (BSA-NH2/PNIPAAm) is formed through the coupling of mercaptothiazoline-activated PNIPAAm polymer chains with the primary amine groups of cationized BSA-$NH_2$. b) Production of proteinosomes. An aqueous suspension of the amphiphilic BSA-NH2/PNIPAAm nano-conjugates along with other water-soluble functional components (e.g. DNA, ribosomes, nucleotides, amino acids, enzymes, proteins and inorganic nanoparticles), were emulsified in a continuous oil phase. The aqueous micro-droplets were stabilized through the self-assembled monolayer of closely packed protein-polymer nano-conjugates. These are subsequently cross-linked into a continuous membrane at the oil/water droplet interface, and transferred into aqueous solutions by the removal of the oil layer. [48] Copyright © 2013, Springer Nature. Reprinted with permission from Nature Communications.

Besides semi-permeability, proteinosome membranes are elastic, stimuli-responsive (e.g., temperature), and tolerate higher temperatures over multiple cycles (70 $^{o}$C for 90 min). [48] These properties make them suitable to study the amplification of genetic material in protocells using the polymerase chain reaction (PCR).[48] Alternatively, the temperature-sensitive polymer, PNIPAAm, can act as a thermally-controlled gate for regulating the diffusion of substrates for enzyme-mediated processes in proteinosomes.[44] Proteinosomes have been

used to mimic different cellular functions including but not limited to gating enzymatic cascades,[52] phagocytosis,[46,53] prototissue formation,[17] cell to cell communication (see chapter 1.3).[7,42,50] Taken together, proteinosomes are great model compartments with a high degree of programmability to develop artificial cells, given their robustness, tunable functionality and structure, semi-permeability and capability to house cellular processes.[51]

## 1.3 Communication between synthetic cells

### 1.3.1 Inspiration from nature

The concept of molecular communication is widely observable in nature and communication through mobile signaling molecules is found at the macro- and micro-scales. For instance, animals exchange information through pheromones, different organs in the body coordinate their function through hormones and during embryonic development stem cells differentiate into diverse cells and tissues based on morphogen gradients.[1,54] At the same time, microorganisms cooperate, synchronize their activities, and autonomously operate in the body without being detected by the immune system.[55–57] Microorganisms accomplish these complex tasks and act like a multicellular organism by using the soluble chemical signaling molecules.[55,58]

### 1.3.2 General characteristics of molecular communication

Intercellular communication among artificial cells is a crucial element in order to design consortia of functional minimal cells arising from the coordinated operation of individual compartments.[21] Through the distribution of information in the form of soluble signals, synthetic cell communities can attain collective and

multicellular behavior, facilitating the occurrence and maintenance of higher-order structures.[49,59,60] Communication between artificial cells has vast applications in many fields, from lab-on-a-chip applications to tissue engineering.[61–63]

In simple terms of molecular communication, the transmitter (also called the sender), sends a message encoded as a molecule that propagates to the receiver. The receiver detects the transported molecules and decodes the message (Figure 1.3.1).

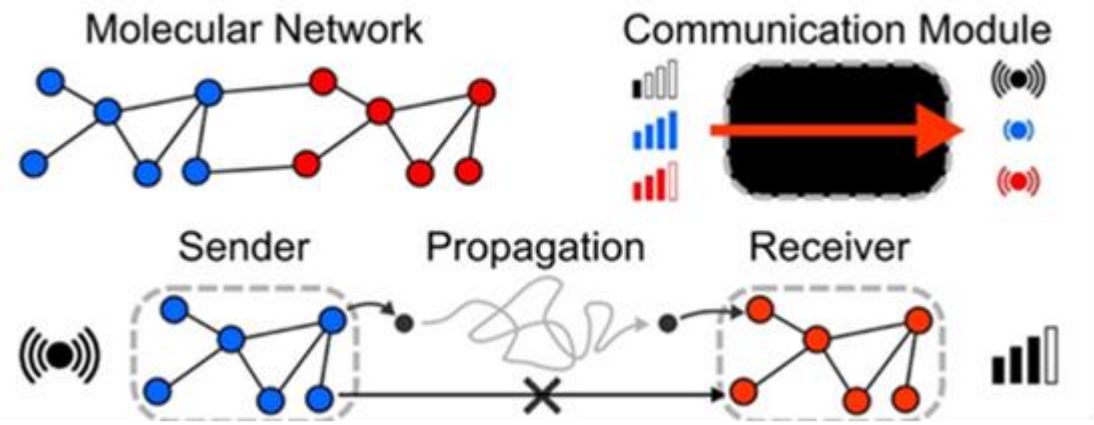


**Figure 1.3.1** Sender-receiver architecture. a) Schematic of a sender-receiver system. A chemical reaction network can be represented by nodes (molecules) connected by edges (reactions). Compartmentalization can be used to isolate parts of a molecular network..[21] Copyright © 2019, Wiley-VCH Verlag GmbH & Co. KGaA. Reprinted with permission from Chemistry - A European Journal.

The required components for efficient molecular communication are a transmitter (i.e., sender), a transport medium, and a receiver One of the examples of molecular communication is a lipid-based protocell that can initiate a quorum-sensing response in the marine bacterium *Vibrio harveyi* (Figure 1.3.2).[64] In this study, i) protocells (senders) autocatalytically synthesize carbohydrates (e.g., *D*-ribose, the message) that mimic autoinducers for quorum sensing of *V. harveyi* through formose reaction, ii) the carbohydrates propagate

by diffusion through the lipid membranes in the medium, iii) as a result the message is transported to the bacteria, iv) the bacteria (receivers) detects the carbohydrates, and v) initiate quorum sensing observable as the bioluminescence light production (decoding).

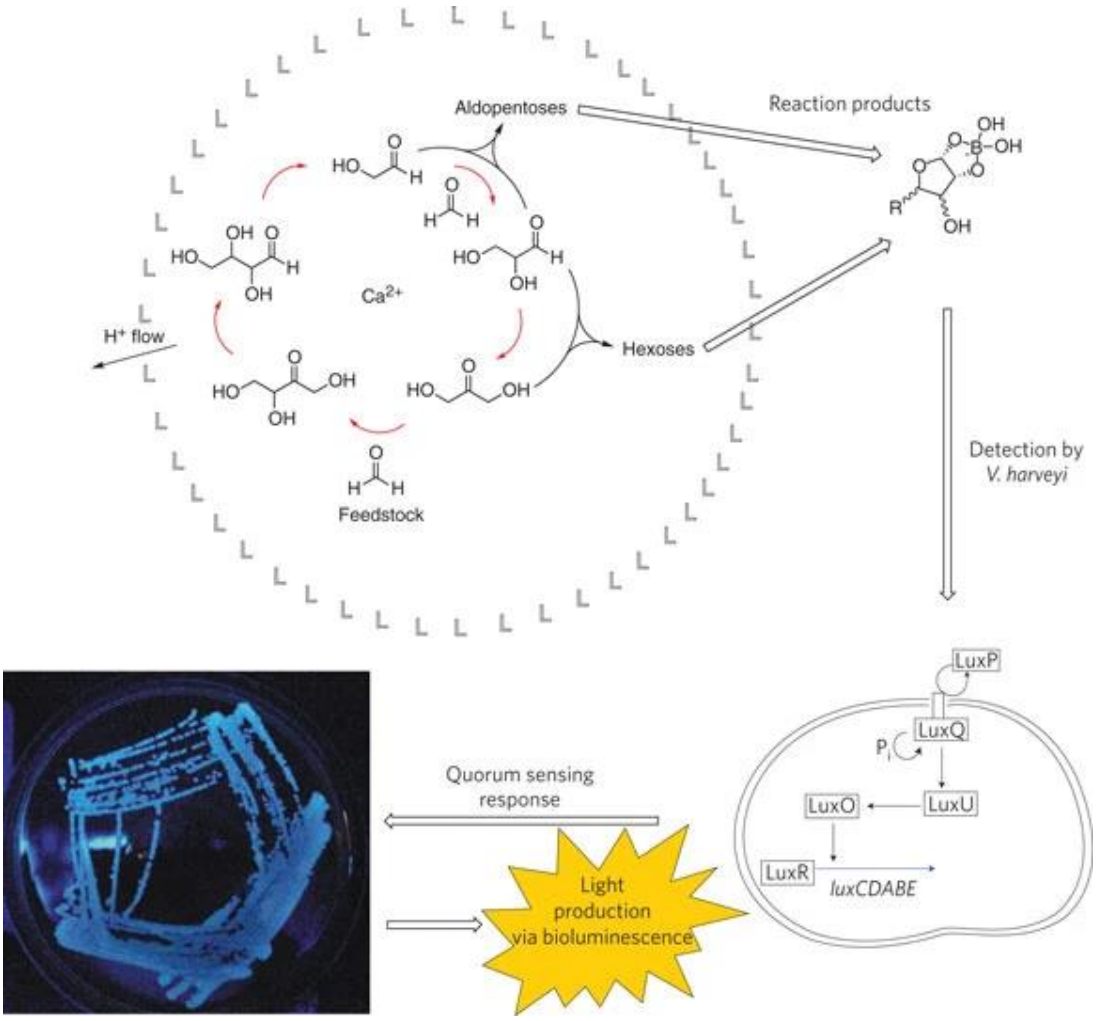


**Figure 1.3.2** Sugar synthesis encapsulated in a lipid-based protocellular model (L). The increase in the environmental pH induces the formate reaction which causes the formation of sugar molecules (Carbohydrate–borate) as the signaling molecule. The sugar diffuses through the medium to interact with the bacterium Vibrio harveyi (bottom right). Successful binding to the LuxP/LuxQ signal transduction proteins of the V. harveyi bacterium results in a protein phosphorylation response, and the subsequent expression of the genes luxCDABE (Pi, inorganic phosphate). The proteins produced give rise to a detectable bioluminescent output (bottom left, a photograph of an agar plate of V. harveyi stimulated with formose). In this way, the products of the protocellular metabolism of a chemical cell allow signaling to the cells of a natural

organism.[64] Copyright © 2009, Springer Nature. Reprinted with permission from Nature Chemistry.

### 1.3.3 Increasing complexity of molecular communication between synthetic cells

Early examples were inspired by molecular communication between bacteria. In one of the early examples, quorum sensing-based artificial microbial communication in *E. coli* was designed using the native quorum-sensing signal 3-oxohexanoyl-homoserine lactone (3OC6-HSL).[65] Many follow-up studies built in the same principle as also described in chapter 1.3.3, for the communication between a liposome and quorum sensing of the marine bacterium *Vibrio harveyi*.[64]

Soluble signals have been used as a means to communicate between artificial cells and living cells. A notable example is a communication between the trapped colonies of GUVs on micro-arrays, cancer cells and bacterial cells (*E. coli*).[66] In this study, spatially organized trapped GUV colonies containing enzymes such as glucose oxidase (GOx) or horseradish peroxidase (HRP) had the capacity to produce enzyme-dependent chemical signaling. For instance, upon the entry of the glucose substrate through pores of the pore-forming peptide (melittin), the inter-vesicular enzyme GOx/HRP cascade reaction is activated. Co-trapped cancer cells are consequently exposed to the toxic levels of hydrogen peroxide coming from the GUVs and result in cell death. Similarly, by co-trapping *E. coli* transformed with T7 promoter/lac operator plasmid encoded for green fluorescent protein (GFP) expression, with IPTG containing GUVs can lead to the synthesis of GFP upon adding melittin and forming membrane pores.

Ions, such as calcium ions have also been used as a soluble signal for the communication between artificial cells. An elegant example of using calcium ions which activates the internal enzyme activity between lipid-based artificial cells, which is observed as an increase in fluorescence.[13] Herein, a calcium-dependent phospholipase ($sPLA_2$ (P1)) was incorporated into the GUVs, which through the hydrolysis of the phospholipids in the presence of calcium, changes the mechanical properties of the lipid membrane. Thus, the permeabilities of the compartment membranes changed which causes the controlled release of encapsulated calcein dye.

Cell-free transcription-translation (TXTL) has been one way to avoid natural cells and built communication between purely synthetic minimal cells. For instance, TXTL reagents such as the Tet Repressor proteins (i.e., TetR) have been implemented into artificial cells that contain nucleus-like porous DNA-hydrogel compartments.[67] Upon the supply of TXTL reagents, expression of the proteins which are encoded in the DNA in the nucleus of cell-mimics takes place. These cell mimics can communicate with the neighboring cells by exchanging expressed diffusive protein signals and exhibit quorum sensing like communication. Likewise, cell-free protein synthesis systems (CFPS), and now known as PURE (Protein Synthesis Using Recombinant Elements) are also used for the synchronized synthesis of functional proteins in communicating artificial cells.[68]

### 1.3.4 DNA-based communication between artificial cells

Using DNA molecules as the signal is especially attractive due to its high programmability and tunability.[69] Moreover, unlike the above-described protein-based molecular machinery is much simpler to program.

Recently, polymerase–exonuclease–nickase (PEN) toolbox has become popular as model systems to study cell to cell communication.

Living organisms use gene regulatory networks to integrate signals from their environment and convert these signals to cellular responses.[70] The essential characteristics of gene regulatory networks have been reproduced to create an artificial approach, DNA PEN toolbox, which uses a set of three enzymes; a polymerase, a nickase cleaving one side of a DNA duplex (i.e., restriction site), and an exonuclease which hydrolyzes the DNA duplex. DNA PEN toolbox relies on a set of short ssDNA strands that encode the information of enzymatic activation and enzymatic inhibition interaction that is mediated by these three enzymes.[71] The design mainly relies on the three ssDNA strands: the main strand and two shorter ssDNA strands that are complementary to the main strand. When the two of the shorter strands hybridize with the main strand, they form the DNA duplex without any overhangs in the presence of the polymerase. The addition of the nickase cuts the two ssDNA strands. Similarly, the exonuclease hydrolyzes the DNA duplex. Most of the PEN based designs are followed through a double-strand specific dye (EvaGreen), which emits fluorescence in the presence of double strands of DNA templates, which is called the active state (Fluorescent ON). When the DNA duplex is disturbed, the fluorescence

diminishes, which is called the inhibited state (Fluorescent OFF). Through the combinations of various DNA templates with the nickases´, PEN based systems enable well-defined programmable communication systems such as amplifiers, and bistable systems.[71,72]

The PEN toolbox has been used to program the exchange of single-strand DNA (ssDNA) between DNA-modified polymer particles.[71] In this example, the particles' were modified with complementary strands of DNA. When the particles carrying these complementary strands were in the vicinity with respect to one another, they were able to interact with one another via the DNA they carry. The emergence of fluorescence signal from the double-strand specific dye (EvaGreen), reflected the number of double DNA strands, on the interacting particles. With the addition of the nickase, the DNA duplex was disturbed and the fluorescent signal diminished. Through the interaction of the complementary DNA strands on the neighboring particles, the fluorescent signal from the particles was switched ON and OFF based on the local density and the spatial organization of the other particles, which is similar to the quorum sensing behavior of the bacteria.

Although the DNA based communication using the PEN toolbox is highly modular, it still requires enzymes for its function.[21] A great way to avoid the use of enzymes in protocell communication are enzyme-free toehold mediated DNA strand displacement (DSD) circuits. DSD circuits rely only on DNA and have been implemented into proteinosomes that communicated with ssDNA molecules.[7]

Toehold-mediated strand displacement (TMSD), is an enzyme-free tool in dynamic DNA nanotechnology.[73,74] TMSD is based on the principle of spontaneous toehold exchange of one strand of DNA (output) with another strand of DNA (input) which is driven forward by entropy (Figure 1.3.3).[74,75] Two complementary strands of DNA are hybridized via based on their Watson-Crick pairing (G-C/A-T), where one of the strands has an exposed overhang domain called toehold, which is complementary to a third ssDNA input strand.[75] The input ssDNA strand is fully Watson–Crick complementary to the strand with the toehold and can displace the complementary strand.[73,75] Here, the higher binding affinity of the input strand to the original strand is the driving force for the strand displacement reaction.[74,75] Consequently, TMSD is a thermodynamically favored process.

By utilizing different ssDNA sequences, which are highly programmable, provide improved control over the communication process and allow for the design of catalytic cascades,[74] oscillations,[76,77] digital logic circuits[74,78] and Boolean neural networks.[79]

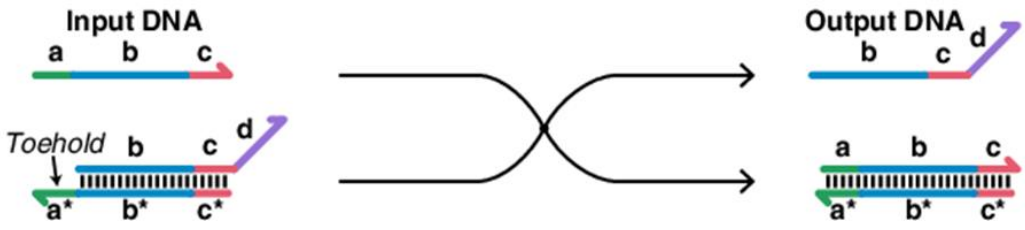


**Figure 1.3.3** Schematic showing a toehold-mediated nucleic acid interaction. The two-strand complex has an exposed toehold domain a* that is complementary to the domain in the input DNA. The input DNA binds to the complex and strand displacement through domains band b* leads to the release of an output DNA that can be used for downstream DNA reactions. [80] Copyright © 2019, Portland Press. Reprinted with permission from Emerging Top Life Science.

In particular, Joesaar *et al*., implemented TMSD based communication between different protocells. Here, proteinosomes that had encapsulated ssDNA logic gate complexes are able to detect, decode, and secrete ssDNA as signaling molecules (Figure 1.3.4a). The sender proteinosomes contained biotin-ssDNA that is immobilized within the membrane and labeled with a fluorescent probe (F). Before the input strand was added F was quenched due to the hybridization with a complementary quencher strand (Q). Upon addition of an input strand, which initiates a TMSD reaction, Q is released and the fluorescence signal within the proteinosomes is observable (Figure 1.3.4b). Moreover, the Q can diffuse freely into the medium and act as a signal for further communication steps with neighboring proteinosomes. Using versatility and tunability of the TMSD, consortia of proteinosomes can perform complex tasks from signal detection, transduction and amplification, to Boolean logic operations, cascaded signaling reactions and feedback loops (Figure 1.3.4b).[7]

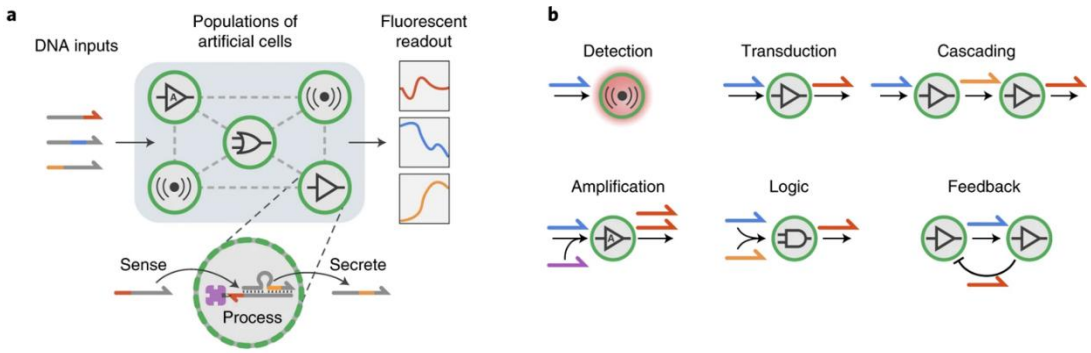


**Figure 1.3.4** a) Protocells with encapsulated DNA gate complexes are localized on a two-dimensional (2D) spatial grid and can sense, process, and secrete short ssDNA-based signals. The system is initiated by adding ssDNA inputs, and the response dynamics associated with the compartmentalized DSD reactions for each protocell are followed by confocal microscopy. b) Individual protocells can be configured to perform various tasks ranging from signal detection to Boolean logic operations. Individual modules can be combined to implement more complex population behaviors such as cascaded signaling, bidirectional communication, and distributed computing.[7] 

### 1.3.5 Transport mechanisms for artificial cell-cell communication

The transport of soluble signaling molecules from one synthetic cell to the next is an important aspect to consider and can happen by passive diffusion, flow-driven transportation of the molecules (e.g., om microfluidic devices with a constant flow), and active propagation (e.g. using motors).[7,76,81,82]

The majority of the communication between the artificial cells relies on the passive diffusion of the signaling molecules, which limits its signaling range.[61] Passive transport is the simplest approach for transporting molecules as it does not require an energy supply or a complex transport biomachinery. However, it is required to have switching and filtering mechanisms both for secretion and detection in order to regulate the propagation selectively.[83] As explained below, there are several studies demonstrating filtering mechanisms either by using closed membranes with membrane channels for selective permeability or using permeable membranes for selective binding (anchoring) of signaling molecules in the senders or receivers.

Lipid-based membranes are tightly enclosed, preventing the exchange of membrane-impermeable large and charged molecules.[21] Forming membrane pores using transmembrane proteins or pore-forming small molecules allows the passing of a diffusible signal.[84,85]

A commonly used pore-forming transmembrane protein in lipid-based protocells is α-hemolysin, a membrane protein originally from *Staphylococcus aureus*.[86] α-hemolysin can be used to transfer chemical messages, from protocells to *E. coli*. For example, Lentini *et al.* constructed protocell secreting

Isopropyl-*β*-D-thiogalactopyranoside (IPTG) through α-hemolysin membrane pores. This allowed for the activation of a fluorescent protein gene regulated under the inducible IPTG *lac* operator on *E. coli*.[87] The recognition of IPTG in *E. coli* results in the expression of a fluorescent protein. Likewise, Tang *et al*. demonstrated the molecular communication between two compartments with different membrane permeabilities, more precisely a lipid vesicle and a proteinosome.[50] In this study, they encapsulated a cell-free protein expression system within lipid vesicles, which upon the external induction with a small lipid permeable lactone (3OC6-HSL) produces α-hemolysin and glucose. The produced glucose is released through the membrane pores formed by in situ produced α-hemolysin and diffused to the receiver cells, the proteinosomes. The proteinosomes which contain glucose oxidase and horseradish peroxidase (HRP) detect the glucose signal, i.e., the glucose oxidase oxidizes the glucose producing hydrogen peroxide. Subsequently, HRP in the presence of hydrogen peroxide catalyzes the conversion of Amplex Red to a fluorescent output.[50]

Pore-forming peptides such as melittin can also be used to regulate chemical signaling. In particular, melittin was used to release a chemical signal in the form of glucose between two different in GUV populations. Likewise, as demonstrated in the study which is explained in detail above, consortia of protocells and living cells were able to communicate through melittin, where the presence of the $H_2O_2$ signal of the protocell induced cell death with cancer cells, and the IPTG signal from the protocell lead to gene expression within *E. coli*.

Using open compartments with permeable membranes requires careful designs to specifically transport small molecule signals but not dilute intercellular

content. Consequently, the permeability should be tuned in a way that the machinery of the synthetic cells, which enables their function stays encapsulated, but the signaling molecules are allowed to be exchanged. Proteinosomes presents a great example of such tunable permeability as described in detail in the previous chapter. The study reported by Joesaar *et al.* is an example of an open DNA-based communication system in populations of proteinosomes. while proteinosomes were permeable to short (<100 bases) single-stranded DNA (ssDNA), the streptavidin (MW: 60 kDa) immobilized ssDNA with biotin tags remained within the proteinosomes.

An interesting example of the active transport is using chemotactic bacteria (*i.e. E. Coli*) for the delivery of encapsulated imaging agents, genes, and drugs (i.e. anticancer doxorubicin drug molecules) to cells, which will be discussed in chapter 1.5.[88,89]

### 1.3.6 The role of spatial organization in chemical communication and emergent behavior among synthetic cells

As described in the previous chapters, living cells communicate with their environment and coordinate their behavior with their neighbor cells. Among various intercellular communication types, paracrine signaling is a type of signaling where cells secrete diffusive extracellular messenger molecules, which induces changes in the cells in proximity.[1] Paracrine signaling is used in a whole range of cellular processes; however, they are especially important during development and cell differentiation.[90] It allows cells to dictate neighboring cells what identity to acquire.[72] Embryogenesis is an important example of this phenomenon. From a simple form, it develops into a complex organism by going

through differentiation as a response to the spatial and chemical information that directs the structure and the function of the cells constructing the embryo.[72] As such, the diffusion range of the secreted paracrine signaling molecules is kept very limited, ensuring its delivery to the proper target cells and at a defined distance.[90] Moreover, the action of the most paracrine signaling molecules depends on the binding of neighboring cells to specific plasma membrane receptors.[90]

In the context of soluble and diffusing chemical signals, the speed and range of the transmission of a signal depend on the signaling molecule and the transport medium. However, it is often restricted to a sub-domain either within a cell or a couple of cells.[61] When the signaling range is smaller than the average separation of cells, the cells act like isolated cells, leading to no communication.[21]

Consequently, the communication between cells, based on diffusible signals, relies heavily on the distances between them, their spatial organization, as well as the contacts between the cells. Thus, the collective behavior of cells, including complex cellular processes such as differentiation, and information processing cannot be achieved by cells in isolation. In parallel, controlling the spatial organization and the contacts between the synthetic cells in order to regulate the intercellular communication between synthetic cells is a crucial step for the emergence of complex cellular processes, collective behavior, and achieving a functional minimal cell.

As a result, also for the communication and emergent or collective behavior of synthetic cells controlling their spatial organization has been of interest. The rest

of this chapter gives the most prominent examples of how spatial organization of synthetic cells impacts their behavior and the emergence of properties.

An essential step towards recapitulating morphogenesis in synthetic cellular consortia is a different response to chemical cues depending on their spatial distribution and, thereby, their differentiation to different states. To this end, as described in chapter 1.3.3, Gines *et al*. reported the programming of the DNA-modified polymer particles that can communicate selectively with each other using the PEN toolbox.[71] In this example, the communication between the particles having complementary DNA strands depends on their spatial organization as they require to be in the vicinity to achieve hybridization. As a result, the particles as a collective were able to mimic some fundamental features of quorum sensing and morphogenesis. In a later study, Zadorin *et al.* introduced bistable reaction networks using the PEN DNA toolbox, which allowed to generate three different patterns of particle aggregation.[72] In this study, two different sets of microparticles were used. From these particles all aggregated on the one side of a glass substrate, only one set was aggregated in the middle of the substrate and none of them aggregated on the other side of the substrate. For this, they used microparticles functionalized with ssDNA strands that can be programmed to either aggregate with each other or repel other populations. The aggregation of the particles can be triggered by the external addition of a linker-DNA, which is the main strand (as explained in detail in Chapter 1.3.4) complementary to the all short ssDNA strands that were immobilized on the microparticles. The DNA on the complementary microparticles hybridized together with the linker DNA in the presence of the polymerase. In other words,

the linker DNA here acts as the crosslinker. The aggregation can be turned off (i.e., reversed by the nicking and exonuclease). By generating concentration patterns of the linker ssDNA concentration on the glass substrate and the enzymes and combining with the functionalized particles, they regulated the aggregation of the particles in real-time. The particles autonomously exhibited different aggregation behaviors which is inspired by the cell patterns formed during *Drosophila* (fruit fly) embryogenesis.

An outstanding example of how the spatial arrangement of sender and receiver cells alters the cell-to-cell communication *in vitro* was reported by Dupin *et al*. (Figure 1.3.5).[84] In emulsion-based synthetic cells containing DNA/RNA circuits, the droplets are connected at the through bilayers at the droplet-interfaces and the spatial organization of the droplets in the network is precisely controlled. In other words, receiver cells with or without pore-forming α-hemolysin (shown in red in Figure 1.3.5) are connected to a central sender cell (S) in a geometrically controlled arrangement. As a consequence the chemical signal (shown in blue in Figure 1.3.5) can only diffuse through droplets with α-hemolysin and their direct neighbors, thus only moving along the red path to the neighbors. The integrated positive feedback circuit further increases the differences in the protein expression levels between droplets within the same cell network, thereby led to a primitive form of differentiated gene expression.

Optical tweezers are an attractive way to spatially organize lipid-based vesicles with high precision. Once sender and receiver cells were brought in proximity in the desired configuration, $Ca^{2+}$ ion exchange was possible using α-hemolysin pore-forming proteins. The forces applied with the optical tweezers can be high

enough even to induce fusion between vesicles, which allows separating different components and mixing them on demand. In particular, transcription and translation components placed in different vesicles could be combined and trigger protein expression.[91]

The contact-dependent chemical exchange between different protocells can also be used to kill a population, which is analogous to predatory behavior.[38,49] For instance, protease loaded coacervate microdroplets, which lyses the proteinosomes upon electrostatically induced contacts has been reported.[38] The lysed proteinosomes release their load to the medium, which then can be selectively encapsulated in a different protocell population.[38] In a follow-up study, a three-step process for contact-dependent response retaliation was introduced using ternary proteinosome/coacervate communities.[49] This consortium consists of GOx containing proteinosomes, a pH-sensitive coacervate droplet containing proteinase K, and a pH resistant polymer coacervate adhering to the proteinosomes. Upon the introduction of glucose signal, protons secreted by the proteinosomes kills pH-sensitive coacervate droplets, releasing the proteinase K, which is then transferred into the polymer coacervate. Through the contact between the polymer coacervate and the proteinosomes proteinase K, a delayed killing of the proteinosomes was demonstrated.

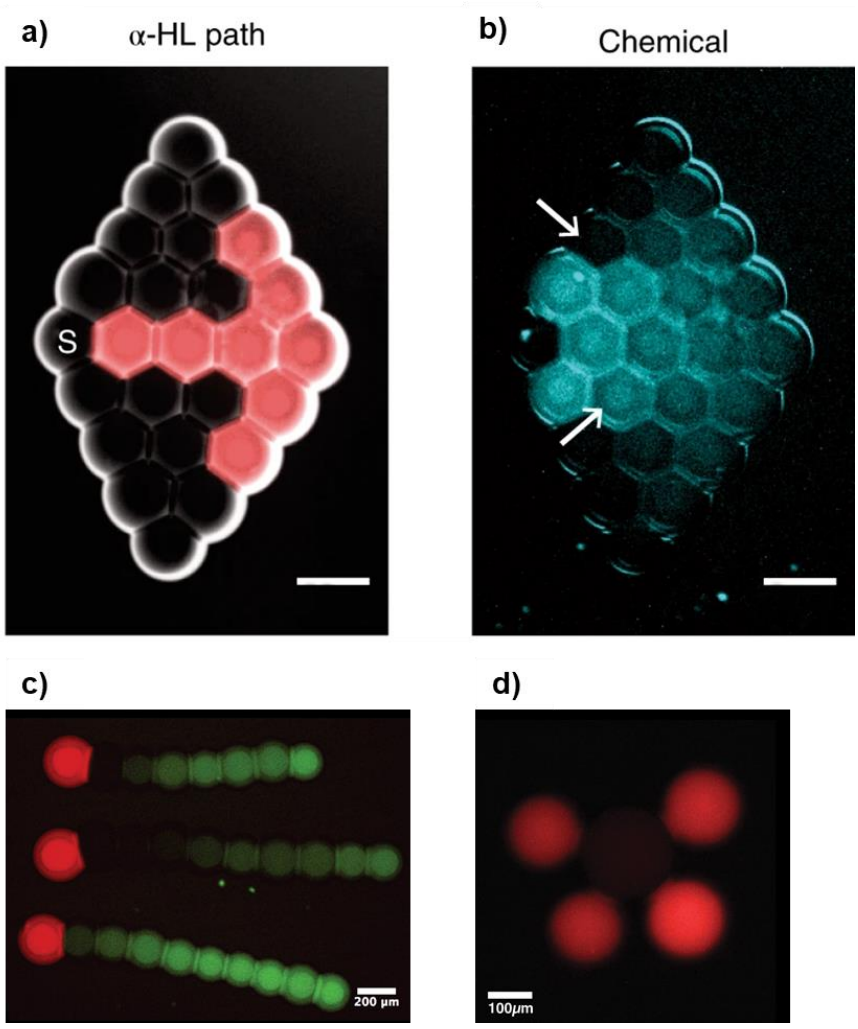


**Figure 1.3.5** a) A droplet network is assembled with a sender droplet (S) and receivers containing α-HL (red) or not. b) A diffusing chemical (blue) can only translocate through bilayers where α-HL is incorporated, so it diffuses along the red path and into the direct neighbors. Arrows point to two initially identical droplets, which differentiate based on their environment. Scale bars, 200 μm. c) Propagation of the pulse from a sender droplet (red) to an array of receivers. Fluorescence is shown in green at different time points. Scale bar, 200 μm. d) Fluorescence images of three different positions, with a sender in the center and receivers on the edges, display differentiated protein expression levels.[84] 

## 1.4 Controlling the adhesion in synthetic cells as a step towards spatial control

In the previous chapters, the importance of the spatial organization of synthetic cells for intercellular communication has been described. In order to regulate communication, the spatial control among protocellular communities is either

achieved on templated closed systems such as on chips or microfluidic arrays[7,43,71,72,76,82] or by inducing cell-cell adhesions between synthetic cells.[38,46,49,53,60,84,91]

Biological cells adhere to their matrix through surface receptors (i.e. integrin transmembrane receptors) specific to extracellular matrix proteins, including but not limited to fibronectin, collagen, and fibrinogen. Similarly, adhesion models for synthetic cells for adhesions include an adhesion receptor on the cell membrane and a complementary adhesion ligand either on the matrix for matrix adhesions or on the different types of cells for cell-cell adhesions (Figure 1.4.1).

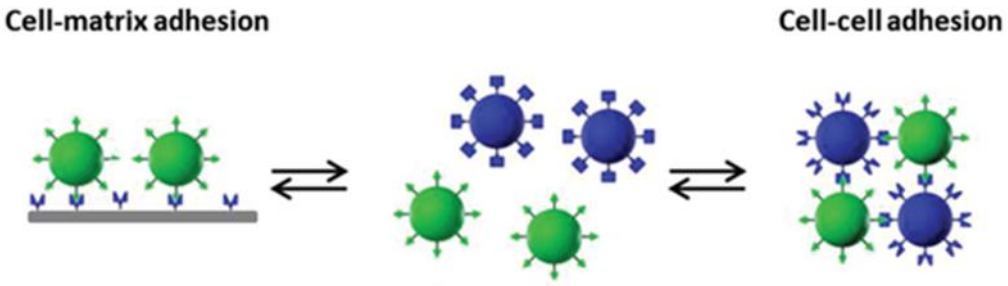


**Figure 1.4.1** Mimicking cell adhesion in minimal synthetic cells. Minimal synthetic cells, here shown as green and blue spheres, are functionalized with cell receptors. Cells can adhere to substrates functionalized with the ligands recognized by their surface receptors to form cell-matrix adhesions. Different or the same cell types that have complementary receptors on their surfaces can form cell-cell adhesions.[92] Copyright © 2019 WILEY-VCH Verlag GmbH & Co. KGaA. Reprinted with permission from Advanced Biosytems.

Adhesions between synthetic cells have been induced using the native cell-cell adhesion proteins, cadherins as well as other types of interaction partners. Especially, early synthetic cell models decorated with cadherins including GUVs have provided insight into cell-cell adhesion and the fusion of oil in water droplets.[93,94]

Lectins, which are carbohydrate-binding proteins employed by cells to actuate cell adhesion have also been used as adhesion mediators in synthetic cells. For instance, glycophorin functionalized liposomes specifically adhere to lectin coated surfaces even under flow conditions.[95], and glycan functionalized GUVs were crosslinked to form cell-cell junctions and prototissues in the presence of lectin.[96,97]

The above-mentioned natural adhesion partners can be substituted with other receptors and ligands. For such, the strong binding affinity of tetrameric protein avidin (or its analogs such as streptavidin and neutravidin) to biotin has been utilized to induce the adhesion of GUVs to biotin functionalized supported bilayers (SBL),[98,99] and assembled vesicles into prototissues.[94,100] Additionally, hybrid systems composed of bacteria and vesicles have been assembled through the specific biotin-streptavidin binding (see chapter 1.5).[89,101–103]

In addition to specific protein interactions, unspecific electrostatic and van der Waals forces, as well as permanent covalent interactions, were also used to induce cell adhesions. For instance, in the above-described assembly of lipid vesicles with optical tweezers, the vesicle adhered to one another through electrostatic and van der Waals forces, which can be overcome by the addition of high concentrations of salt.[91] Likewise, the adhesion of coacervate microdroplets to proteinosomes relies on electrostatic interactions.[38,60] A similar strategy is employed to attach positively charged vesicles (e.g. liposomes) to bacteria, which have a negative net surface charge under physiological conditions.[104] On the other end of the spectrum in terms of binding strength, synthetic cells can also

be covalently bound to each other, for example, through click chemistry to form stable prototissues.[17]

To regulate the spatial organization in response to external stimuli adds another level of control. By this means, we can achieve high spatiotemporal control over the architectures and dynamically alter the interactions between the different cells to program intercellular communication.[105] As such, external stimuli such as temperature and light have been used to control adhesions between synthetic cells.[17,105–109 ] In particular, DNA coated nano or micrometer-sized particles have been employed for temperature-responsive and reversible self-assembly.[108,110–112] Upon cooling the adjacent particles functionalized with complementary strands below the melting point the DNA strands anneal with each other, driving the self-assembly of the particles. DNA also provides flexible control over the interparticle interactions with high programmability in this context. However, it should be noted that temperature-responsive methods find limited application under biological conditions and provide limited spatiotemporal control.[112,113]

Photo-responsive systems where light directs the interaction between minimal cells under isothermal conditions are especially attractive as light offers independent control with high spatiotemporal resolution as well as the ability to trigger bioorthogonal reactions.[114] Other advantages of using light as a stimulus are; the possibility to effortlessly deliver light to a defined area of the sample down to the diffraction limit of a couple of hundred nanometers; the possibility to turn light ON/OFF at any desired time; the tunable and dynamic control; the sustainable availability of light as a continuous trigger on a sample without consuming it or forming byproducts like with a chemical reagent; its high

biocompatibility in the visible range; and finally its non-invasiveness, which makes it suitable for biological applications. So far, the assembly of micron-sized objects has been controlled with light through the functionalization of the particles with light-responsive small molecules such as azobenzenes[109,115–117], spiropyrans[118,119], and coumarins[120] is used to trigger the self-assembly of particles by using light as the stimuli. Although light is an attractive stimulus for all the reasons listed above, none of these examples are biocompatible, due to their response to UV-light and the use of organic solvents. As an alternative, photoswitchable proteins (see Chapter 1.6) that respond to the visible light can be used to drive the interaction between minimal cells. For instance, two different pairs of photoswitchable proteins (iLID/Nano and nMagHigh/pMagHigh) that reversibly heterodimerizes with the complementary pair upon blue light illumination were used to control the self-assembly of four different type of model minimal cells. [107] The colloids (as model minimal cells) were functionalized with the only type of the protein. Colloids functionalized with the complementary protein pairs bind reversibly and orthogonally only to one another (i.e., iLID to Nano and nMagHigh to pMagHigh) thereby sorting into two separate families with controlled arrangements. The study demonstrates the precise control of the organization of various compartments as a step for achieving prototissiues.

## 1.5 Bacteria driven biohybrid microswimmers

Bacteria-driven biohybrid microswimmers (i.e., bacteriabots) are composed of motile bacteria cells integrated with a functional synthetic cargo (e.g.,

microparticles, encapsulated bioactive molecules, fluorophores, or drugs).[88,89,103] They are extensively studied for active and targeted delivery of the cargo.

Bacteria have unique characteristics, which makes them well-suited as smart delivery agents: they are self-propelled and can pass biological barriers, which provides access to otherwise inaccessible regions (e.g., tumor sites), they can sense and respond to the environmental stimuli (e.g., chemotaxis), which provide specificity and high spatiotemporal control of the delivery, they can express proteins *in situ* for delivery, and they can be externally detected.[121] Straightforward genetic engineering of bacteria allows manipulating their function and precisely tuning their mode of action. For instance, bacteria cells can be genetically engineered to express light-sensitive ion-channels, providing a high degree of transcriptional control.[122] Another study reported a bacterial LOV protein that binds to DNA upon blue light illumination, which utilizes bacteria to activate transcription in eukaryotic cells.[123]

Multifunctional bacteriabot systems present exceptional possibilities for the production of soft micro-robots, which can overcome the problems with conventional drug delivery including but not limited to the need for repeated administration of high doses of the drug, and off-target distribution of the drug molecules leading to severe side-effects.[121] For instance, *E. coli* strains with lectin pili allow anchoring a fluorescently labeled cargo to the mannose expressing epithelial cells found in the urinary tract and gastrointestinal tract through the lectin-mannose interaction.[103] Bioadhesiveness of the bacteria can be used to target specific cell types through specific adhesion moieties for the delivery of

the cargo. Another study reported the combination of the engineered bacteria with the microemulsions encapsulating imaging agents for the active transport and delivery of the desired cargo to the breast cancer cells, MCF7, (Figure 1.5.1).[88] The attached bacteria body transports the microemulsion to the cell, and the delivery of the cargo can be observed through the emergence of fluorescence in the target cells as a result of the diffusion of the imaging agent into the cell.

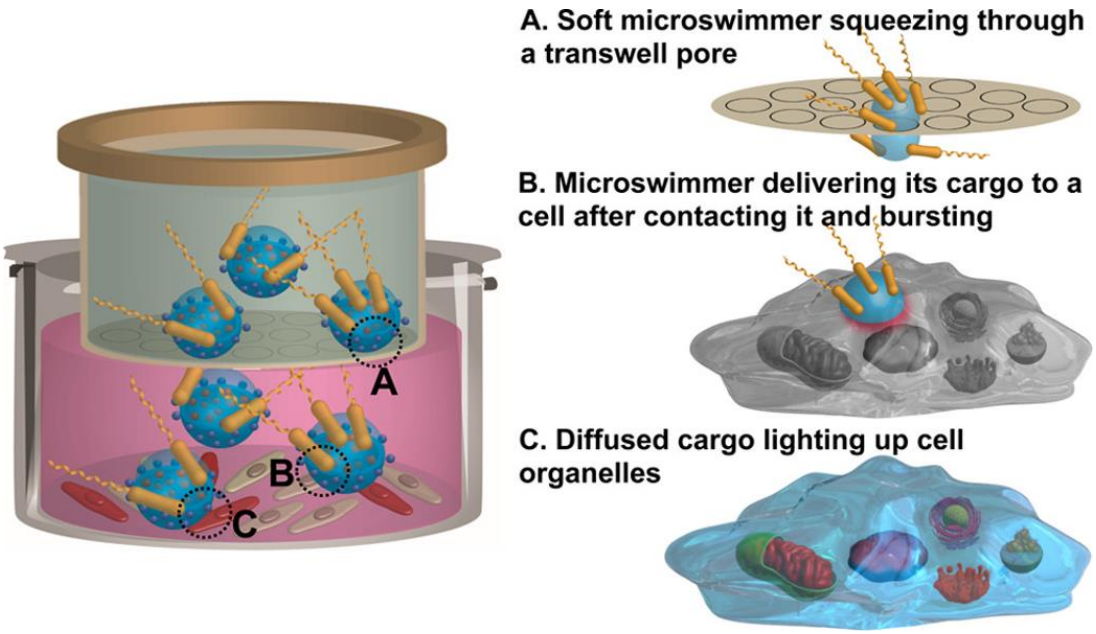


**Figure 1.5.1** Schematic diagram of the *in vitro* experimental set-up of the microemulsion-based bacteribots for active cargo delivery.[88] Copyright © 2017 American Chemical Society. Reprinted with permission from ACS Nano.

Designing systems involving molecular communication can be applied to improve healthcare applications for diagnosis and drug delivery when combined with bacteriabot technology.[61–63] In bacteriabot designs, thousands of bacteria need to detect the disease sites, coordinate with one another, act autonomously, and release the drugs at the target site. Accomplishing such complex tasks, require communication between these robots. Although bacteriabots present a promising technology, there are many challenges that need to be addressed before employing bacteria in delivery systems. One of the main points when

designing a bacteriabot is cargo integration onto the bacteria and its release. Living motile bacteria and the cargo should be coherently integrated to produce a delivery system with maximum functionality. What is more, controlled delivery of the cargo provided with the stimuli-responsive cargo drop is need to ensure effective delivery. Bacterial adhesion on synthetic surfaces has been extensively studied. The adhesion can either be induced by electrostatic interactions; where the bacteria have a natural negative net surface charge and adhered to the positively charged surfaces[124,125], by covalent attachment[126], or by bioaffinity/specific attachment (e.g. antibody-antigen or biotin-streptavidin)[101,127]. A few reports also exist demonstrating a stimuli-responsive cargo drop by using UV-light, chemicals, or ultrasonic waves.[128–130] However, as these methods only offer minimal control and are not biocompatible, controlled cargo integration and release need further investigation and development in order to achieve the full potential of the bacteriabot systems.

## 1.6 Light sensitive proteins for optogenetic control

Light-responsive proteins present a promising alternative to the small molecules mentioned earlier to generate light-controlled systems. Such proteins stem from plants, fungi and bacteria, which use these proteins to regulate their vital functions such as growth and development, circadian rhythms, chloroplast motility in response to light.[131,132 ] Light-responsive proteins have been crucial in the emergence of the field of optogenetics, which uses light to control cellular processes. Engineering and introducing these proteins into cells enabled scientists to turn on or off processes selectively with unprecedented

spatiotemporal control and their dynamic regulation. Cellular events that have been controlled with light including but not limited to gene expression,[123,133–135] signaling pathways[136–139], protein localization,[140] cell polarity and migration of enzymes[141–145]. Besides intracellular events, neuronal optogenetics utilizes light-responsive channel proteins cell to cell signaling in neural networks,[146,147] and has the potential for improving neurological disorders and restoring vision loss.[148,149]

The light-responsive proteins that are utilized in this thesis are reversible light-induced dimerizes. All these proteins form specific homophilic or heterophilic protein-protein interactions upon illumination, which dynamically revert in the dark (and under far-red light for red light-triggered interactions. These proteins differ in their response to specific wavelengths i.e. colors of visible light: blue (470 nm), red (650 nm) and far-red (750 nm), enabling their orthogonal photoactivation to one another.[141,150,151] When choosing the suitable photoswitchable proteins, factors to consider are the reversion time in the dark, the dynamic range of the protein-protein interaction, and wavelength compatibility with fluorescence imaging. Orthogonal and independent activation of independent modules can be achieved by combining multiple photoswitchable proteins that respond to different colors of light. For instance, Gaigai et al. reported the selected localization of two proteins from the cytoplasm to the plasma membrane by utilizing blue and red light-sensitive proteins.[152] This allowed for the light-controlled intercellular signal transduction of $Ca^{2+}$ and cyclic adenosine monophosphate (cAMP). Likewise, Yüz et al. employed blue and

red light-sensitive proteins to independently trigger the adhesion of two different cell types on the matrix in the presence of other cell types.[153]

### 1.6.1 Red light-responsive proteins

Phytochromes are photoreceptors derived from plants, fungi, and bacteria that are responsive to red (≈ 650 nm) and far-red (≈ 740 nm) light.[150,154,155] Phytochromes posses a covalently bound light-sensing bilin chromophore, which consisting of an open chain of four pyrrole rings.[150] When the chromophore absorbs red/far-red light, it photoisomerizes (Z to E dimerization), which leads to conformational changes in the protein resulting in binding with the interaction partner (Figure 1.6.1). The phytochromes exist in two photo-interconvertible forms; upon red light illumination, the Pr form (red light absorbing form) converts to the Pfr form (far-red light-absorbing form).[156,157] The process is reversed upon far-red light illumination or can take place spontaneously in the dark by thermal relaxation.[150]

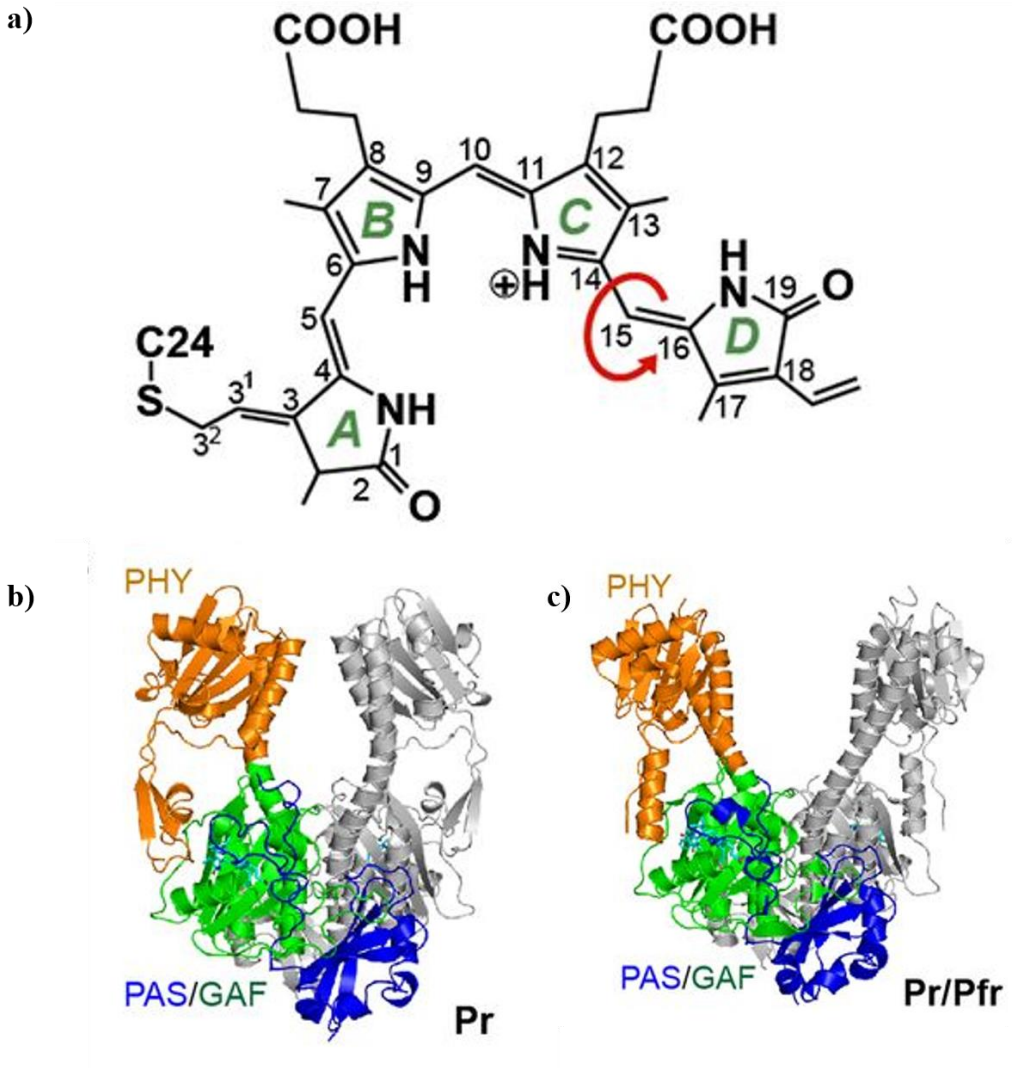


**Figure 1.6.1** a) Chemical diagram of the bilin chromophore. The four pyrrole rings (A-D) are labeled, arrow shows the Z to E photo-isomerization location. [158] Copyright © 2014, American Society of Plant Biologists. Adapted with permission from the Plant Cell. [158]. Crystal structures of PAS-GAF-PHY dimer b) in the dark, and c) illuminated forms. [155,159] Copyright © 2014, Springer Nature. Adapted with permission from Nature.

### 1.6.1.1 PhyB/PIF protein pair

Phytochrome B (PhyB) is a red/far-red light-absorbing photoreceptor derived from the plant *Arabidopsis thaliana*.[144,160] The photosensory core of PhyB containing 650 amino acids and has a covalently bound phycocyanobilin (PCB) as the chromophore. Upon red light illumination, the protein switches to the Prf state and rapidly binds to downstream transcription factors, phytochrome interaction factors (PIFs In far-red light or in the dark, the Pr state has a lowered

binding affinity towards PIFs leading to their dissociation from PhyB (Figure 1.6.2).[138] For optogenetic applications, a 100 amino acid segment of PIF6 and PIF3 have been used as interaction partners.[138,161]

The light-dependent heterodimerization of PhyB with PIF6 has been utilized to control various processes within cells. Levskaya et al. were able to perturb and direct the morphology of mammalian cells by using red/far-red light as the stimuli.[138] For this purpose, PhyB was anchored to the cell membrane and a small signaling G protein fused to PIF6 was recruited upon redlight illumination. The local recruitment of the small signaling G protein, which controls the actin polymerization, from the cytoplasm to the membrane with micrometer spatial resolution, enabled the precise control of cell shape. PhyB/PIF6 dimerization has also been used to control gene expression in yeast and mammalian cells, as well as in zebrafish.[162–166] For instance, Beyer *et al*. were able to dynamically photo-regulate the nuclear localization of proteins of interest and gene expression in zebrafish and mammalian cells.[162] In this study, a PhyB was fused to a protein of interest and a nuclear export signal, while PIF3 was harboring a nuclear localization signal. As a result, the nuclear import could be turned on ON under red light with the complexation of PhyB-PIF and OFF under far-red light.

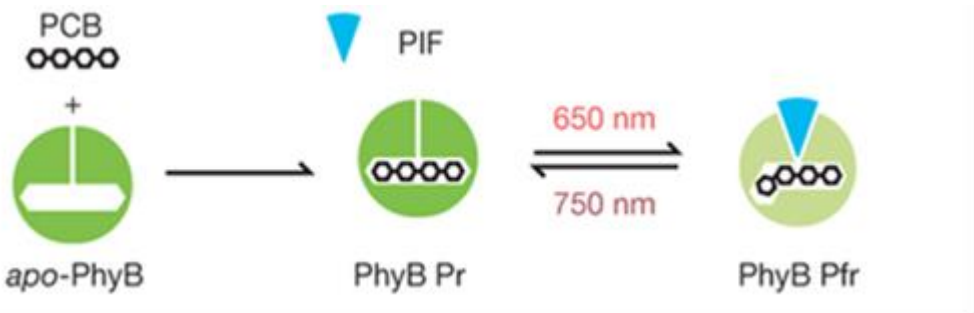


**Figure 1.6.2** Schematic representation of red light-induced interactions (PhyB /PIF system). Upon red light irradiation chromophore (PCB) undergoes a conformational change that causes switching from Pr (red light sensing form) that does not interact with the PIF to Pfr (far-red light sensing form) that can interact with the PIF. [138] Copyright © 2009, Springer Nature. Adapted with permission from Nature.

### 1.6.1.2 Cph1 protein

The cyanobacterial phytochrome 1 (Cph1) from *Synechocystis* PCC 6803 is another red/far-red light-absorbing photoreceptor protein.[157] Similar to PhyB, the cofactorPCB binds to apo-Cph1.[157,167] Upon red light illumination, Cph1 switched to the Pfr state and homodimerizes. Similar to PhyB, also Cph1 reverts to the monomeric Pr state upon far-red light illumination and the homodimer disassembles.[167]

Cph1 has been widely used in bacteria for spatiotemporally programmed gene expression and protein interactions.[168–172] For example, Levskaya et al. demonstrated a bacterial system that can replicate a photograph light pattern as a chemical image by fusing Cph1 to an *E. coli* intercellular histidine kinase domain.[170] Upon red light illumination, the gene expression is inhibited, resulting in an image as the pattern of applied light on the biological film appeared. ] Similarly, Cph1 was combined with blue and green light-responsive proteins to regulate the expression of different genes in *E. coli* with respect to red, green, and red light (RGB).[171] Consequently, spatiotemporally controlled colored chemical

images (i.e. color photographs) on bacteria culture plates could be generated by controlling the color pigment production.

Cph1 has also been used in order to control cell signaling pathways in mammalian cells. For instance, Cph1 has been fused to receptor tyrosine kinases, of which native ligand-binding domain was truncated.[167] The red light-induced homodimerization of the receptor tyrosine kinases initiates the downstream signaling pathways,[173] and the activation of the signaling not in response to its ligand but red light.[167]

### 1.6.2 Blue light-responsive proteins

The Light-Oxygen-Voltage (LOV) domain is a blue light-responsive photoreceptor from the phototropin protein family found in a large variety of plants (e.g. *Arabidopsis thaliana* and *Avena sativa*), bacteria, microalgae, and fungi (*Neurospora crassa)*.[141,174–176] LOV domains have the blue light-absorbing flavin cofactor, which tightly binds to the folded protein through noncovalent interactions. Upon blue light absorption, the flavin reacts with a cysteine residue forming a covalent bond and leading to major conformational changes in the protein (Figure 1.6.3).[141,177] There exist different variants of LOV-based proteins from various organisms and further versions were engineered to enhance dimerization, broaden and/or optimize the kinetic range as well to adjust binding affinities suited for the various applications.[141,151,177,178]

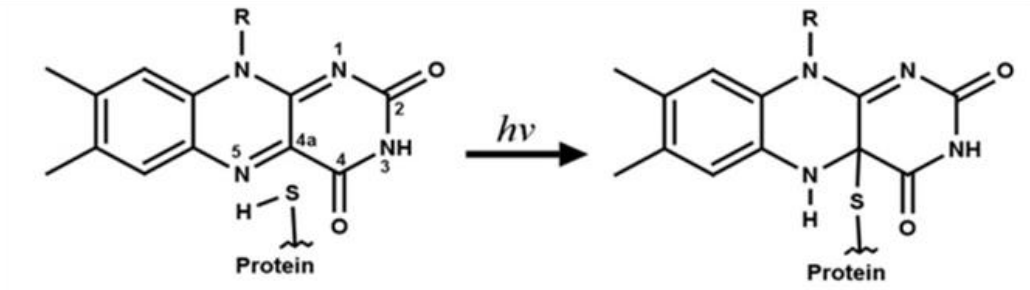


**Figure 1.6.3** Photoreaction of the flavin mononucleotide (FMN). Blue light illumination causes singlet excited state FMN to undergo intersystem crossing to the triplet state, which results in a covalent bond with the cysteine residue of the protein.[179] Copyright @ 2016 American Chemical Society. Reprinted with permission from the Journal of Physical Chemistry Letters

### 1.6.2.1 iLID/Nano protein pair

iLID protein has been engineered from the LOV2 domain of phototropin 1 from *Avena sativa.* The LOV2 domain posses a flavin mononucleotide (FMN) chromophore, which is crucial for the blue light responsiveness. The LOV2 domain has a well-folded the core protein domain (core-per-arnt-sim, i.e., PAS fold), which has two α-helixes with 20 amino acids on both N- and C- termini and conserved cysteine and glutamine residues.[180] Upon blue light illumination, the excited FMN goes through a singlet to triplet transition, forming a covalent bond with the cysteine, which subsequently disturbs the hydrogen bond between the glycine residue and FMN. This causes the glycine to flip and protein to change its structure, resulting in the unfolding of the C-terminal α-helix (i.e. Jα-Helix). The covalent bond between the cysteine and the FMN breaks within tens of seconds, leading to the spontaneous refolding of the Jα-Helix in the dark.[180]

iLID protein is an improved light-inducible dimer derived from the LOV2 domain, which has a seven amino acid binding peptide, SsrA from *E. coli*, incorporated into the Jα-Helix.[141] In the design, the Jα-Helix unfolds upon blue

light illumination (488 nm), exposing SsrA peptide to its binding partner, the SspB peptide (Figure 1.6.4).[141]

Different point mutants of the SspB peptide have different binding affinities for iLID and have been named Nano (wild-type SspB), Micro, and Milli. The photoreceptor iLID and its binding partners have been employed to control various processes from protein localization[141,181,182], transcription[183], self-assembly of oligomeric enzymes[184], signaling pathways[185] to cell migration[186,187] in mammalian cells. Moreover, these blue light-controlled protein-protein interactions have also been used in synthetic cells for the spatiotemporal control of cell mimetic processes. For instance, the movement of a giant unilamellar vesicle was guided by light.[106] Two lipid vesicle populations either functionalized with iLID proteins or Nano, adhered to one another upon blue light illumination.[120]

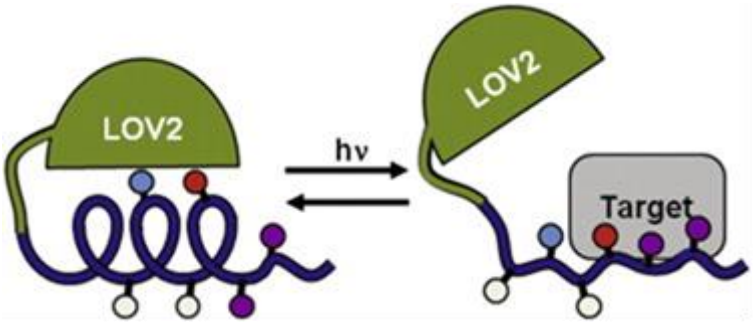


**Figure 1.6.4** Schematic representation of the photoswitchable LOV2 based light-inducible dimer design. SsrA peptide is caged under the Jα-Helix. The amino acid residues which are important for protein-core/ Jα-Helix interactions are cyan, the ones for SsrA/target peptide (i.e. SspB) are purple. Blue light illumination leads to the unfolding of Jα-Helix, making the SsrA peptide available for SspB binding.[177] Copyright @ 2012 Elsevier. Reprinted with permission from Chemistry and Biology.

In the context of chemical communication, Chakraborty et al. demonstrated blue light-controlled communication in minimal synthetic cells.[105] Two lipid vesicle

populations either functionalized with iLID proteins or Nano, adhered to one another upon blue light illumination.[120] The spatiotemporal control over the adhesions between the vesicles allowed to regulate the $Ca^{2+}$-dependent chemical communication between them. Consequently, the adhered vesicles communicate with one another, which was followed with a fluorescent output, where the distant vesicles in the dark showed no output.

#### 1.6.2.2 VVD protein

VVD is a LOV based photoreceptor derived from *Neurospora crassa*.[176] VVD switches from a monomer state to a homodimer state in response to blue light.[176,188] The protein binds to flavin adenine dinucleotide (FAD) as the cofactor and reacts to the blue light through the photochemically driven formation of a cysteinyl-flavin adduct.[188] Upon excitation, FAD is protonated and the flavin protonation state leads to a series of conformational and hydrogen bonding changes, exposing the amino acid chains that are responsible for the dimerization, thereby facilitating the dimerization.[176] The light state dimerization is driven mainly by the conformational changes in the part of the N-cap sequence and the hinge to the PAS core.[176]

Homodimerization of VVD has been utilized to regulate the transcription and gene expression in fungi, bacterial, and mammalian cells.[189–195] For instance, by fusing split fragments of T7 RNA polymerase to VVD protein, blue light-activated gene expression was implemented in *E.coli*.[191] Moreover, a study demonstrating the blue light-inducible recombinase for *E. coli* has been reported.[195] Similarly, the split fragments of recombinase were coupled with the photodimers, where

the blue light illumination brings the fragments together to yield a functional recombinase.[195] This offers precise control over the DNA excision. More recently, the photoreceptor was integrated into the neuronal cells for a blue light-inducible recombinase for precise single-cell manipulation and analysis.[196]

In summary, light-responsive protein-based systems were demonstrated to control protein localization, protein states, transcription, gene expression, cell contacts, and information exchange in a spatiotemporal manner. These proteins offer reversible and dynamic control over the engineered systems and have the potential to address the drawbacks of the existing stimuli-responsive methods, as discussed in the previous chapters. Ultimately, the proteins, as mentioned above, provide a versatile tool to achieve high spatiotemporal and dynamic control over processes such as cell-adhesion and complex communication processes.

# Chapter 2: Results and Discussion

## 2.1 Blue-light triggered cell adhesion and DNA-based communication in synthetic protocell communities

### Aim

The ability to manipulate the collective decision making within artificial cellular networks is a key step to achieve higher-order synthetic systems. Here, the optogenetic protein pair iLID and Nano is utilized as a tool to control the self-assembly of artificial model cells in order to regulate the DNA-based communication cascade between the cells. This presents the first example of a DNA-based communication cascade that can be manipulated by visible light under physiological conditions.

### Contributions

I performed all the experiments including the analysis of the data[redacted]and [redacted] helped in establishing the DNA-strand-displacement reaction and assisted in the troubleshooting of DNA-localization. [redacted] synthesized the NTA-PNIPAam polymer conjugate. [redacted] supervised the work.

### Abstract

Living cells exchange diffusible signals, where the sender cell secretes a chemical signal that is detected and decoded by the receiver cell. This chemical communication between the living cells is the basis of the complex collective information processing leading to the higher-order multicellular networks. The

spatial organization of the sender and receiver cell is one of the major factors that affect the local cell-cell communication and many important biological processes such as differentiation. Development of the artificial cell-like compartments performing chemical communication provides for a simplified tunable platform to study intercellular communication, which can also lead to the synthetic communication networks among artificial cells. Controlling the assembly and the spatial organization of the artificial cells with external stimuli is an important step in achieving highly programmable communication networks with higher spatiotemporal complexity. Towards this goal, we present a blue light-responsive communication cascade between artificial cells containing previously reported DNA-encoded sender-receiver architectures, where semi-permeable protein-polymer microcapsules (proteinosomes) used as the model cells and DNA is the diffusive chemical signal. For this purpose, we functionalized the microcapsules with proteins iLID and Nano, which interact under blue light and dissociate in the dark. Upon blue light illumination, the proteinosomes self-assemble allowing the DNA-based communication cascade to take place between the proteinosomes in the vicinity. Consequently, the communication does not take place in the dark. Our system presents a strategy for a stimuli-responsive control over the spatial organization of the proteinosomes in bulk systems, that paves the way for mimicking collective behavior in living cells.

## Introduction

In multicellular organisms, intercellular communication is essential for coordinating individual cells to attain collective behavior.[197] Cells use a variety

of signaling pathways to operate, organize, synchronize, and differentiate into specialized tissues.[90,198] These signaling processes allow cells to exchange information with neighboring cells, to monitor their environment, sense and adapt to the changes. Signals in the form of diffusible chemicals are secreted from sender cells and recognized by receiver cells. In many cases where the diffusion range of these chemicals is limited to a sub-domain of a single cell or only to a couple of cells, the spatial organization of the cells within cellular communities is critical for the perception of the signal.[199] Consequently, the action of such signaling molecules relies on the direct contacts of the neighboring sender and receiver cells.[1] A prominent example of such communication is the paracrine signaling during development, allowing cells to identify neighboring cells and differentiate into the appropriate cell type.[1,72]

Artificial cell-like compartments offer a simplified platform to understand how intercellular communication can lead to the coordination of individual cells in communities and engineer synthetic communication networks among artificial cells. Early examples include implementing the quorum sensing machinery in bacterial cells for artificial microbial communication.[65]Studies reporting quorum-sensing mimicking communication between artificial and living cells have followed up.[64,67,200] Pore-forming transmembrane proteins, such as α-hemolysin, have been used for the transduction of larger membrane-impermeable signals between sender and receivers.[50,86,201] The variety of artificial model cells, as well as the complexity of the signals and the communication network increased, where minimal synthetic cells were combined with information processing networks using DNA-based

communication,[7] molecular sensing architectures using ions to activate internal protein communication,[15] feedback loops through *in vitro* gene circuits,[7,13,84] and cell-free protein expression machinery mimicking quorum sensing behavior in synthetic cell communities.[67] These studies illustrate the capabilities of a variety of artificial cell networks utilizing chemical communication and the potential for emergent behavior Similarly, contact-dependent response in cell communities including retaliation and predatory behavior between minimal synthetic cells through the chemical signal transduction has been reported.[38,49] These studies illustrate the capabilities of a variety of artificial cell networks utilizing chemical communication and the potential for emergent behavior.

Similar to the multicellular communities in Nature, the spatial arrangement of different synthetic protocells is critical towards the emergence of higher-order behavior. In recent studies, the distribution of synthetic cells on defined positions on microfluidic chips or by using optical tweezers has been demonstrated.[7,76,84,91] The spatial organization of the protocells was shown to lead the rudimentary examples of emergent behavior such as synchronization of cell-free genetic oscillations and artificial differentiation of microbeads.[72,84,91] Nevertheless, the self-assembly of synthetic cells into prototissues such that they can perform tasks as a collective remains unexplored. Yet being able to precisely define the spatial organization of the components of the artificial cell networks is an important step towards seamlessly combining individual compartments capable of carrying out above mentioned tasks in a collective manner, which leads to higher-order architectures.

One of the visions for artificial multicellularity is controlling the self-assembly of the synthetic cells with external stimuli. Such control would allow regulating the communication and constructing networks with the desired cell-cell interactions. A promising approach to this challenge is assembling multicellular structures through the stimuli-responsive specific adhesions between protocells. To date, several examples of programmed assembly of protocells with respect to external stimuli such as temperature,[17] metal ions[202] and light[105] have been reported. Controlling the spatial organization of sender and receiver cells by implementing light-responsive adhesions between them is attractive since light as a stimulus provides tunable and non-invasive control over the assembly process with high spatiotemporal resolution.[107,114,203]

Herein, we demonstrate the blue light-responsive assembly of sender and receiver populations of semi-permeable protein-polymer microcapsules (proteinosomes),[48] carrying DNA based communication cascades. The DNA based communication modules build on the previously developed enzyme-free DNA strand-displacement (DSD) cascades and are highly programable.[7] The semi-permeability of the proteinosomes allows for the encapsulation of large protein conjugates and the exchange of ssDNA as signaling molecules. Utilizing sequence-specific DNA provides high tunability to program functions including but not to oscillations,[76,77] digital logic circuits[74,78] and Boolean neural networks.[79] Through the combination of the light-responsive protocell adhesions with the DSD reactions, we aim to photo-regulate the self-assembly and communication between the sender and receiver proteinosomes with visible light as the stimuli.

We recently demonstrated the blue light triggered adhesion and aggregation of GUVs that are decorated with photoswitchable proteins, which enables us to photo-regulate the calcium(II) based chemical communication between the sender and receiver GUVs, based on their spatial proximity.[105] Similarly, our blue light-responsive communication cascade relies on the toehold mediated DNA-strand displacement reaction and consists of sender and receiver proteinosomes, which are functionalized with photolabile proteins and encapsulated with two complementary single-strand DNAs (ssDNA).[7]

**Results and discussion**

In order to follow the each DSD reaction, DNA-complexes consisting of; i) fluorescent strands (F) that are anchored within the proteinosomes through the streptavidin-biotin interactions, ii) complementary quencher (Q) strands, were employed. By the addition of the Input (invading strand), the ssDNA exchange reaction in the sender population is induced, the replaced strand (Q1) is secreted by the sender, and transmitted as the chemical signal in the communication process. The replacement of the quencher strand (Q) results in the recovery of the fluorescence of F-strand, which can be observed under the microscope. Under blue light, the aggregation of the proteinosomes will be induced, then the chemical signal (Q) between the proteinosomes that are in contact can be transmitted, whereas the communication is disturbed between the isolated proteinosomes in the dark due to the dilution of the signaling molecules (Figure 1). The process is observed by the emergence of Cy5 signal from the F strand of receiver population, which only takes place when the proteinosomes are under blue light (Figure 2.1.1)

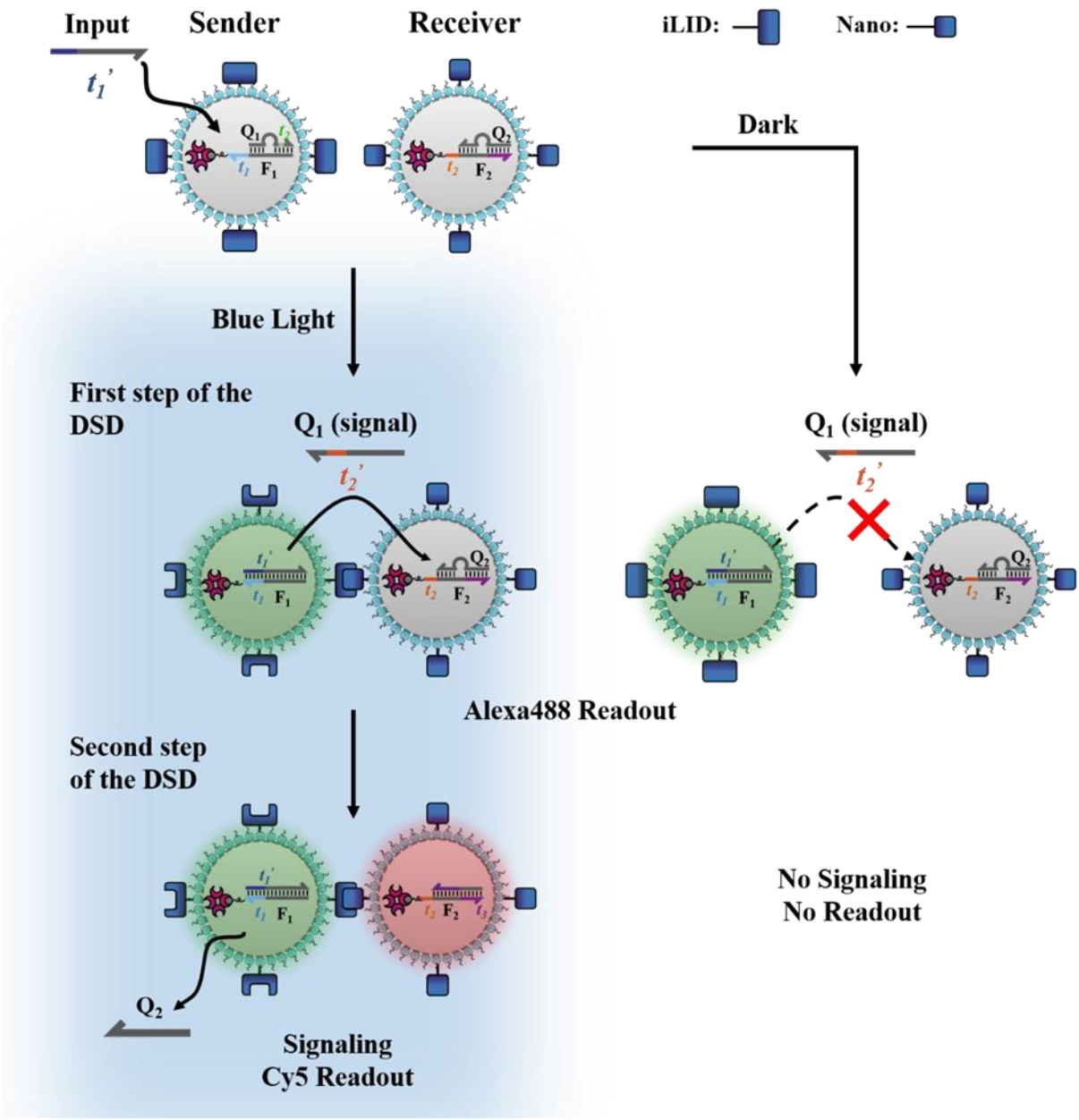


**Figure 2.1.1** Molecular reaction diagram of the blue light triggered signaling cascade between the protocell populations. Under blue light, sender cells functionalized with the photoswitchable protein iLID on their surface bind to receiver cells functionalized with Nano, due to the blue light-dependent interaction of iLID and Nano. Sender proteinosomes sense the added input strand, triggering the first step of the DNA-strand-displacement (DSD) reaction and secreting a signal strand (Q1) to the medium. Removal of the Q1 stand activates the Alexa488 fluorescent DNA gate complex, enabling the detection Q1 secretion. Only when the sender and receiver cells are in close proximity as a part of a cluster, the Q1 signal can be sensed by the receiver cells, triggering the second step of the DNA-strand-displacement (DSD) reaction, secreting the Q2 strand. Removal of the Q2 strand activates the Cy5 fluorescent DNA gate complex, which can be detected and recorded as the readout of the signaling process. The signaling does not take place in the dark. The sequences for this system are given in the Methods section.

In order to control the adhesions between the sender and receiver proteinosomes, and hence their spatial organization, we employed a pair proteins iLID and Nano, which bind to each other under blue light (480 nm) and dissociate in the dark. [105] These photoswitchable protein interactions specifically respond to low-intensities of light and function in buffered solutions, which makes them highly biocompatible and attractive for biological applications.[28]

To later functionalize the proteinosomes with the proteins, we prepared Rhodamine labeled proteinosomes from NTA-PNIPAAm polymer-BSA conjugates (1% NTA-PNIPAAm to -PNIPAAm ratio) (Figure 2.1.2).

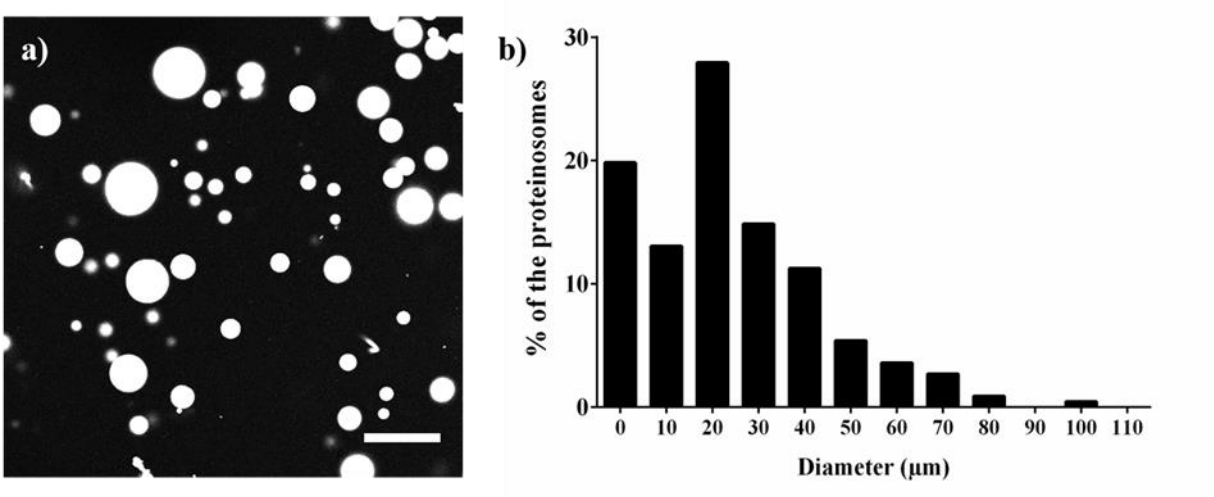


**Figure 2.1.2** a) Confocal microscopy images of NTA-co-PNIPAAm Rhodamine-B labeled proteinosomes. The scale bar is 100 µm. b) Graph demonstrating the distribution of the diameters of the proteinosomes. At least the sizes of the 200 proteinosomes from three different images was measured.

Loading the NTA (nitrilotriacetic acid) groups with $Ni^{2+}$ ions allowed us to immobilize any His-tagged (polyhistidine sequences) protein of choice on the surfaces of the proteinosomes in a specific and oriented way (Figure 2.1.3). To demonstrate the functionalization of the proteinosomes, we used the His-tagged fluorescent protein, miCy (Figure 2.1.3 c and d). While the proteinosomes with Ni2+ loaded NTA groups showed bright fluorescence at the periphery upon

incubation with His-tagged miCy, control proteinosomes that were not functionalized with $Ni^{2+}$ were not fluorescent. The binding of His-tags to $Ni^{2+}$-NTA groups is a very reliable method to functionalize materials and was used also to immobilize the photoswitchable protein interaction partners iLID and Nano through their His-tags onto proteinosomes.

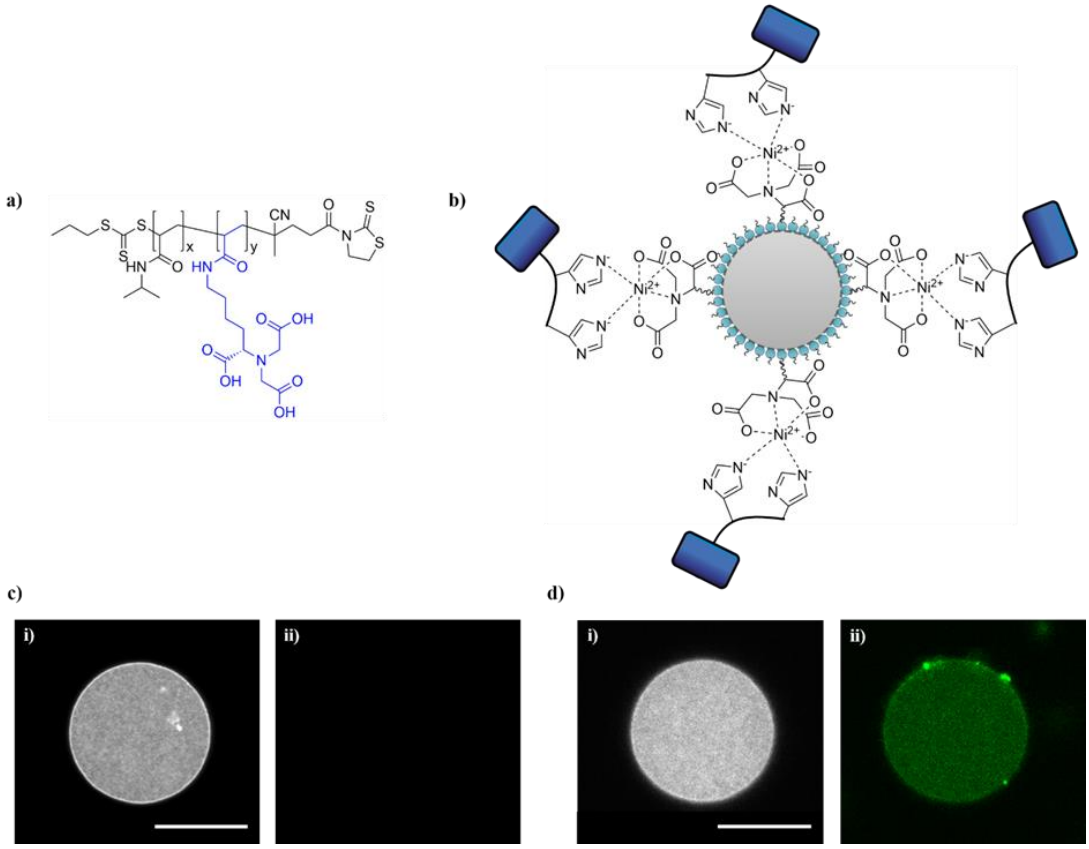


**Figure 2.1.3** a) Molecular structure of the NTA-co-PNIPAAm. b) Surface chemistry of protein functionalized $Ni^{2+}$-NTA proteinosomes. Confocal fluorescence microscopy images c)NTA-PNIPAAm proteinosomes, i) proteinosome membrane, ii) fluorescent His-tagged miCy protein labeling. No fluorescent signal indicated that without the $Ni^{2+}$ complexation, His-tagged proteins have no affinity for the proteinosomes. d) $Ni^{2+}$ NTA-PNIPAAm proteinosomes i) proteinosome membrane, ii) fluorescent His-tagged miCy protein labeling. Localization of the miCy on the membrane is shown, indicating the His-tagged proteins can be immobilized on the proteinosomes. The scale bar is 50 µm.

Following the above-detailed design strategy, we first tested if the adhesion between iLID and Nano functionalized proteinosome populations can be triggered under blue light (Figure 2.1.4 and Appendix Figure A3). For this

purpose, the two different populations of proteinosomes each functionalized with one of the proteins, were mixed in equal proportions and either incubated under blue light (480 nm) or kept in the dark for 90 min. Under blue light illumination, the proteinosomes formed large aggregates, while in the dark, they remained dispersed as single proteinosomes, as observed using fluorescence microscopy (Figure 2.1.4b). These qualitative observations were further supported by quantifying the aggregation ratio of the proteinosomes. The aggregation ratio was defined as the area of proteinosomes involved in clusters (fluorescent objects with an area > 2000 $\mu m^2$) divided by the area of all proteinosomes. It should be noted that proteinosomes have a broad size distribution (from 2 μm diameter to 100 μm), and the size limit for proteinosomes involved in a cluster is larger than the largest single proteinosomes to avoid counting any single proteinosome as a cluster. Consequently, this method underestimates proteinosome clustering as clusters composed of multiple small proteinosomes are not accounted. Despite the underestimation of proteinosome clustering, it was still significantly higher for the proteinosomes that were incubated under blue light compared to the ones that were kept in the dark (Figure 2.1.4c). We also quantified the number of clusters with the same size threshold, and we observed the number of proteinosomes clusters is significantly higher when they were kept under blue light (Figure 2.1.4d). Taken together, the results show that the assembly of the two different populations of proteinosomes, that were functionalized with photoswitchable iLID and Nano proteins, could be controlled by using blue light as the stimuli.

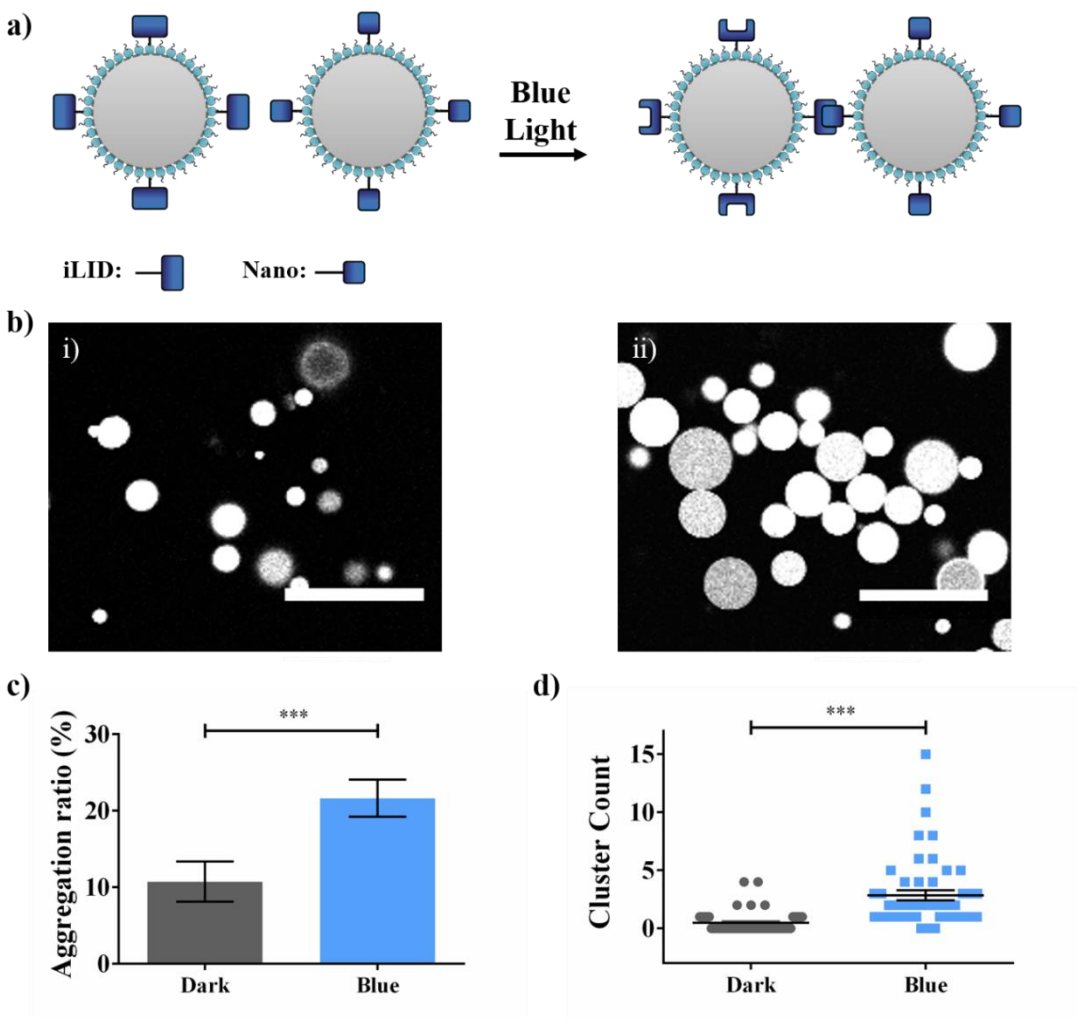


**Figure 2.1.4** a) Photoswitchable proteinosome adhesions. b) Microscopy images of iLID and Nano functionalized proteinosomes, i) in the dark, proteinosomes do not stick together and remain dispersed in the solution, ii) after 90 min of blue light illumination includes the heterodimerization of iLID and Nano proteins, results in the aggregation of the proteinosomes. The scale bars are 100 µm, c) Aggregation ratios of the proteinosomes functionalized with iLID and Nano proteins. d) The number of proteinosome clusters in the dark and under blue light. Unpaired t-test was used as the statistical test, $p < 0.001$. Error bars are the standard error of the mean from >45 images.

Next, we sought to integrate the DNA based communication module into these proteinosomes and control the proximity of sender and receiver cells with blue light and thereby their communication. For this purpose, the streptavidin was encapsulated into the proteinosomes to later localize biotin tagged DNA strands inside of the proteinosomes. We could confirm the encapsulation of streptavidin in the proteinosomes using a FITC labeled streptavidin with confocal

microscopy. Based on these images, the streptavidin concentration in the proteinosomes was calculated to be ≈15 μM (Figure 2,1.5).

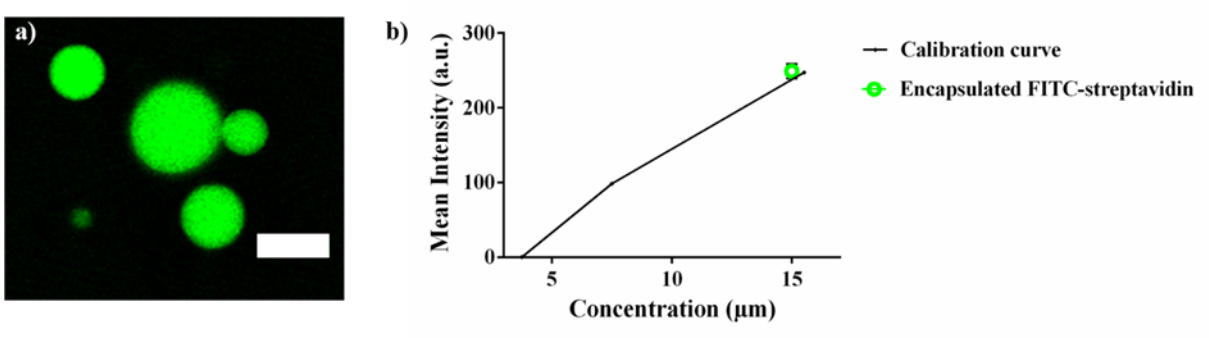


**Figure 2.1.5** Encapsulation of the FITC-steptavidin in proteinosomes. a) Microscopy images of the proteinosomes in FITC channel. b) Calculation of the concentration of encapsulated FITC-Streptavidin in the proteinosomes, n=3.

To demonstrate that the DNA-based signaling cascade between the sender and receiver proteinosomes depends on their proximity and contact and can only take place upon light illumination, we combine iLID functionalized sender cells with Nano functionalized receiver cells. The sender and receiver cells were loaded with different elements of DNA based logic operators using the encapsulated streptavidin and the biotinylated-DNA strands. The sender cells were equipped with the first step of the DSD, the F1 strand labeled with an Alexa488 fluorophore and the Q1 strand, which quenches Alexa 488 and can be displaced by the I (input) strand. The receiver cells are loaded with components of the second step of the DSD, the F2 strand with a Cy5 fluorophore and the Q2 strand, which quenches Cy5 and can be displaced by the Q1 strand (Figure 2.1.1). The mixture of the sender and the receiver proteinosomes were incubated for 90 min either in the dark or under blue light. After the formation of the adhesions between the protocells, we placed the sample under the confocal microscope, added the I strand and observed the signal from the sender (Aleca488) and

receiver (Cy5) cells (Figure 2.1.6 and Appendix Figure A4). At this point, quencher strands, Q1 and Q2 quenches the fluorescence of the biotin-anchored F1 and F2 strands within the proteinosomes and no signal was detected.

As the I strand diffused into the sender proteinosomes, the toehold-mediated displacement of the quencher Q1 strand (DSD-Step 1) took place, which results in an emergence of the Alexa488 signal from these proteinosomes. Both for proteinosomes in the dark and under blue light the Alexa488 fluorescence was observed for 20 min. The Q1 strand diffusing out of the sender cells acts as the signal and the input strand for the receiver cells for Step-2 of the DSD. When the receiver cell was in contact with the sender cells as a result of blue light-induced aggregation, the signal (Q1) was perceived and the toehold-mediated displacement of the quencher Q2 strand (DSD-Step 2) took place after 20 min (Figure 2.1.6a, ii). As a consequence, the Q2 strand was released into the medium leading to the emergence of the Cy5 fluorescence inside the receiver cells and is the readout of the communication between the sender and receiver cells due to this cascade. It should be noted that Q1 only quenches the F1 strand and not F2. On the other hand, for proteinosome mixtures kept in the dark the DSD-Step2 was not observed in the form of an increase in Cy5 fluorescence in receiver cells even after 20 min (Figure 2.1.6a, i). These findings show that the transmission of the Q1 strand, which acts as the mediator of communication, relies on the spatial proximity of the sender and receiver cells.

For population-level quantification of the two DSD reactions and the communication process, we analyzed the changes in the fluorescence intensity for the Step-1 and Step-2 DSD (Figure 2.1.6b). For such, we randomly selected 60

sender and receiver proteinosomes and measured their fluorescence intensities in 5 min intervals. For Step-1 of the DSD reaction, an increase in the Alexa488 fluorescence was observed after the addition of the input strand in all the sender cells, whether in the dark or under blue light. Based on the data, we demonstrated the input strand dissipates homogenously and triggered the DSD reaction, regardless of the light illumination. On the other hand, we observed the emergence of the Cy5 fluorescence as a result of the Step-2 DSD, which indicates the uninterrupted communication, only after the blue light illumination. The results confirmed that the molecular communication between the proteinosomes relies on the adhesions of the proteinosomes and can be controlled by using light as the stimuli.

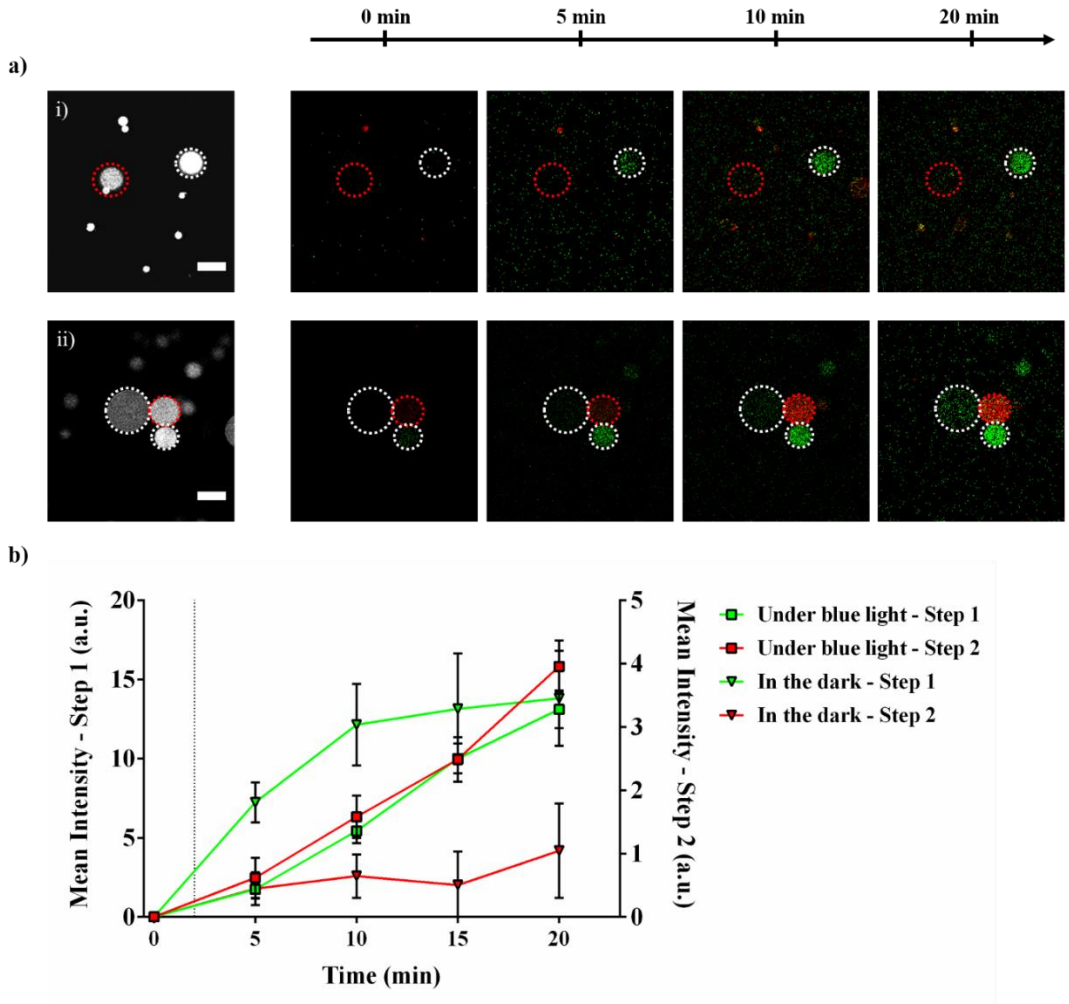


**Figure 2.1.6** Adhesion dependent communication of the proteinosomes. a) Confocal images of the signaling cascade between the sender cells (green), and the receiver cells (red). t=0 is the time point when the input strand was added. i) In the dark, the proteinosomes are dispersed in the buffer. Upon the addition of the input strand, the sender cell secretes the signal and Alexa488 is activated, which can be observed as the generation of the green fluorescence. However, the receiver cells do not receive the signal and the communication is impaired. ii) Under blue light, proteinosomes are aggregated and upon the input strand, the sender cells secrete the signal and Alexa488 is activated. The secreted signal is received by the neighboring receiver cell, activating the Cy5 signal, observed as the generation of the fluorescence signal (represented in red color). The scale bars are 50 μm b) Change in the Alexa488 (first step of the DSD, green profile) and Cy5 signals (second step of the DSD, red profile) in the dark and under blue light were measured for individual proteinosomes in confocal microscopy images, from three independent experiments (n>60).

**Conclusion**

Herein, we demonstrated how population dynamics can be easily tuned, while increasing the complexity, by photo-regulating contact-based DNA-based communication between the binary populations of abiotic protocells. The DNA-based strategy offers highly programmable and predictable communication processes within protocellular assemblies. For this, we used highly bio-orthogonal, well-characterized internal molecular circuits that can encode and decode DNA-based messages using toehold mediated strand displacement reactions (DSD). Adhesions between the sender and receiver proteinosomes (semi-permeable protein-polymer based microcapsules), of which each functionalized separately with photoswitchable proteins, iLID and Nano, are controlled through the photo-regulated dimerization of those proteins. The dynamic nature of the photoswitchable proteins provided us with the high spatiotemporal control over the proteinosome assembly. The two-step toehold mediated strand displacement reaction (DSD), can then be triggered on demand, upon blue light illumination. Unlike the many other examples on chemical communication systems between the protocellular models, our system offers high spatiotemporal control over the communication process in bulk solutions, without the need for encapsulation of the protocells in gels, chips or in microfluidic arrays.[7,43,76,204,205] Taken together, the here described model system that combines DNA-based tuneable specific responses with the programmable assembly with high spatial control and environmental adaptivity presents a step towards a better understanding of cell mimicks, and eventual production of model protocells.

## 2.2 Independent blue and red light-triggered narcissistic self-sorting self-assembly of colloidal particles

### Aim

Two different types of colloids self-assemble orthogonally either under blue or red light and reversibly disassemble in the dark. Further, in a mixture these colloids self-sort into separate clusters, a behavior known as narcissistic self-sorting. This concept will allow for the assembly of addressable and adaptable materials into higher-order tissue-like structures.

### Contributions

Protocols for the self-assembly of colloids were designed and established by [redacted] The experiments for the proof-of-principle of the self-assembly and, the kinetics and the reversion of the self-assembly of colloids were also conducted by [redacted] and analyzed by me. Experiments showing the light-induced asocial sorting of the colloids were conducted by me. [redacted] supervised.

### Copyright

The following chapter is based on the publication Senturk et al. *Small,* 2019. 15(25), 1901801. The results are reprinted with permission from Wiley, Small.


### Abstract

The ability of living systems to self-sort different cells into separate assemblies and the ability to independently regulate different structures is one ingredient

that gives rise to their spatiotemporal complexity. Here, this self-sorting behavior is replicated in a synthetic system with two types of colloidal particles; where each particle type independently self-assembles either under blue or red light into distinct clusters, known as narcissistic self-sorting. For this purpose, each particle type was functionalized either with the light-switchable protein VVDHigh or Cph1, which homodimerize under blue and red light, respectively. The response to different wavelengths of light and the high specificity of the protein interactions allows for the independent self-assembly of each particle type with blue or red light and narcissistic self-sorting. Moreover, as both of the photoswitchable protein interactions are reversible in the dark; also, the self-sorting is reversible and dynamic. Overall, the independent blue and red light controlled self-sorting in a synthetic system opens new possibilities to assemble adaptable, smart and advanced materials similar to the complexity observed in tissues.

**Introduction**

Living systems have the remarkable ability to self-assemble and self-sort different micro-sized components, creating higher-order functional structures.[206] For example, during early embryo development different cell types self-sort (also known as sorting-out in the biology community) into discrete domains, which later give rise to different tissue types.[207,208] Likewise, different bacteria species self-sort into separate colonies to avoid competition for resources.[209] Replicating self-sorting with microscopic synthetic objects and controlling different sub-assemblies within the same mixture with orthogonal triggers is an ongoing challenge but would allow the assembly of smart, adaptive

and autonomous advanced materials.[19,38,210] Beyond this, as more and more bottom-up assembled synthetic cell-like compartments, which house different life functions are developed, their assembly into prototissues opens the door to perform tasks as a collective that are incompatible within a single compartment.[2,14,17,85,211,212] Moreover, as observed within a tissue, the spatial organization of different synthetic cells within the assembly determines the communication and material exchange between them.[213,214]

Colloids are great models to establish concepts of self-assembly and self-sorting as units of advanced materials and for the assembly of synthetic cells into prototissues.[19,210] Decorating colloids with DNA, proteins and supramolecular interaction partners allows to program their self-assembly and modify assemblies in response to external triggers such as temperature,[111–113], pH[117,215,216] and light.[109,118,120,217] Among these stimuli, photo-responsive assemblies are especially attractive since light provides non-invasive, tunable and specific control with high spatiotemporal resolution.[19,114,118,203,218] Self-sorting of a mixture of different colloidal particles into distinct assemblies is far more challenging, as it requires multiple and orthogonal interactions to drive the assembly and sorting. Previous examples achieved the pairwise sorting of 4 different colloids, also known as social self-sorting, by implementing two pairs of orthogonal heterodimerization partners on the colloid surface.[107,116] The sorting of 2 different colloids into discrete clusters, also known as narcissistic or asocial self-sorting, has not been realized with colloidal systems but is what is observed during embryo development and colony segregation in bacteria.[207–209] Furthermore, within a self-sorted mixture dynamically switching different

assembly types with orthogonal stimuli would provide a valuable model to create adaptive smart materials.

Here, we describe how in a mixture of two types of colloids each type orthogonally self-assembles either under blue or red light and self-sorts into separate clusters. This example of narcissistic self-sorting mirrors the self-sorting observed with cells in biology and provides independent control over each assembly type using different colors of light. These self-sorted assemblies also reversibly disassemble either in the dark or under far-red light, which introduces adjustable dynamics. Additionally, unlike most other light-triggered systems for the self-assembly of colloids, which require UV-light and organic solvents,[115,116,120,219–222] the systems described here respond to non-invasive low intensity visible light and operate in buffered solutions. The biocompatible conditions for the narcissistic self-sorting pave the way for the assembly of synthetic cells into prototissues with new self-sorting behavior, build-up complexity in synthetic systems analogous to natural ones and coupling with living systems.

**Results and discussion**

To achieve narcissistic self-sorting and control the assembly of each subtype independently requires decorating the colloids with two different homodimerizes that mutually do not interfere with each other and react to orthogonal triggers. For this purpose, we used the photoswitchable proteins, VVDHigh[176,223,224] and Cph1,[167,225] which specifically homodimerize under blue and red light, respectively. The homodimerization of VVDHigh and Cph1 is

reversible in the dark and for Cph1 as well under far-red light. By decorating the surfaces of colloids with either VVDHigh or Cph1, we aim to reversibly control the self-assembly of VVDHigh and Cph1 decorated particles without any crosstalk with blue and red light, respectively (Figure 2.2.1). Moreover, building on the high specificity of the protein interactions, we aim to achieve narcissistic self-sorting upon the co-illumination with blue and red light. To realize this scheme, the photoswitchable proteins VVDHigh and Cph1 were recombinantly expressed and purified as His6-tagged proteins. Subsequently, each protein was immobilized separately on 2 µm $Ni^{2+}$-NTA functionalized polystyrene beads through their His6-tags, yielding two different bead types with ca. 200 proteins/bead.[107]

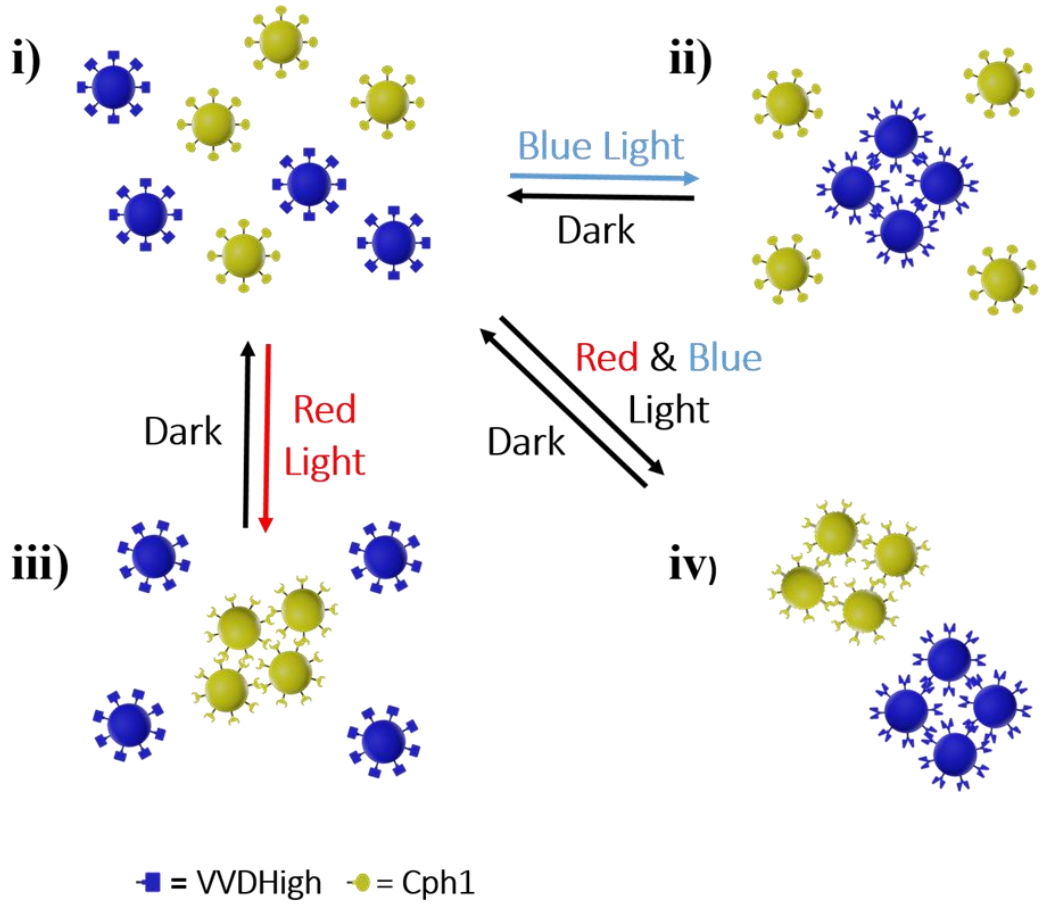


**Figure 2.2.1** Asocial self-sorting self-assembly in a mixture of particles functionalized with VVDHigh (blue particles) and Cph1 (yellow particles). (i) In the dark, particles remain dispersed. (ii) Upon blue light illumination, only VVDHigh functionalized particles self-assemble due to the homodimerization VVDHigh. (iii) Upon red light illumination, only Cph1 functionalized particles self-assemble with each other due to the homodimerization of Cph1. (iv) Upon coillumination with red and blue light, both VVDHigh functionalized and Cph1 functionalized particles self-assemble into distinct clusters. In the dark (or under far-red light for Cph1) the homodimerization of VVDHigh and Cph1 are reversed and aggregates disassemble.

As a first step, we tested if the light-dependent homodimerization of the photoswitchable proteins can be used to drive the self-assembly of these colloids. A key point in independently controlling the self-sorting of two different colloid types was the specific response of each protein to either blue (460 nm) or red (630 nm) light, but not both. When particles functionalized with the blue light responsive protein VVDHigh were incubated under blue or red light for 2 hours, particles formed large aggregates only under blue light, while they remained

dispersed under red light (Figure 2.2.2a). Conversely, particles functionalized with the red light responsive protein Cph1 were also incubated under blue or red light for 2 hours. In this case, the particles self-assembled into large clusters only under red light but not under blue light (Figure 2.2.2b). We support the qualitative observations with the quantification of the aggregation ratio of the particles. Aggregation ratio was defined as the area of clusters (objects with an area > 10 individual beads) divided by the total area of all beads and correlates with the percentage of particles assembled into a cluster. It should be mentioned that this 2D analysis method of aggregation ratios underestimates clustering, especially for larger clusters, as it only relies on the 2D projections of 3D clusters. Nonetheless, it reflects the differences in aggregation under different conditions and provides a high throughput analysis method. Under blue light, the aggregation ratio of VVDHigh functionalized particles was much higher than for Cph1 functionalized ones (Figure 2.2.2c). On the other side, under red light, the reverse was true and the aggregation ratio was higher for Cph1 functionalized particles than for VVDHigh functionalized ones.

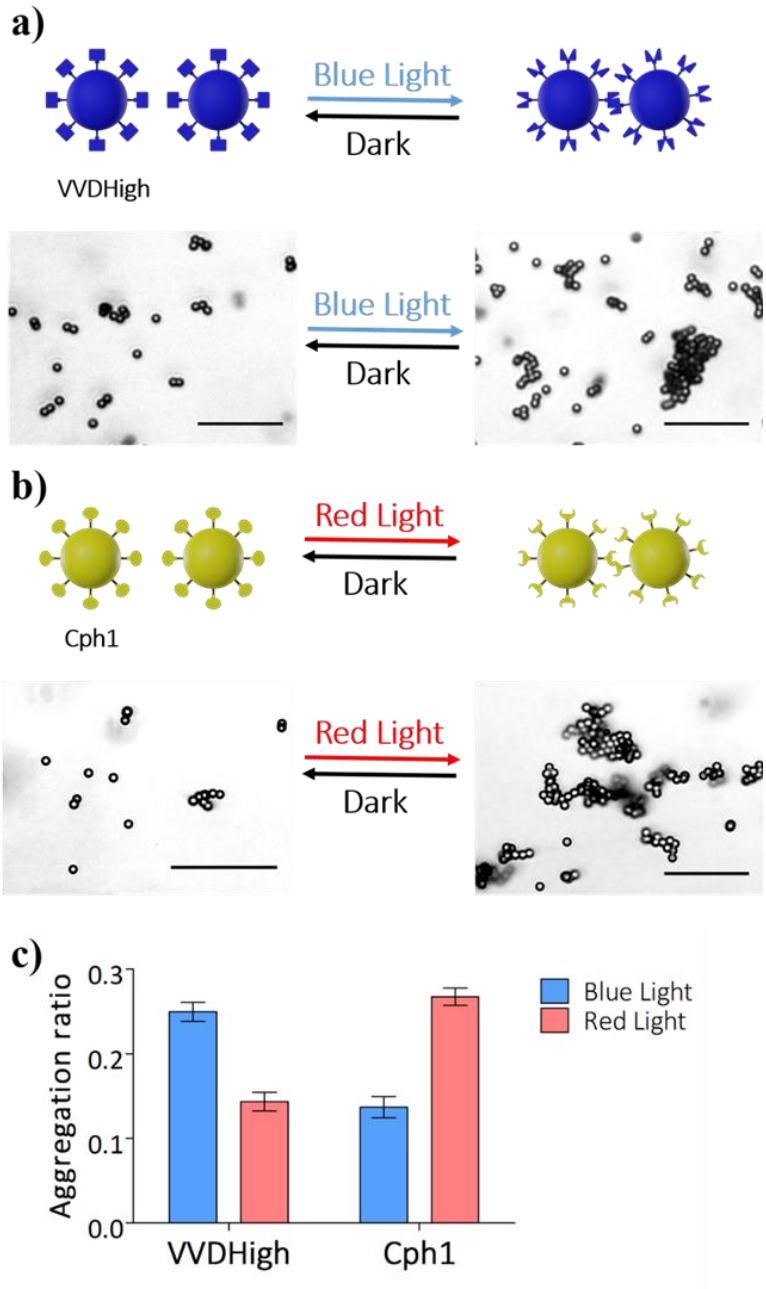


**Figure 2.2.2** Blue and red light triggered self-assembly of beads. Bright field images of 2 µm polystyrene particles functionalized with a) VVDHigh and b) Cph1. The scale bars are 25 µm. Blue light induced homodimerization of VVDHigh, results in the aggregation of VVDHigh functionalized particles upon blue light illumination (+ far-red light) and the reversion of the process in the dark (+ red light). Red light induced homodimerization of the Cph1, results in the assembly of Cph1 functionalized particles into clusters under red light and the reversible disassembly in the dark or under far-red light (+blue light). c) Aggregation ratios of the particles functionalized with VVDHigh and Cph1 proteins. Under blue light, VVDHigh functionalized particles form aggregates and Cph1 functionalized particles do not; while, under red light, VVDHigh functionalized particles do not form aggregates and Cph1 functionalized particles do. . Unpaired t-test was used as the statistical test (p-value<0.05). Error bars are the standard error of the mean from > 45 images.

Additionally, other measures of aggregation including the average cluster sizes and the number of clusters were also higher for VVDHigh beads under blue light and for Cph1 beads under red light than under the light of the other color (Figure 2.2.3).

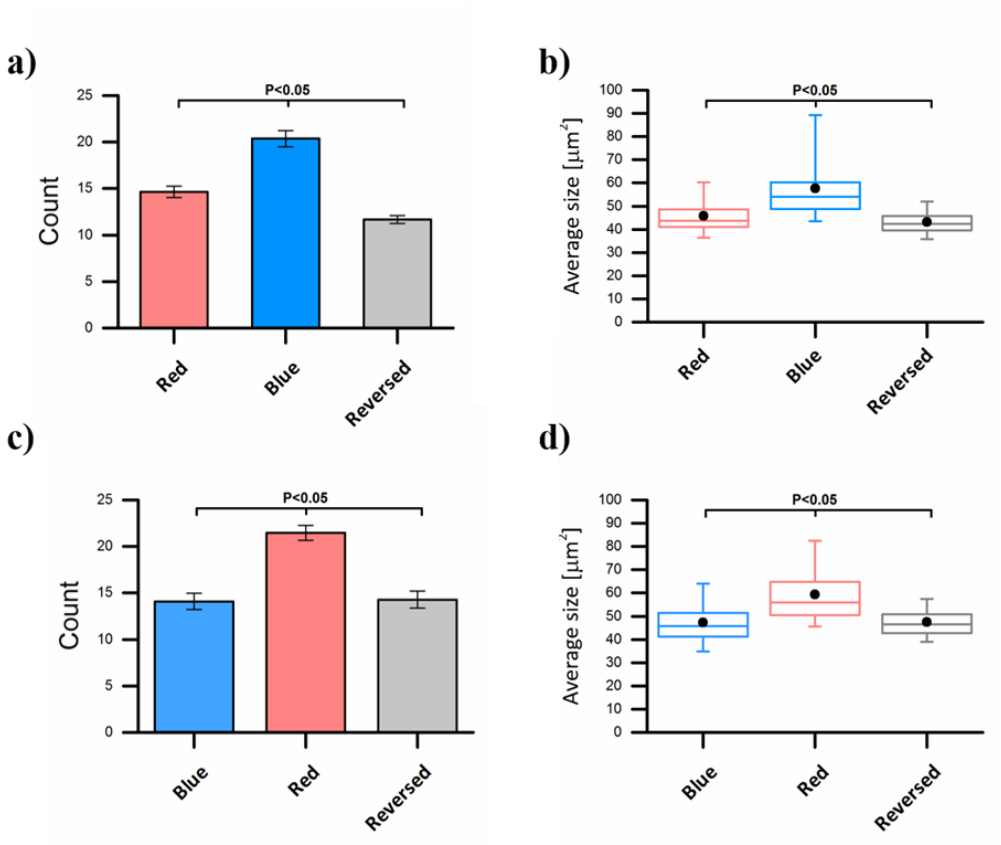


**Figure 2.2.3** a) Cluster number for VVDHigh protein functionalized beads: Light-induced aggregation and reversion and b) Average cluster size. Samples kept under red light are depicted in red; samples kept under blue light (+ far-red light) are depicted in blue; reversed samples kept under red light are depicted in grey. c) Cluster number for Cph1 protein functionalized beads: Light-induced aggregation and reversion. d) Average cluster size. Samples kept in under blue light (+far-red light) are depicted in blue; samples kept under red light are depicted in red; reversed samples kept under far-red light are depicted in grey. One-Way ANOVA test (significance level 0.05) was performed to analyze the statistical difference followed by Dunn-Sidak post hoc test (significance level 0.05). Error bars are the standard error of the mean from > 45 images.

The orthogonal response of VVDHigh and Cph1 to blue and red light as well as their response to far-red light was also observed in the UV-Vis absorption of these proteins, which changes upon photoactivation (Figure 2.2.4). For VVDHigh

the absorbance at ca. 450 nm decreased upon activation with blue light, but was unchanged under red or far-red light. Conversely, for the Cph1 protein the absorbance at ca. 650 nm decreased and a new peak at ca. 720 nm appeared upon photoactivation with red light but the spectra under far-red light and coillumination with blue and far-red light showed a single peak at ca. 650 nm. For aggregation studies, the samples were handled under wavelengths of light that do not activate/interfere with the protein and are specified in the figure legends. (e.g. VVDHigh in the dark was handled under red light, Cph1 with far-red light was handled under blue light.) Overall, based on these findings, we concluded that the photoswitchable proteins VVDHigh and Cph1 respond to orthogonal wavelengths of light and their interactions are highly specific. Therefore, the self- assembly process of each particle type is triggered by either blue or red light and is not affected by the other wavelength of light for both cases. The orthogonality of the assembly process is a crucial advantage over the existing methods and fundamental to address each assembly type within a mixture independently.

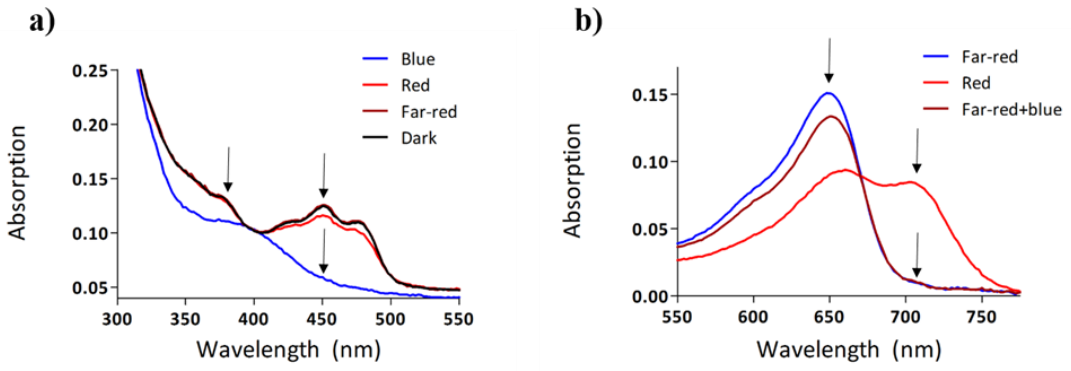


**Figure 2.2.4** UV-visible spectra of photoswitchable proteins. a) VVDHigh protein after blue light illumination (30 s), followed by a 2 h incubation in the dark and subsequent illumination under far-red light (30 min) and red light (30 min). The absorption of VVDHigh at ca 450 nm decreases only under blue light, due to the photoactivation of the

protein but not under red or far-red light. b) Cph1 protein after red light illumination (30 s), followed by far-red light illumination (1 min) and subsequent illumination with far-red and blue light (30 min). The absorption of Cph1 decreases at ca 650 nm and increases at ca 710 nm upon red light illumination due to the photoactivation of the protein but does not absorb at ca. 710 nm under far-red or far-red and blue light illumination. These spectra show the orthogonal photoactivation of VVDHigh and Cph1 under blue and red light, respectively.

Subsequently, we investigated the self-assembly kinetics of each particle type under light that triggers the response. As the particle self-assembly is a multistep process, this kinetic investigation provides insight into rate limiting steps. For this purpose, the aggregation of VVDHigh and Cph1 decorated particles was followed over 2 h under blue and red light, respectively and compared to the assembly in the dark. For both particle types, the aggregation ratio reached a plateau for light-activated samples within 2 h and the aggregation ratios were were much lower for the dark samples (Figure 2.2.5). Specifically, for VVDHigh decorated particles the aggregation ratio increased by ca. 7% in the dark (+ red light) and by ca. 15% under blue light after 2 h. For Cph1 decorated particles, the aggregation ratio increased by ca. 9% in the non-activating conditions and by ca. 21% upon red light illumination. It should also be noted that as soon as particles are decorated with proteins some aggregation was observed even for non-activated samples and from the very beginning (t= 0 min), possibly due to the unspecific protein interactions and the sticky nature of proteins. A comparable contribution of nonspecific interactions independent of photoactivation has also been between beads that were functionalized with other photoswitchable proteins.[107]

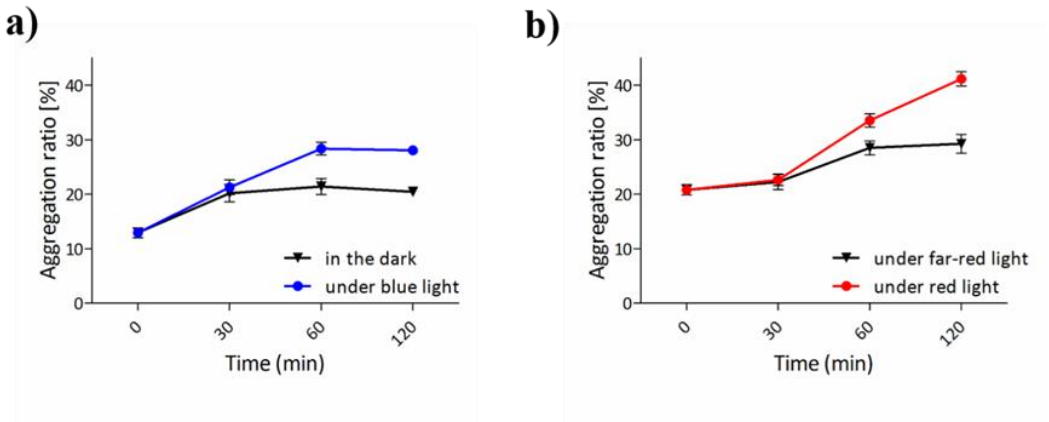


**Figure 2.2.5** Bead aggregation dynamics. a) VVDHigh protein functionalized beads in the dark (+ red light) and under blue light (+ far-red light). b) Cph1 protein functionalized beads under far-red light (+ blue light) and under red light. Error bars are the standard error of the mean from > 30 images.

While at the molecular level, the proteins VVDHigh and Cph1 undergo light-induced conformational changes, which expose the specific homodimerization interphases, within seconds the assembly processes is are much slower. This indicates that the rate-limiting step is two colloidal particles coming into proximity and not the photoswitching of the proteins.

A significant characteristic of assemblies in Nature is their reversibility and adaptability under changing conditions. In the system described here, we aim to capture this important property and we investigated the reversibility of the blue and red light-triggered assemblies. As mentioned, the homodimerization of both proteins is dynamically reversible in the dark and the Cph1 interaction reverses even faster under the far-red light. For such, we repeatedly switched the interactions on protein-decorated particles on and off. For each type of colloid, the particles were altered between 1h under light to trigger aggregation (blue light for VVDHigh and red light for Cph1 coated particles) and then 30 min under far-red light (730 nm) to reverse the aggregation. We observe that VVDHigh and

Cph1 decorated particles assemble into clusters after each blue and red illumination cycle, respectively and disassemble after each far-red illumination cycle (Figure 2.2.6). Moreover, the reversion of Cph1 mediated clusters under far-red light was complete, whereas for the aggregation of VVDHigh functionalized particles were reduced by ≈60%. It should be noted that the reversion of VVDHigh protein interactions takes place in the dark (i.e. in the absence of blue light) and is not triggered by far-red light. Yet, keeping in mind the perspective of combining both the VVDHigh and the Cph1 based assemblies in the same mixture, VVDHigh beads were also placed under far-red light for reversion to ensured that far-red light does not interfere with the disassembly of the VVDHigh mediated clustering. Overall, both the blue light triggered VVDHigh and red light-triggered Cph1 based assemblies can be switched on and off repeatedly and dynamically.

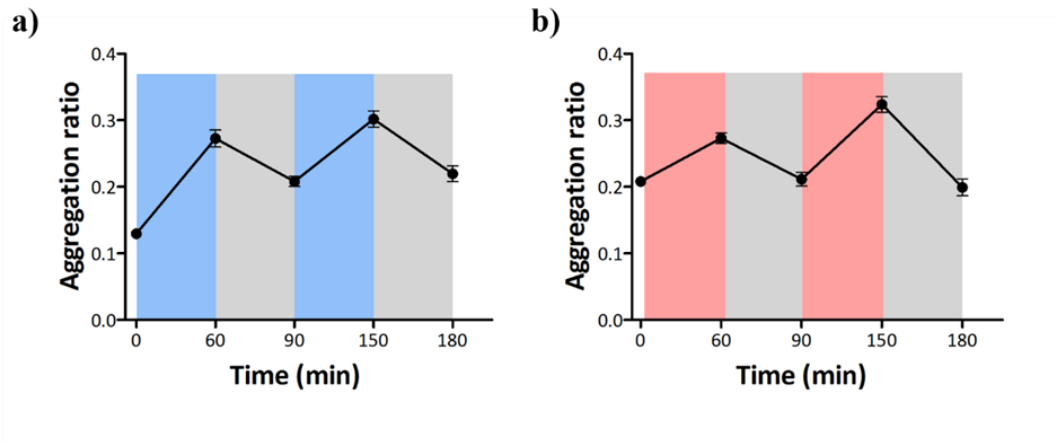


**Figure 2.2.6** Repeated switching on/off of blue and red light triggered self-assembly. a) VVDHigh functionalized particles. Periods, when samples are kept under blue light (+ far-red light) are marked blue; periods in the dark (+ red light) are marked in grey. b) Cph1 functionalized particles. Periods, when samples are kept under red light are marked red; periods under far-red light (+ blue light) are marked in grey. Error bars are standard error from 15 images.

Finally, we sought to achieve narcissistic self-sorting within a mixture of two different colloids such that each colloid type self-sorts into distinct assemblies and to control each of the assembly types independently with different colors of light. Such behavior in synthetic and colloidal systems would be comparable to self-sorting behavior observed in multicellular systems. For this purpose, we combined equal numbers of blue light-responsive particles (VVDHigh functionalized, labeled with a green fluorescent dye) and red light responsive particles (Cph1 functionalized, labeled with a red fluorescent dye). In the dark, both populations of beads were well dispersed (Figure 2.2.7a, i) and their self-assembly could be induced for one type of particle at a time by using two different wavelengths of visible light. Upon blue light illumination, only VVDHigh functionalized particles (green fluorescence) assembled into clusters, whereas Cph1 functionalized particles (red fluorescent) remained dispersed (Figure 2.2.7a, ii). Conversely, upon red light illumination, only Cph1 decorated particles self-assembled, while VVDHigh decorated particles remained dispersed (Figure 2.2.7a, iii). Most interestingly, the co-illumination with blue and red light, resulted in the narcissistic self-sorting of green and red labeled particles into distinct cluster families and no intermixing of green and red particles within the same cluster (Figure 2.2.7a, iv). Furthermore, the self-sorting could be reversed when these colloidal mixtures were placed in the dark (Figure 2.2.7b).

The quantitative evaluation of the self-sorting under different colors of light was in accordance with the fluorescent images acquired before (Figure 2.2.7c). When a mixture of VVDHigh and Cph1 functionalized particles was placed under blue and red light the aggregation ratio increased by 6 % and 13 %, respectively.

When the same sample was co-illuminated with blue and red light the aggregation ratio increased by 19%, which is exactly the sum of the increased observed under blue and red light separately. In view of these quantifications, the aggregation due to blue and red light are highly orthogonal without any interference between different wavelengths and two specific protein interactions. Hence, these interactions allow controlling the asocial self-sorting behavior of two different families of cell-sized compartments by using two different wavelengths.

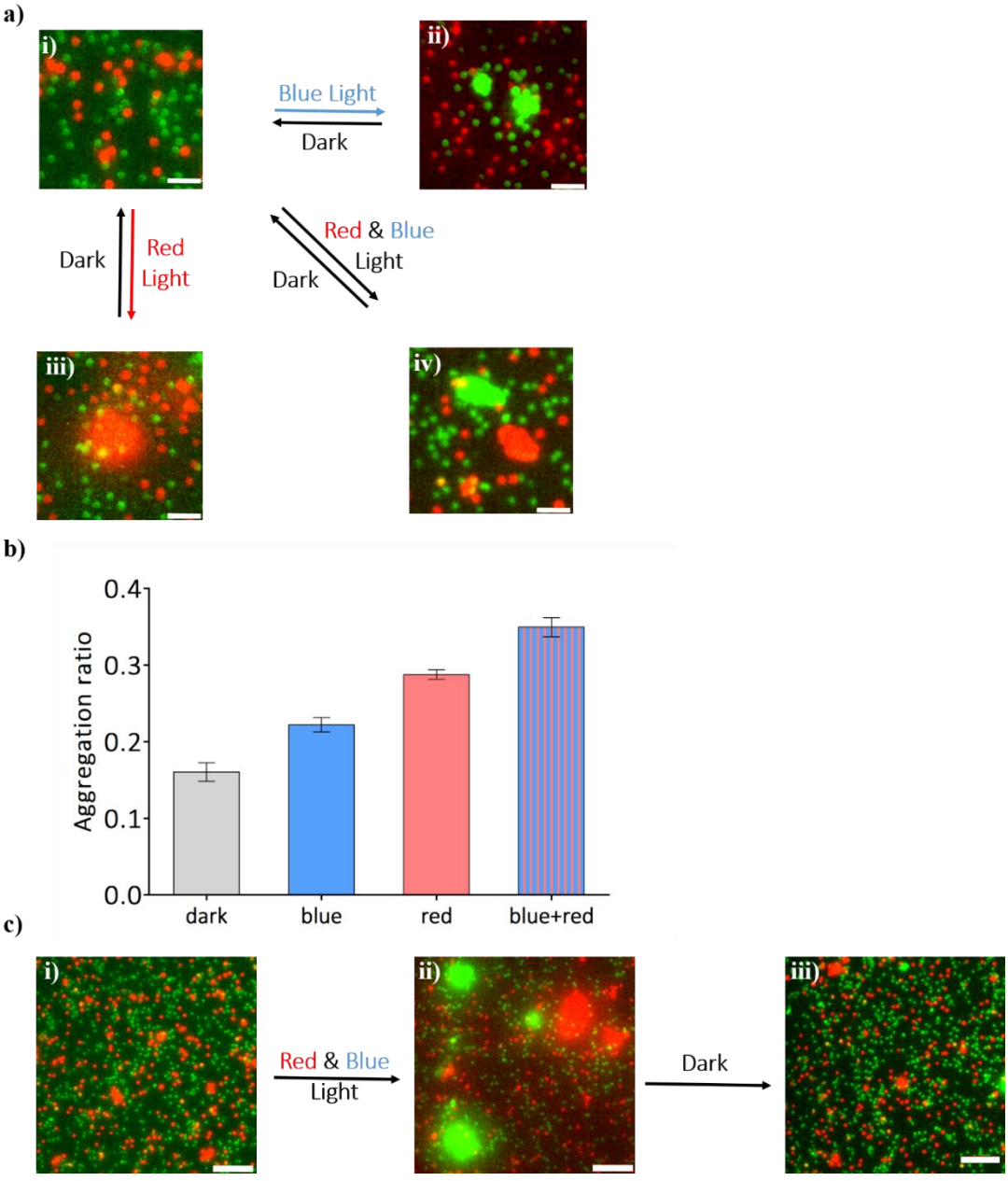


**Figure 2.2.7** Light induced reversible asocial sorting. a) Fluorescence microscopy images of the mixture of VVDHigh functionalized (green) particles and Cph1 functionalized (red) particles . i) in the dark (+ far-red light); ii) under blue light (+ far-red light); iii) under red light, vi) under red and blue light. Scale bars are 10 µm. b) Quantification of the aggregation ratios in the dark (+ far-red light), blue light (+far-red light), red light and coillumination with red and blue light from left to right, respectively. Each sample was illuminated under the respective light for 2 h prior to the analysis. Error bars are standard error from 15 images. c) Fluorescent microscopy images of the reversible asocial sorting of VVDHigh (green fluorescence) and Cph1 (red fluorescence) functionalized particles i) after 2h in the dark (+ far-red light); ii) 2h of blue and red light illumination; iii) after 2h of blue and red light illumination, the sample was kept in the dark (+ far-red light) for 30 min for the reversion. The scale bars are 25 µm.

## Conclusion

In this study, we have demonstrated for the first time narcissistic self-sorting in a colloidal system, where the self-assembly of each colloidal type is independently triggerable with either blue or red light. This behavior is parallel to the narcissistic self-sorting of two cell types in early embryos that will later give rise to different tissues driven by orthogonal molecular interaction modes and different interaction strengths. Moreover, in the synthetic system, the independently addressable assemblies with blue and red light and their reversibility provide exquisite control in space and time. The molecular building blocks that make light controlled the narcissistic self-sorting possible are the two photoswitchable proteins, VVDHigh and Cph1, which homodimerize upon illumination and dissociate in the dark. Here, their orthogonal response to blue and red light as well as the high specificity of these interactions are of a key for this orthogonal narcissistic self-sorting. This concept demonstrated with colloidal particles is transferable to other micro-sized objects such as synthetic cells and functional particles to reproduce narcissistic self-sorting and to organize them into higher-order, adaptable and smart tissue-like structures and materials.

## 2.3 Red/far-red light switchable cargo attachment and release in bacteria-driven microswimmers

### Aim

Photoswitchable bacteriabots bind to their cargo under red light, transport it to the target site and release it on demand upon far-red light illumination. The photo-regulation of bacteriabots with red/far-red light provides noninvasive remote control high spatiotemporal precision and good tissue penetration, which opens new possibilities in engineering biohybrid systems.

### Contributions

The adhesion of bacteria on surfaces and on the particles, the viability of the bacteria and the chemotactic assay were performed and analyzed by me. The cell viability experiment was performed by [redacted] and analyzed by me. [redacted] provided the Ag43-BAP displaying MG1655 *E. coli* strain and helped in the design of experiments and questions about the bacterial motility. [redacted] supervised.

### Copyright

**Abstract**

In bacteria-driven microswimmers, i.e. bacteriabots, artificial cargos are attached to flagellated chemotactic bacteria for active delivery with potential applications in biomedical technology. Controlling when and where bacteria bind and release their cargo is a critical step for bacteriabot fabrication and efficient cargo delivery/deposition at the target site. Towards this goal, we propose photo-regulating the cargo integration and release in bacteriabots using red and far-red light, which are noninvasive stimuli with good tissue penetration and provides high spatiotemporal control. In the bacteriabot design, we functionalized the surfaces of *E. coli* and micro-sized model cargo particles with the proteins PhyB and PIF6, which bind to each other under red light and dissociate from each other under far-red light. Consequently, the engineered bacteria adhered and transported the model cargo under red light and released it on-demand upon far-red light illumination due to the photoswitchable PhyB-PIF6 protein interaction. Overall, we demonstrate the proof-of-concept for red/far-red light switchable bacteriabots, which opens new possibilities in the photo-regulation in biohybrid systems for bioengineering, targeted drug delivery, and lab-on-a-chip devices.

**Introduction**

Biohybrid microrobots combine cells and synthetic cargos (mainly micro- and nanoparticles) for potential applications in biomedical technology including diagnostics and targeted delivery of sensitive materials such as imaging agents, genes and drugs.[88,89,125,226–229] In this context, cells offer unique characteristics that make them well-suited as delivery agents, such as self-propulsion,

environmental sensing abilities, production of biomolecules on-site and taxis.[89,230] Among different microorganisms that have been employed to this end, biohybrid microrobots with bacterial cells, i.e. bacteriabots, are particularly of interest due to their viability in diverse environments, robust motility, efficient conversion of chemical energy into mechanical energy and straightforward genetic engineering.[231–234] Most importantly, their ability to detect and follow gradients of diverse external stimuli (i.e. pH, oxygen, glucose, and temperature) provides a unique opportunity for controlling their taxis behavior.[235,236] This feature has allowed designing bacteria to follow specific cues for active delivery of cargo based on chemotaxis,[102,237,238], phototaxis,[239] pH-taxis,[240] thermotaxis,[241] and magnetotaxis.[229,231]

The efficient integration of the cargo onto the bacteria and the controlled release of the cargo from the bacteria are critical factors for successful application of bacteriabots. To attach bacteria to the surface of cargo, different types of unspecific and specific interactions (electrostatic interactions, hydrophobic interactions, covalent attachment, streptavidin-biotin, and antibody-antigen) have been used.[101,102,125–127] Yet, the controlled on-site release and active delivery of the cargo, which improve the bioavailability of the administration have only been demonstrated in a few studies. In these examples, the cargo has been released in response to external stimuli such as chemicals, pH and UV-light.[128–130] Controlling bacterial attachment to and release from a synthetic surface with visible light instead of UV light would be especially attractive since it would offer better biocompatibility while preserving the bioorthogonal and high spatiotemporal control.[138,242] In particular, for *in vivo* applications, photo-

regulation of bacteria-cargo interactions with red/near-infrared light (650-1350 nm) would be desirable due to good tissue penetration.

Here, we report a new approach to photo-regulate the interaction between bacteria and their cargo in bacteriabots using red/far-red light, which would offer good biocompatibility and overcome the above-mentioned limitations. In the design, we envisioned that the bacteria attach to the cargo upon red light illumination, transport it to the target site and release it on demand upon far-red light illumination. To photo-regulate the cargo integration in bacteriabots, we employed the photoswitchable protein phytochrome B (PhyB, amino acids 1-651) from *Arabidopsis thaliana*, which under red light (660 nm) binds to the protein phytochrome interaction factor 6 (PIF6, amino acids 1-100).[138,243] The red light-triggered binding of PhyB/PIF6 is reversible under far-red light (740 nm) within seconds (Figure 2.3.1).[243] We thus engineered *Escherichia coli (E. coli)* bacteria to display PhyB on their surface, such that the bacteria could bind to PIF6 decorated cargo under red light illumination and release it under far-red light illumination. This design offers reversible and dynamic control over cargo attachment and release in bacteriabots and improves the spatiotemporal control of biohybrid systems with future possible applications in engineering, targeted drug delivery, and lab-on-a-chip devices.

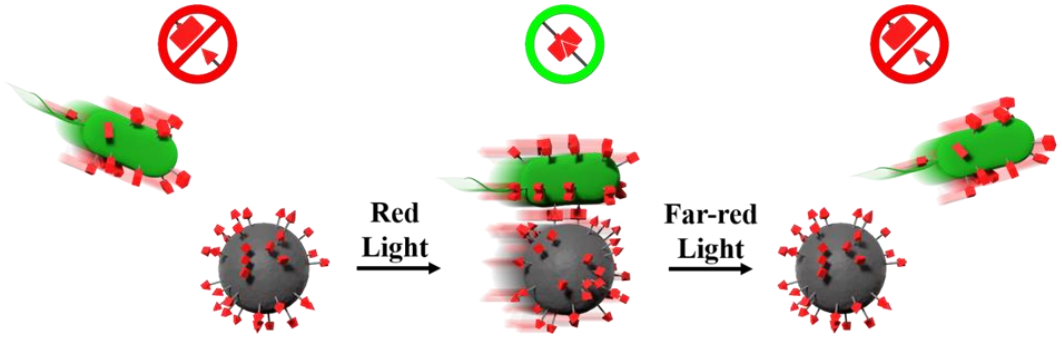


**Figure 2.3.1** Red/far-red light controlled bacteriabots. Under red light, bacteria displaying the photoswitchable protein PhyB on their surface bind to cargo particles functionalized with PIF6, due to the red light-dependent interaction of PhyB and PIF6. Upon far-red light illumination, the PhyB-PIF6 interaction is reversed and the cargo is released from the bacteriabot on demand.

## Results and discussion

To realize the envisioned design, we used the most commonly studied model organism for bacteriabots, *E. coli*, due to its well-characterized taxis abilities, easy genetic manipulation, established cell surface display systems and wide use in bioengineering for therapeutic applications. To display the red light-switchable protein PhyB on the surface of *E. coli*, we utilized a biotinylated Ag43 (Ag43-biotin) protein expressed on the cell surface[30], which allowed linking recombinantly expressed and purified biotinylated PhyB through a streptavidin linker to the *E. coli* surface (Figure 2.3.2). We chose this strategy for the surface functionalization of the bacteria with PhyB since the direct expression and display of large proteins such as PhyB (651 aa) on bacteria surfaces is challenging. On the other side, the complementary interaction partner PIF6 was linked to $Ni^{2+}$-NTA functionalized materials as a PIF6-GFP-His6-tag, relying on the specific $Ni^{2+}$-NTA binding to His-tags.

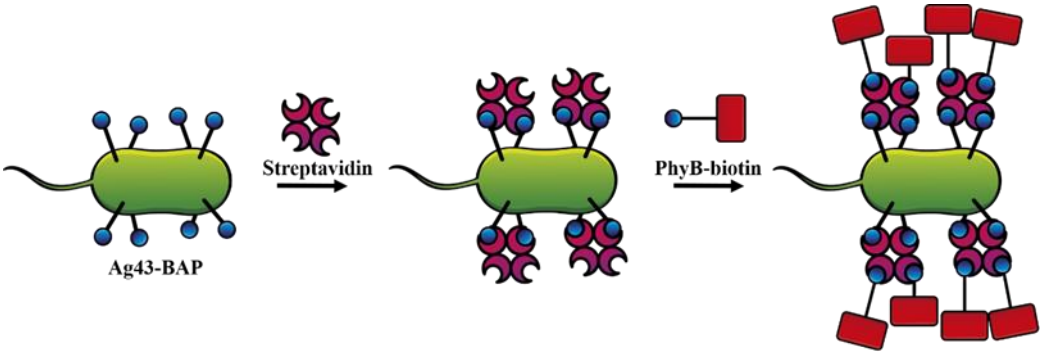


**Figure 2.3.2** Surface chemistry of PhyB functionalized E. coli. Bacteria transformed with Ag43-BAP display biotin at their surfaces and were first incubated with streptavidin and then with biotinylated PhyB (PhyB-biotin).

As the first step of a red/far-red light controlled bacteriabot fabrication, we tested whether the photoswitchable PhyB/PIF6 interaction could be used to control the adhesion of bacteria to synthetic surfaces (Figure 2.3.3). For this purpose, we initially immobilized PIF6 onto glass substrates with a poly(ethylene glycol) (PEG) coating and $Ni^{2+}$-NTA terminal groups. This PEG coating provided an inert background by preventing unspecific binding of proteins and bacteria and allowed for the specific immobilization of His-tagged PIF6 onto the glass substrate. Then, PhyB functionalized bacteria, which were fluorescently labeled for visualization, were incubated on these surface for 1 h either under far-red or red light (Figure 2.3.3, i-ii). These PhyB displaying bacteria were only able to adhere to the PIF6 functionalized substrates under red light illumination, while no bacteria were observed on the substrate under far-red light. Also, the quantification of the bacteria that adhered to the substrate showed that the bacteria adhered significantly under red light and that the number of bacteria under far-red light and substrates that were not functionalized with PIF6 was insignificant (Figure 2.3.3c). Taken together these results show that the PhyB immobilized onto the bacteria is accessible and active

and that the bacteria adhesion is due to the highly specific red light-dependent PhyB-PIF6 binding.

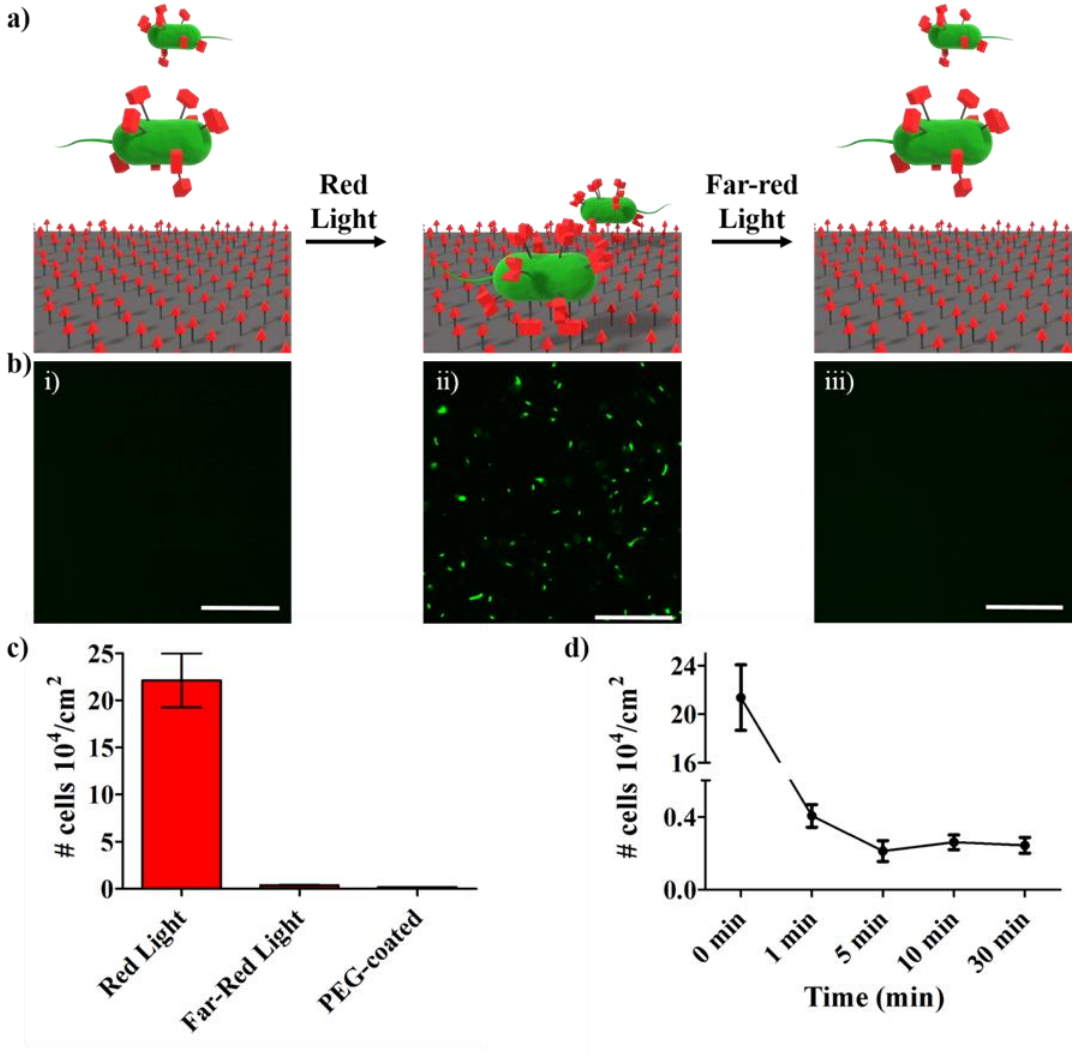


**Figure 2.3.3** a) PhyB functionalized E. coli adhere on PIF6 functionalized substrates under red light and detach from the substrate under far-red light, due to the red light-dependent PhyB-PIF6 interaction and its reversion in far-red light. b) Fluorescence microscopy images of GFP expressing and PhyB functionalized E. coli functionalized on PIF6 functionalized PEG-coated glass substrates. i) 1 h far-red light. Bacteria did not adhere to the substrate. ii) 1 h red light. Bacteria adhere to the substrate. iii) 1 h red light followed by 30 min far-red light. The adhered bacteria detach from the substrate upon far-red light illumination. Scale bars are 50 µm. c) Quantification of PhyB functionalized bacteria on PIF6 functionalized substrates under red light, under far-red light, and on PEG-coated substrates without PIF6. Error bars are the standard error from 15 images. d) Detachment kinetics under far-red light of PhyB functionalized bacteria from PIF6 functionalized substrates after 1 h red light illumination. Error bars are the standard error from 15 images of three biological replicates.

Since the triggered reversion of the bacteria adhesions is the key point in releasing the cargo from bacteriabots, we investigated if and how fast the PhyB-PIF6 mediated interactions between bacteria and synthetic surfaces could be switched off under far-red light. When PhyB functionalized bacteria, which had adhered onto PIF6 functionalized glass substrates described above for 1 h under red light, were placed under far-red light for 30 min all bacteria detached from the substrate (Figure 2.3.3b,iii). The time-dependent analysis of the detachment was showed that even after 1 min of far-red illumination 98 % of the bacteria detached (Figure 2.3.3d). To verify that the observed differences in bacterial attachment were not a result of phototoxicity and to demonstrate the high biocompatibility of red/far-red light, we checked the viability of the bacteria and mammalian cells (MDA-MB-231 cells) under different light illumination (Figure 2.3.4). This analysis showed that after 1 h illumination with different light sources used in this study there was no loss in viability compared to untreated cells. Overall, this demonstrates that the red/far-red light switchable PhyB/PIF6 interactions can be used to reversibly and noninvasively photocontrol the attachment and detachment of PhyB functionalized *E. coli* to PIF6 functionalized materials.

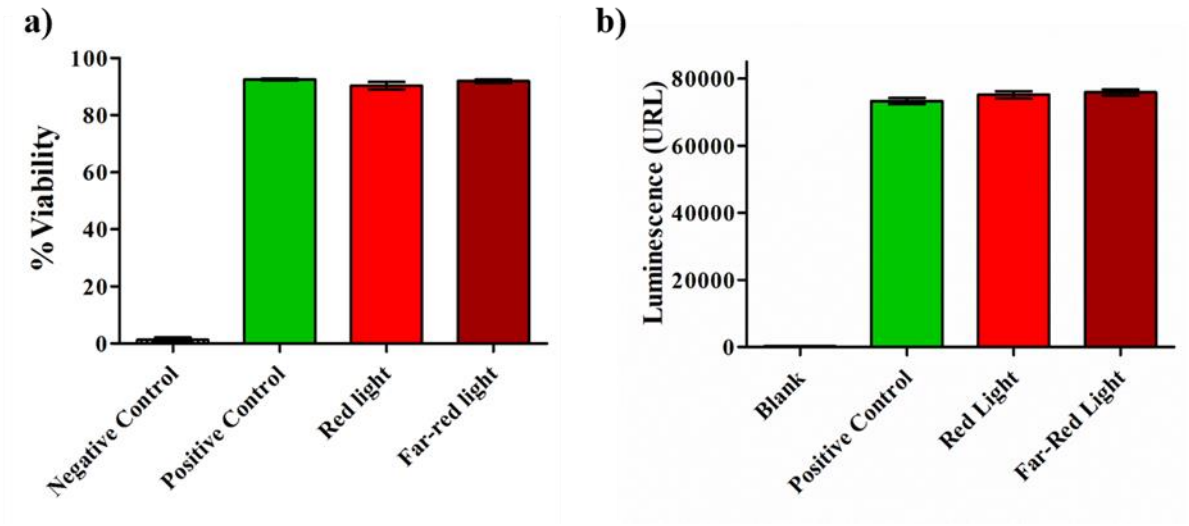


**Figure 2.3.4** Cell viability under different illumination conditions. a) E. coli were illuminated with red light or far-red light for 1 hour. Bacteria treated with isopropyl alcohol were used as negative control and untreated bacteria were used as positive control. The experiment was performed in three biological replicates with three technical replicates each. b) MDA-MB-231 cells were illuminated with red light or far-red light for 1 h. Cells that were kept in the dark used as positive control and the bioluminescence reagent without any cells used as the blank control. The experiment was performed in three biological replicates with three technical replicates each.

Once it was established that the binding of PhyB functionalized bacteria to PIF6 functionalized materials could be reversibly turned on and off using red and far-red light, we sought to control bacteria-cargo interactions using the PhyB-PIF6 binding. This would allow generating bacteriabots under red light using PhyB functionalized bacteria and PIF6 functionalized cargos and release the cargo at the desired location upon far-red light illumination (Figure 2.3.1). As a model for synthetic cargo, we used 2 µm $Ni^{2+}$-NTA functionalized magnetic polystyrene (PS) particles, which were functionalized with His6-tagged PIF6. In initial tests, *E. coli*, which were functionalized with PhyB and expressing GFP for detection, were incubated with these PIF6 functionalized magnetic particles under different illumination conditions. Subsequently, the bacteria interacting with the magnetic particles were separated using a magnet and quantified (Figure 2.3.5a). After 10 min of red light and far-red light illumination, the number of bacteria

that adhered on the particles under red light was substantially higher than under far-red light. Moreover, under red light illumination, these PhyB displaying bacteria (labeled with GFP) and fluorescently labeled PIF6 functionalized 2 μm PS particles form direct contacts and assemble into bacteriabots as observed with fluorescence microscopy (Figure 2.3.5b).To demonstrate the reversibility of this attachment, samples incubated for 10 min under red light illumination, were subsequently either illuminated with far-red light or kept in the dark for 10 min. The number of bacteria adhering on the particles after the far-red light treatment was comparable to the sample which was only illuminated with far-red light. On the other hand, in the sample that was kept in the dark after red light illumination, the number of bacteria that adhere to the particles was comparable to the red light illuminated sample and showed no reversion of the adhesions. These results show that the formation of bacteriabots could be triggered with red light and the cargo remains stably attached until illuminated with far-red light using PhyB-PIF6 as chemical building blocks between the bacteria and the cargo.

Binding kinetics of bacteria to the cargo is an important aspect for bacteriabot fabrication and understanding the temporal modulation the PhyB-PIF6 interaction offers. At this point, we also investigated the contribution of unspecific interactions in the formation of bacteriabots. Therefore, we incubated bacteria with and without PhyB functionalization with PIF6 functionalized PS particles for up to 2 h under red light illumination (Figure 2.3.5c).Within 10 min of red light illumination, attachment of PhyB functionalized bacteria was 2 fold higher compared to the non-functionalized bacteria (blank). As the incubation

time under red light increased, the number of PhyB functionalized bacteria that attach to the PIF6 beads increased rapidly and reached a plateau around 60 min. On the contrary, the unspecific binding between particles and bacteria did not increase significantly with time and was similar to the attachment of PhyB displaying bacteria under far-red light after 2 h incubation. Although the PhyB-PIF6 interaction is highly specific as also demonstrated with the PEG-coated substrates, unspecific interactions between *E.coli* and the PS particles contribute to the binding of bacteria to the model cargo. Therefore, the contribution of unspecific interactions needs to be considered in the design of photoswitchable bacteriabots.

As a complementary process, the reversion of the bacteria particle interaction was studied to gain insight into how quick cargo can be released from the bacteriabots. For this purpose, bacteriabots were first assembled under red light for 10 min before illuminating them with far-red light or placing them in the dark. We observed that within 5 min of far-red light illumination most of the bacteria dissociate from the particles and the number of bacteria attached to the particles was comparable to the unfunctionalized control bacteria (Figure 2.3.5d).On the other hand, the bacteriabots remained intact when placed in the dark over 30 min. The lack of reversibility in the dark is actually an advantage as it shows that one the bacteriabots are assembled under red light, illumination can be stopped and the bacteriabots will remain intact until illuminated with far-red light. It should be noted that if PhyB functionalized bacteria and PIF6 functionalized particles were incubated under red light for 30 min rather than 10 min, the attached cargo could not be released even after 30 min far-red light

illumination. This lack of reversibility after longer bacteria-bead contact could be due to secondary nonspecific interactions that form when bacteria are in close proximity to the PS particles. In fact, the biding of PhyB and PIF6 reverses within seconds at the molecular level. This fast reversion was also mirrored in the complete detachment of bacteria from PIF6 functionalized PEG-coated substrates within one minute. To achieve faster cargo drop in future bacteriabots, the cargo should be coated with PEG like molecules that prevent undesired secondary interactions. In this sense, the quick and specific reversion of the PhyB-PIF6 interactions with far-red light is critical for the cargo release.

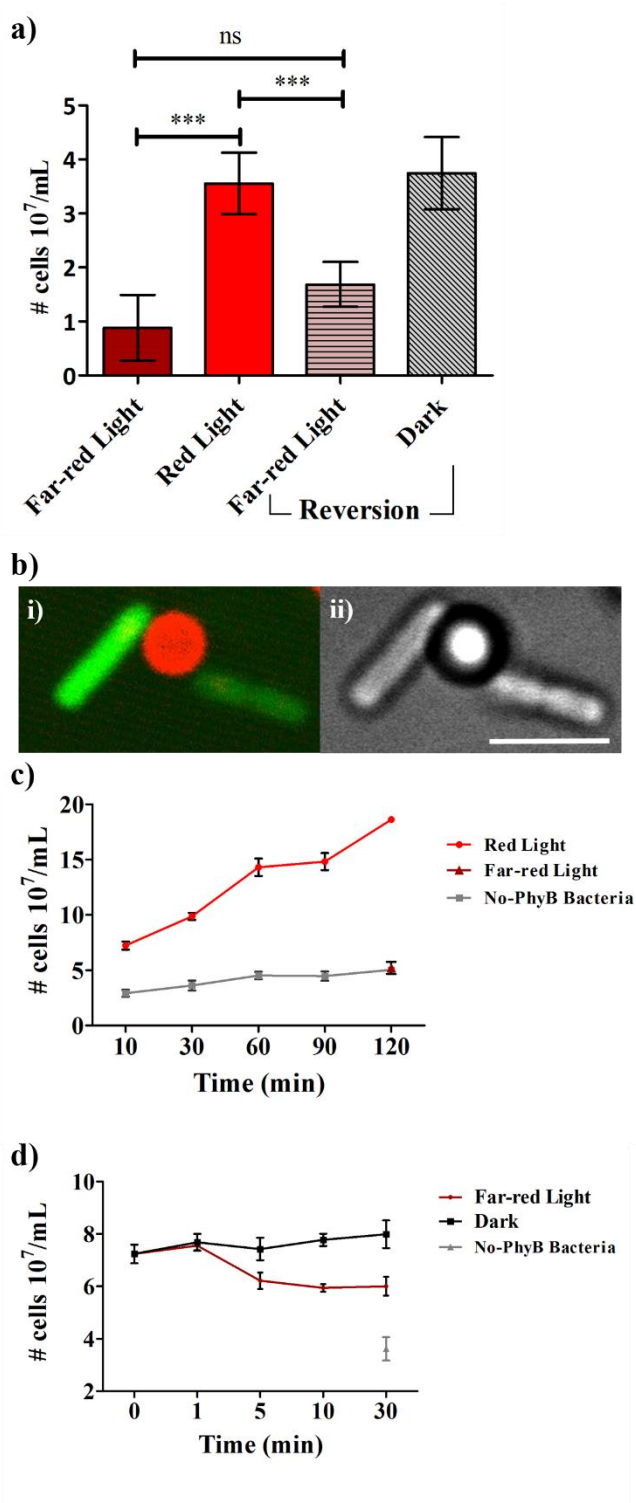


**Figure 2.3.5** a) Number of PhyB functionalized E. coli that adhered to PIF6 functionalized 2 µm magnetic PS particles upon 10 min far-red or red light illumination and the reversion under 10 min far-red light or in the dark after 10 min red light illumination. Bacteria adhere to the particles only under red light and not under far-red light. The red light-dependent interaction is reversible under far-red light but not in the dark. The numbers were background corrected for unspecific binding between bacteria and unfunctionalized PS particles. Error bars show standard error of the mean from three biological replicates each done in three technical replicates; paired t-test was used

for statistical analysis, $p<0.001$. b) i) Confocal fluorescence microscopy image of the GFP labeled PhyB functionalized E. coli (shown in green) interacting with a PIF6 functionalized and far-red dye-labeled 2 μm PS particle (shown in red). ii) Optical microscopy image in bright field. Scale bar is 5 μm. c) Attachment kinetics of PhyB functionalized and unfunctionalized E. coli to PIF6 functionalized PS particles under red light. d) Reversion kinetics of PhyB functionalized E. coli and PIF6 functionalized PS particles under far-red light and in the dark after 10 min red light illumination. Error bars show standard error of the mean from three biological replicates each done in three technical replicates.

As a final step, we demonstrated that the red light-triggered assembly of the bacteriabots and far-red light-triggered detachments of the cargo from the bacteria can be used to control cargo transport in bacteriabots. For this purpose, we evaluated the movement of cargo particles (fluorescently labeled PIF6 functionalized 2 μm PS particles) transported by bacteriabots moving in a chemotactic gradient (Figure 2.3.6 and 2.3.7). This analysis showed that particles transported by bacteriabots assembled for 10 min under red light had a mean speed of 8.44 μm/s. On the other hand, when the cargo was released from these bacteriabots by illuminating them for 10 min with far-red light, most particles remained still and the mean speed dropped to 4.22 μm/s. Likewise, for the tracked particles the accumulated distance and the Euclidean distance in the chemotactic gradient, showing directional movement, dropped after far-red light illumination (Figure 2.3.7). Furthermore, the mean speed of unfunctionalized PS particles, used as a negative control to account for random movement, was only 3.29 μm/s.

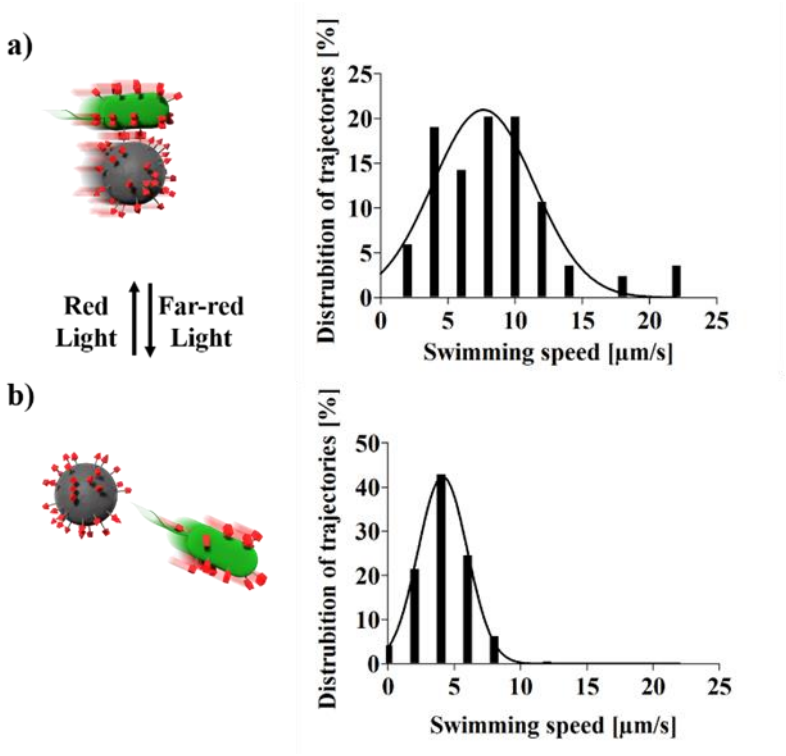


**Figure 2.3.6** Particle transport by bacteriabots. PhyB functionalized E. coli transported PIF6 functionalized and far-red dye-labeled 2 µm PS particles, which were tracked under the fluorescence microscope. a) After 10 min of red light illumination. The mean PS particle speed was 8.44 µm/s, showing attachment and transport by the bacteria. b) After 10 min red light followed by 10 min far-red light illumination. The mean PS particle speed reduced to 4.22 µm/s, as a result of the cargo release. Data were obtained from at least 80 tracks per experiment.

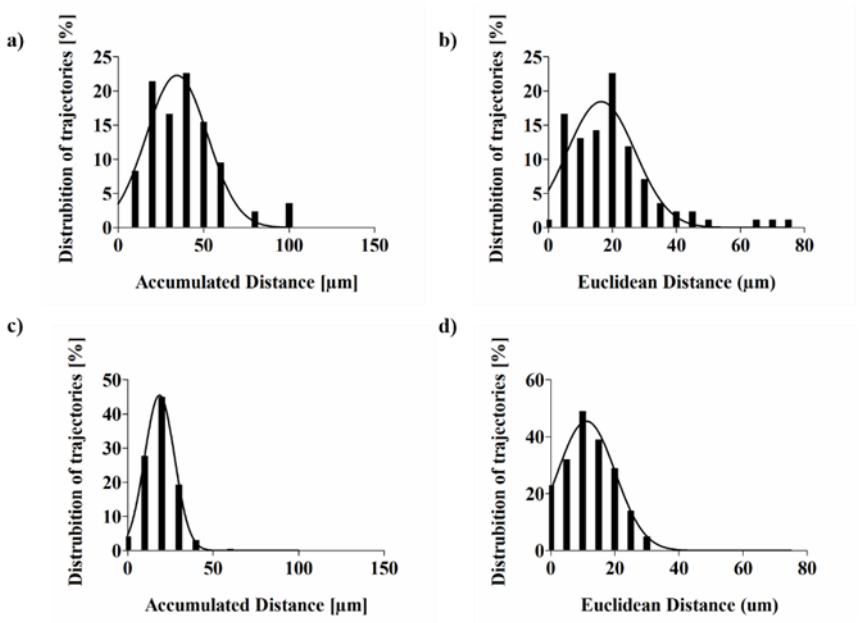


**Figure 2.3.7** Particle transport by bacteriabots. PhyB functionalized E. coli transported PIF6 functionalized and labeled with a far-red dye 2 µm PS particles, which were tracked under the fluorescence microscope a-b) After 10 min red light illumination. c-d) After 10 min red light followed by 10 min far-red light illumination. For the PS particles, the accumulated distance reduced from 38.99 µm after red light illumination to 19.01 µm after far-red light illumination. Similarly, the Euclidean distance reduced from 20.34 µm after red light illumination to 12.17 µm after far-red light illumination.

## Conclusion

In summary, we developed a red/far-red light switchable specific bacterial adhesions to synthetic materials based on the photoswitchable PhyB-PIF6 interactions. These photoswitchable interactions were employed to photo-regulate the integration of cargo into bacteriabot using benign visible light and providing unprecedented control over the cargo-bacteria interphase in biohybrid microrobots. The assembly of the bacteriabot under red light, the stability of the once formed bacteriabot in the dark and the fast cargo release within 10 min under far-red light at the desired location are ideal for later applications *in vivo* due to the good tissue penetration of red/far-red light. As a proof-of-concept, our results demonstrate the possibility of a dynamic and effective cargo integration and release in bacteriabots with red and far-red light,

respectively. This study paves the way towards improving the control of biohybrid systems in bioengineering, targeted drug delivery, and lab-on-a-chip devices.

# Chapter 3: Summary and Outlook

Cells have the unprecedented ability to sense, respond, and adapt to spatial and temporal changes in their environment. Similarly, the exchange of diffusible signals between the cells is the fundament of the collective and multicellular behavior. These chemical signaling cues regulate many critical cellular processes, such as cell differentiation, chemotaxis, and cancer development. Understanding the underlying mechanisms as well as the physicochemical determinants that play the role in intercellular communication is challenging due to the inherent complexity of the living systems. Therefore, the development of cell mimics, which can be precisely controlled in space and time is highly desirable. Having high spatiotemporal control over the interactions between artificial cell-like compartments is critical for their self-assembly in which separate compartments work collectively to perform complex functions. Optogenetic proteins such as iLID/Nano, PhyB/PIF6, VVD and Cph1 offer such control with high precision using biocompatible visible light as the external stimuli.

This thesis demonstrates the usage of optogenetic proteins as tools to first to achieve DNA-based communication between cell-mimics, then the self-sorting behavior of colloidal cell-mimics which is a critical step for the embryonic differentiation, and finally, to design a bacterial biohybrid bacteriabot for the drug-delivery applications.

In the first part of the thesis, the DNA-based communication cascade between the binary populations of abiotic protocells was controlled by using blue light.

Each of the heterodimerizing optogenetic proteins iLID/Nano was immobilized separately on the surfaces of the two different populations of the protein-polymer microcapsules (proteinosomes). As the communication architecture, DNA-based two-step toehold mediated strand displacement reaction (DSD) were used. Upon blue light illumination, due to the interaction of the proteins, the adhesion of the separate populations protein-coated proteinosomes to each other was triggered. The proteinosomes carried DNA-complexes required for the DSD reactions. The communication cascade relies on the transfer of the diffusible ssDNA-molecules as the signals between the binary proteinosomes populations, where the secretion of the signal is highly localized. Therefore, when proteinosomes of two populations were in the immediate vicinity as a result of their blue-light triggered aggregation; the secreted ssDNA signal from the sender cell reached the receiver cell in high concentration and the DSD reactions took place, which was followed by the emergence of the fluorescent signal. When the proteinosomes were kept in the dark, the ssDNA signal diffused away in the solution, the local concentration dropped, impairing the detection by the receiver cell. As a result, communication cascade did not take place. The study demonstrates how population dynamics can be easily tuned, by photo-regulating contact-based DNA-based communication between the binary populations of abiotic protocells. The DNA-based strategy offers highly programmable and predictable communication processes within protocellular assemblies. The dynamic nature of the photoswitchable proteins provided us with the high spatiotemporal control over the proteinosome assembly. The existing strategies for controlling the spatial organization of the protocells for complex artificial

communication architectures rely on the encapsulation of the protocells in gels, chips or microfluidic arrays.[7,43,76,204,205] The here described system is the first light-responsive example of a spatially organized DNA-based communication cascade accomplished in the bulk solution.

In the future, NTA-co-PNIPAam based proteinosomes can be combined with a variety of orthogonal optogenetic proteins to control the assemblies of multiple (i.e., ternary, quaternary) populations of proteinosomes to construct higher-order configurations with DNA-circuits exhibiting a variety of complex functions such as oscillations,[76,77] digital logic circuits[74,78] and Boolean neural networks such as AND, NOR, and XOR.[79] Implementation of an additional external stimulus such as magnetism, and different light-responsive molecules would improve the specificity of the response. The platform offers the functional combination of cell-like compartments housing these complex functions, into prototissues, so that they can perform tasks as a collective in multicellular populations.

In the second part of this thesis, narcissistic self-sorting of two different types of colloids where the self-assembly orthogonally triggered with either under blue or red light. The two photoswitchable proteins, VVDHigh and Cph1, which homodimerize upon illumination and dissociate in the dark, made the light controlled narcissistic self-sorting possible. Each population of the colloids were functionalized with either blue light-responsive protein VVD or with red light-responsive protein Cph1. Upon light illumination, dimerization of the proteins resulted in the adhesion of the colloids carrying the same type of protein on the surface. In this study, the orthogonal response of proteins to blue and red light

as well as the high specificity of the protein interactions are the key for this orthogonal narcissistic self-sorting.

The behavior reported here is parallel to the narcissistic self-sorting of two cell types in early embryos that will later give rise to different tissues driven by orthogonal molecular interaction modes and different interaction strengths. Independently addressable reversible assemblies of the cell-mimics with blue and red light provide precise control in space and time. In the future, this platform can be transferred to other micro-sized objects such as synthetic cells (e.g. proteinosomes) to reproduce narcissistic self-sorting and to organize them into higher-order, adaptable tissue-like structures. Adapting this platform into communication cascades has the potential to develop programmable synthetic multicellular architectures of multiple combinations of cell-like compartments capable of carrying out communication protocols for collective decision making.

In the third part of this thesis, red/far-red light switchable bacteriabots were developed. In this design, bacteriabots bind to their cargo under red light, transport it to the target site and release it on demand upon far-red light illumination. The here described red/far-red light switchable specific bacterial adhesions to synthetic materials was a result of the photoswitchable PhyB-PIF6 interactions. The adhesion of PhyB functionalized bacteria to the PIF6 coated surfaces and to a micro-meter sized model cargo was triggered with red light and reversed far-red light illumination. Moreover, the red light-triggered adhesion did not reverse in the dark.

The good tissue penetration of red/far-red light and the stability of the bacterial adhesion in the dark is ideal for later applications *in vivo*. This study demonstrates a platform for dynamic and effective cargo integration and release in bacteriabot designs. Having such control over the bacteriabots can potentially improve the biohybrid systems in bioengineering. Further, the demonstrated bacteriabots can be used for active delivery of the sensitive signaling molecules between synthetic cells for the intercellular communication over longer distances or under harsh conditions. Combining molecular communication platforms on-chip designs with the photoswitchable bacteriabots has the potential to achieve higher-order communication networks.

Bacteria can autonomously communicate and carry out specific tasks once administered in the body. In the future, instead of the model cargo, bacteria can be combined with liposomes or functional cargo encapsulating drug molecules to test the efficiency of the delivery. The introduction of the magnetic steering of the bacteriabots would enable the steering of the bacteria once it is administered in the body for targeted drug delivery applications.

Here, the utilization of the optogenetic proteins, i.e., iLID/Nano, Cph1, VVD, PhyB/PIF6 for manipulating the assembly of synthetic cells as versatile tools in molecular communication was demonstrated. The proteins lead to reversible light-induced adhesions between various synthetic and minimal cells with high spatial and temporal control under physiological conditions. The combinations of the optogenetic proteins in synthetic cellular systems offer the possibility to achieve collective and higher-order behavior for the creation of cell-like functions.

# Chapter 4: Materials and Methods

## 4.1 Materials

### 4.1.1 Equipment, software, chemicals and consumables

Equipment, software, chemicals, and consumables used in this thesis are listed in Table 1, 2, 3 and 4 respectively.

**Table 1: List of equipment used in this thesis**

| Equipment | Supplier |
|---|---|
| Cell Density Meter CO8000 | Biochrom Ltd., UK |
| Avanti J-26S XP (rotors: JA-10 and JA-25.50) | Beckman Coulter Inc., USA |
| VWR Micro Star 17 | VWR, Germany |
| Rotixa 50 RS | Andreas Hettich, Germany |
| Electroporator (MicroPulser™) | Bio-Rad Laboratories,Germany |
| Gel electrophoresis | Bio-Rad Laboratories,Germany |
| HPLC-ÄKTA Explorer 10 | GE Healthcare, Germany |
| Incubators INCU-Line ® ILS6 and Innova ® 44 | VWR Germany, New Brunswick Scientific, USA |
| Bulbs (blue, red, far-red), 15 Watts | Osram GmbH, Germany |
| Blue light panel Albrillo LL-GL003 | Albrillo |
| Red light panel Albrillo LL-GL002 | Albrillo |
| Magnetic stirrer Heidolph MR 3001 K | Sigma Aldrich, Germany |
| Milli-Q® water purification system | Merck KGaA, Germany |
| NanoDrop 8-sample Spectrophotometer ND-8000 | Peqlab Biotechnologie, Germany |
| Orbital shaker | Carl Roth, Germany |
| pH-meter Hanna HI 208 | Sigma Aldrich, Germany |
| Pipetteboy accu-jet® pro | Brand, Germany |
| Plate Reader (TECAN SPARK) | Tecan, Switzerland |
| Affinity columns HisTrap™ HP and 5 mL | GE Healthcare, Germany |
| Mettler PM460 DeltaRange | Mettler-Toledo, Germany |
| Sonication bath Kern EMB 1000-2 | KERN & SOHN, Germany |
| Ultrasonic homogenizer Omni Sonic Ruptor 400 | Omni International, USA |
| UV-VIS spectrometer | Perkin Elmer, Germany |
| Vortex-Genie 1 | Scientific Industries, USA |
| Confocal microscope Leica SP8 | Leica Microsystems, Germany |
| Confocal microscope Leica SP5 | Leica Microsystems, Germany |
| Fluorescence microscope Leica DMi8 | Leica Microsystems, Germany |
| Lenses: 20x/0.75 NA, 20x/0.75 IMM 40x/0.60 NA | Leica Microsystems, Germany |

**Table 2: List of Software used in this thesis**

| Software | Supplier |
|---|---|
| Microsoft office (Word, Excel, Power Point) | Microsoft, USA |
| Graphpad Prism 5.0 | GraphPad Software, USA |
| ImageJ 1.49h | NIH, USA |
| Leica Application Suite X | Leica Microsystems, Germany |
| Mendeley Desktop | Elservier, USA |
| Ibidi Chemotaxis and Migration Tool | ibidi,Germany |

**Table 3: List of chemicals used in this thesis**

| Chemicals | Supplier |
|---|---|
| Agarose | Sigma Aldrich, Germany |
| Ammonium persulfate (APS) | Sigma Aldrich, Germany |
| Ampicillin | Carl Roth, Germany |
| L-(+)-Arabinose | Sigma Aldrich, Germany |
| Kanamycin | Carl Roth GmbH, Germany |
| Chloramphenicol | Sigma Aldrich, Germany |
| Bromophenol Blue | Sigma Aldrich, |
| BactoTM Tryptone | BD Biosciences, Germany |
| Citric acid | Sigma Aldrich, Germany |
| Chloroform | Fisher Scientific, UK |
| Diethyl ether | Sigma Aldrich, Germany |
| DL-Dithiothreitol (DTT) | Sigma Aldrich, Germany |
| Ethylenediaminetetraacetic acid (EDTA) | Sigma Aldrich, Germany |
| Ethanol | VWR, Germany |
| Ethyl acetate | Sigma Aldrich, Germany |
| α-D-Glucose | Sigma Aldrich, Germany |
| Glycerol | Sigma Aldrich, Germany |
| Hydrogen peroxide (35%) ($H_2O_2$) | Carl Roth, Germany |
| Hydrochloric acid (37%) (HCl) | VWR, Germany |
| 2-Ethyl hexanol | Sigma Aldrich, Germany |
| Imidazole | Sigma Aldrich, Germany |
| Isopropyl-β-D-thiogalactopyranoside (IPTG) | Fisher Scientific, Germany |
| L-Ascorbic acid | Sigma Aldrich, Germany |
| 2-Mercaptoethanol | Sigma Aldrich, Germany |
| Methanol | VWR, Germany |
| α-Methyl-DL-aspartate (MeAsp) | Sigma Aldrich, Germany |
| Magnesium chloride solution 1M ($MgCl_2$) | Fisher Scientific, Germany |
| Nickel(II) chloride (anhydrous) $NiCl_2$ | Sigma Aldrich, Germany |
| Paraformaldehyde (PFA) | Sigma Aldrich, Germany |
| Phenylmethylsulfonyl fluoride (PMSF) | Sigma Aldrich, Germany |
| Phosphate buffered saline (PBS) tablets | VWR, Germany |
| Potassium dihydrogen phosphate ($KH_2PO_4$) | Sigma Aldrich, Germany |
| Potassium hydroxide (KOH) | Carl Roth GmbH, Germany |
| Potassium Chloride (KCl) | Sigma Aldrich, Germany |

| | |
|---|---|
| 2-Propanol | Sigma Aldrich, Germany |
| Sodium chloride (NaCl) | Sigma Aldrich, Germany |
| Sodium dodecyl sulfate (SDS) | Carl Roth, Germany |
| Sulfuric acid $H_2SO_4$ (95-97%) | Sigma Aldrich, Germany |
| N,N,N',N'-Tetranethyl-ethylrnrdiamine (TEMED) | Sigma Aldrich, Germany |
| 3-(Triethozysilyl)propyl isocyanate | Sigma Aldrich, Germany |
| Toluene (anhydrous) | Sigma Aldrich, Germany |
| Trizma® base (TRIS) | Sigma Aldrich, Germany |
| Tris Buffer 1 M pH 8.0 | Fisher Scientific, Germany |
| Tween 20 | Sigma Aldrich, Germany |
| **Biochemicals** | |
| Agar | Carl Roth, Germany |
| Luria-Bertani (LB) | Carl Roth, Germany |
| Bovine Serum Albumin (BSA) | Sigma Aldrich, Germany |
| cOmplete Protease inhibitor cocktail tablets | Roche Diagnostics GmbH, Mannheim, Germany |
| Novex™ Prestained Protein Standard | Fisher Scientific, Germany |
| 4x Protein loading dye (stored at -20 °C)<br>40 % glycerol, 240 mM TRIS pH 6.8, 8 % SDS, 0.04 % bromphenol blue, 5 % beta-mercaptoethanol | Self-made |
| Color Protein Standard Broad Range | NEB GmbH, Germany |
| Unstained Protein Standard Broad Range | NEB GmbH, Germany |
| Streptavidin | Tebu Bio, Germany |

**Table 4: List of consumables used in this thesis**

| Consumable | Supplier |
|---|---|
| Cellulose filters (0.22 and 0.45 µm) | Carl Roth, Germany |
| Cover slips (20 x 20 mm and 24 x 60 mm) | Carl Roth, Germany |
| Eppendorf® tubes (0.5 mL, 1.5 mL, 2 mL) | Eppendorf, Germany |
| Falcon Tubes (15 mL, 50 mL) | Greiner Bio-One, Germany |
| µ-Slide Chemotaxis | ibidi, Germany |
| µ-Slide 4 Well | ibidi, Germany |
| µ-Slide 18 Well – Flat | ibidi, Germany |
| Microplate 96 Well F-Bottom black | Greiner Bio-One, Germany |
| Multiwell plate 6 Well | Greiner Bio-One, Germany |
| Nunc® Lab-Tek® Chamber Slide System (8-well) | Thermo Fisher Scientific, Germany |
| Petri dishes | VWR, Germany |
| Plastic pipettes (1 mL, 5 mL, 10 mL, 25 mL) | Greiner CELLSTAR®, Sigma Aldrich, Germany |
| Pipette tips (10 µL, 100 µL, 1000 µL) | STARLAB, Germany |
| Protein LoBind Eppendorf® tubes (0.5 mL, 1.5 mL) | Eppendorf, Germany |
| UV-VIS semi-micro polystyrene cuvettes | Brand GmbH, Germany |

### 4.1.2 Buffers and media

**Buffer A (binding buffer):**

| Chemicals | Final concentration |
|---|---|
| TRIS pH 7.4 | 50 mM |
| NaCl | 300 mM |
| DTT | 1 mM |

**Buffer B (elution buffer):**

| Chemicals | Final concentration |
|---|---|
| TRIS pH 7.4 | 50 mM |
| NaCl | 300 mM |
| DTT | 1 mM |
| Imidazole | 250 mM |

**IMAC binding buffer (pH 7.5):**

| Chemicals | Final concentration |
|---|---|
| $KH_2PO_4$ | 50 mM |
| NaCl | 400 mM |
| 2- Mercaptoethanol | 0.5 |

**IMAC elution buffer (pH 7.5):**

| Chemicals | Final concentration |
|---|---|
| $KH_2PO_4$ | 50 mM |
| NaCl | 400 mM |
| 2- Mercaptoethanol | 0.5 |
| Imidazole | 500 mM |

**DNA localization buffer:**

| Chemicals | Final concentration |
|---|---|
| Tris pH 8.0 | 10 mM |
| $MgCl_2$ | 12 mM |
| Tween 20 | 0.05 %(v/v) |

**Motility buffer:**

| Chemicals | Final concentration |
|---|---|
| $KH_2PO_4$ | 10 mM |
| $K_2HPO_4$ | 10 mM |
| NaCl | 67 mM |
| EDTA | 0.1 % |

**TB (Tryptone Broth) medium:**

| Chemicals | Final concentration |
|---|---|
| Tryptone | 10 g/l |
| NaCl | 5 g/l |

### 4.1.3 DNA oligonucleotides

All DNA oligonucleotides were purchased from Integrated DNA Technologies with HPLC purification, dissolved in 10 mM Tris (pH=8.0) and stored at -20 °C.

| | | | modifications | |
|---|---|---|---|---|
| | **Sequence** | **Length (# bases)** | 5' | 3' |
| Input (A) | TATTACAG CGAACGAA CGAC ACTAATGC ACTACTAC | 36 | | |
| F1 | GTAGTAGT GCATTAGT GTCG TTCGTTCG CTGTAATA | 36 | Alexa488 | Biotin-TEG |
| F2 | GCATTAGT CTATCATG GTCG TTCGTTCG ACAGTTCC | 36 | Biotin-TEG | Cy5 |
| Q1 | CGAACGAA CGAC CATGATAG ACTAATGC ACTACTAC | 36 | | Iowa Black |
| Q2 | GGAACTGT CGAACGAA CGTGAAAC CGAC CATGATAG | 36 | Iowa Black | phosphate |
| Fuel | GGAACTGT CGAACGAA CGAC CATGATAG | 28 | | phosphate |

## 4.2 Methods

### 4.2.1 Plasmids

The plasmids pQE-80L iLID (C530M) and pQE-80L MBP-SspB Nano were gifts from Brian Kuhlman (Addgene # 60408 and # 60409, respectively).

The Cph1 gene was synthesized by the GeneScript and inserted into pET21b(+) vector between the NdeI and SalI cutting sites to include a C-terminal His6-tag. The VVDHigh gene was introduced into pET21b(+) vector between the NdeI and

XhoI cutting sites to include a C-terminal His6-tag.
The gene coding for PIF6-GFP-TEV-His6-tag was synthesized by the GeneScript and inserted into pET21b vector between the NdeI and HindIII cutting sites. The pellet of bacteria co-expressing PhyB-Biotin-His6tag and the genes for the cofactor PCB (phycocyanobilin) was kindly provided by the group of Prof. W. Weber (Center for Biological Systems Analysis, University of Freiburg)

The *E. coli* strain MG1655 was transformed with a plasmid coding for antigen 43 genetically modified with a biotin acceptor peptide (Ag43-BAP) to display biotin on the E. coli surface (pOS233, IPTG inducible, T5 promoter, kanamycin-resistant) and an EGFP (enhanced green fluorescent protein) coding plasmid (pOS239, arabinose inducible, PBAD promoter, ampicillin-resistant) and the transformed strain was gently provided by the group of Prof. V. Sourjik (Max-Planck-Institute for Terrestrial Biology, Marburg)

### 4.2.2 Preparation of the LB medium and Agar plates for *E. coli* cultures

Media were autoclaved at 120 °C for 20 min. LB powder (Luria/Miller) 20 g/L was dissolved in MiliQ water and autoclaved. LB Agar plates contained 7.5 g Agar, 10 g LB medium per 500 mL dissolved in MiliQ water, and autoclaved. The antibiotics were added shortly before the plate pouring

### 4.2.3 Chemical transformation

48 µL of chemically competent bacteria (*E. coli,* BL21 strain) was mixed with 2 µL of plasmid DNA and incubated for 30 min. Then the bacteria was heat shocked on the heating block at 42 °C for 45 s and quickly transferred back on ice, incubated on ice for 2 min. 450 µL of LB media was added to the bacteria and incubated while shaking at 250 rpm, at 37 °C for 1 h. After the incubation, the bacteria mixture was spread on a LB agar plate with 50 µg/mL of appropriate antibiotic. The plate was incubated overnight at 37 °C before picking the colonies.

### 4.2.4 Protein expression and purification

Each plasmid was chemically transformed into *E. coli* BL21 (DE3). Overnight cultures of *E. coli* BL21 were grown overnight in LB medium supplied with the

50 µg/mL appropriate antibiotic at 37 °C at 200 rpm. The overnight cultures were diluted 1:100 into fresh LB medium supplemented with 50 µg/mL ampicillin and were cultured at 37 °C, 220 rpm until the OD600=0.4-0.6. Protein expression was induced with 0.5 mM isopropyl β-D-1- thiogalactopyranoside (IPTG) and the cultures were cultivated overnight at 16 °C, 200 rpm. Then, the bacteria pellets were centrifugated (6000 rpm, 4 °C, 8 min, Beckman Coulter Avanti J-26S XP, JA-10 rotor) and resuspended in the buffer (50 mM Tris, 300 mM NaCl, pH=7.4) supplemented with 100 µM PMSF (phenylmethanesulfonyl fluoride) and 1 mM DTT (dithiothreitol). The bacteria were lysed on ice by sonication (50% frequency, 40% power, 10 min) and the lysate was cleared by centrifugation. After the centrifugation, the supernatant was collected and filtered twice through a 0.45 µm cellulose filter. The cleared supernatant containing the protein was purified using a $Ni^{2+}$-NTA affinity chromatography (column volume: 5 mL). The column was first set with the Buffer A, then the protein solution passed through the column 2-3 times. Then, the column was washed with 10 mL Buffer A and 50 mL 5% Buffer A/Buffer B solution supplemented with 80 µL 1 M DTT. Elution was done by passing through 10 mL Buffer B from the His-tag column. The protein solution was dialyzed against 2 L Buffer A supplemented with 2 mL 1 M DTT, in dialysis membrane (3.5 kDa MW cut-off) overnight at 4 °C by refreshing the Buffer A at least twice. For Cph1 protein, 20 µM PCB was added during the lysing step. The protein purity was verified by SDS-PAGE. Proteins were aliquoted and stored at -80 °C.

**PhyB-Biotin-His6-tag purification**

The pellet of bacteria co-expressing PhyB-Biotin-His6tag and the genes for the cofactor PCB (phycocyanobilin) was kindly provided by the group of Prof. W. Weber (Center for Biological Systems Analysis, University of Freiburg) and the biotinylated PhyB was purified following the previously established protocol.[243] In short, the bacterial pellet was suspended in the IMAC binding buffer (50 mM $KH_2PO_4$, 400 mM NaCl, 0.5 mM 2-mercaptoethanol, pH 7.5) supplemented with 100 µM PMSF and the bacteria were lysed by sonication. The lysed bacteria were spun down by centrifugation at 10000 x g at 4 °C for 1 h and the lysate was

filtered through a 0.45 µm filter. The biotinylated PhyB was purified over a $Ni^{2+}$-NTA affinity column chromatography taking advantage of the His6-tag of PhyB. and obtained as a blue colored protein due to the PCB cofactor. The purity of the protein was checked with SDS-PAGE (Appendix Figure A2)

### 4.2.5 Light sources and intensities

The light power was measured using a LabMax-TOP meter with an OP-2 VIS power sensor (8 mm in diameter, Coherent Inc.) at 6.5 cm distance (equals to the distance at which the samples were positioned). For all the experiments 0.89 $mW/cm^2$ red light (Albrillo LL-GL002, 225 LEDs, 630 nm, 14 W), 0.71 $mW/cm^2$ blue light (Albrillo LL-GL003, 225 LEDs, 460 nm, 14 W) and 1.12 $mW/cm^2$ far-red light (Philips GreenPower LED, 15 W, 700-800 nm) were used.

### 4.2.6 Microscopy

For the DNA-based communication project, all microscopy images and fluorescent data were acquired using the Leica DMi8 S laser scanning confocal microscope, equipped with 488, 552 and 638 nm solid-state lasers and HyD detectors. Imaging was performed with 20x/0.75 NA or 20x/0.75 IMM (field of view: 0.775x0.775 mm2, slice thickness: 2µ) at a resolution of 512x512 pixels. Line correction mode (x4) was used.

For the bacteriabot project, the adhesion of bacteria was visualized by acquiring the fluorescent at on a confocal laser scanning fluorescence microscope (SP5 Leica) through the 20x dry objective (715x 715 µm) for quantification, and on a Leica DMi8 S through the 63x water objective ($\lambda_{excitation}/\lambda_{emission}$: 488 nm/ 530-600 nm). Bacteria-particle attachment between eGFP labeled bacteria and far-red labeled PS particles ($\lambda_{excitation}/\lambda_{emission}$: 732/758 nm) was visualized by acquiring fluorescent images on a Leica DMi8 S laser scanning confocal microscope with a 63x water objective (GFP: $\lambda_{excitation}/\lambda_{emission}$: 488 nm/530-600 nm/ particles $\lambda_{excitation}/\lambda_{emission}$: 647 nm/720-780 nm). Tracking of the bacteria was done by acquiring the fluorescence images of the PS particles on an inverted fluorescent microscope at with Cy5 Filter (DMi8, Leica) through a 40x objective. Fluorescent images were acquired every 0.5 s for periods of 5 s.

For the narcissistic self-sorting project all images were either acquired on an inverted fluorescent microscope (DMi8, Leica) through the 40x air objective using bright field, FITC ($\lambda_{excitation}/\lambda_{emission}$: 494/520 nm) and TRITC ($\lambda_{excitation}/\lambda_{emission}$: 557/576 nm) channels.

### 4.2.7 Protein immobilization on particles

Polystyrene beads with 2 μm with the $Ni^{2+}$-NTA groups magnetic and non-magnetic with fluorescent labels) were purchased from Micromod Partikeltechnologie GmbH as a water suspension (50 mg/mL, $1.2x10^{10}$ beads/mL). Fluorescently-labelled beads contain fluorescein ($\lambda_{excitation}/\lambda_{emission}$: 485/510 nm), rhodamine B ($\lambda_{excitation}/\lambda_{emission}$: 572/590 nm) and far-red fluorescent dye ($\lambda_{excitation}/\lambda_{emission}$: 732/758 nm). Prior to each protein immobilization, particles were incubated in 0.3% BSA in Buffer A (50 mM Tris, 300 mM NaCl, pH=7.4) at 4 °C for 15 min. 1μM His6-tagged protein was incubated in buffer (50 mM Tris, 300 mM NaCl, pH=7.4) with 5 mg/mL $Ni^{2+}$-NTA functionalized PS particles at 4 °C for 1 h.[107] Subsequently, any excess protein was washed away by centrifugation and washing with Buffer A. Particles were then resuspended in PBS with 0.3 %BSA and diluted to 0.5 mg/mL.

### 4.2.8 Preparation of the streptavidin encapsulated Ni-NTA proteinosomes

Rhodamine B labeled NTA-functionalized PNIPAAm/BSA-$NH_2$ conjugates were synthesized and sent by Dr. Pierangelo Gobbo (Centre for Protolife Research, University of Bristol, United Kingdom). 7.5 μL NTA-functionalized PNIPAAm/BSA-$NH_2$ conjugates (stock concentration: 16 mg/ml), 4.2 μL streptavidin (final concentration: 10 μM) and 1.5 mg of PEG-bis(*N*-succinimidyl succinate) (Mw = 2000, Sigma), dissolved in 3.3 μL, 50 mM sodium carbonate buffer, pH=8.5, mixed in an Eppendorf tube. Then, a Pickering emulsion was produced by the addition of 300 μL 2-ethyl-1-hexanol and shaking for 25 s. The crosslinking reaction takes place at room temperature and runs for 3 h in the dark. During this time, proteinosomes sediment and thereafter the upper layer of the oil is carefully removed. 600 μL of 70% ethanol is added and the proteinosomes are resuspended. The resuspended mixture is dialyzed against

first 70% ethanol for 2h, then 50% ethanol for 2 h, and finally against MiliQ water, overnight. For the Nickel complexation, the resulting resuspension of proteinosomes in MiliQ water is dialyzed against 10 mM $NiCl_2$ for 3 h, at 4 °C. The excess $NiCl_2$ was dialyzed against MiliQ water overnight at 4 °C, by refreshing the MiliQ water at least 2 times.

### 4.2.9 ssDNA localization in streptavidin-containing proteinosomes

The protocol for the DNA oligonucleotide localization was previously reported.[7] The protocol is followed with some modifications. As the buffer, RNAse free 10 mM Tris (pH=8.0), RNAse free 12 mM $MgCl_2$ and 0.05% Tween 20 (v/v) is used. To 10 µL dispersion of proteinosomes, 4x of 5 µL buffer, 2 µL BSA (stock concentration: 2mg/mL), 1 µL of biotinylated F-strands (stock concentration: 10 µM) is added and incubated for 1 h at room temperature, in the dark. For the quenching, 2 µL of Q-strands (Stock concentration: 10 µM) is added and incubated overnight at 4 °C. To remove the excess strands, 10 µL of the supernatant is gently discarded, followed by the addition of 10 µL buffer. After the sedimentation for 7h at 4 ° C, 10 µL of the supernatant is gently discarded and 400 µL buffer is added. Proteinosomes are allowed to sediment for 7h at 4 °C and 390 µL supernatant is carefully discarded.

### 4.2.10 Protein immobilization on proteinosomes

To 10 µL of the $Ni^{2+}$-complexed proteinosomes, 1 µL BSA (stock concentration: 2 mg/mL) is added and incubated for 5 min, followed by the addition of the 2 µL of the protein (final concentration: 500 nm). To remove any excess protein, the dispersion is dialyzed against the buffer for at 4 °C.

### 4.2.11 Blue-light triggered aggregation of the proteinosomes

For the aggregation studies, 15 µL of iLID functionalized sender proteinosomes are mixed with 15 µL of Nano functionalized receiver proteinosomes in a µ-slide 18 well – flat uncoated polymer dish (Ibidi GmbH, Martinsried, Germany). Afterward, the samples are moved under the blue light and incubated for 90 min with the light pulsing (120 s ON, 360 s OFF) while shaking on a 2D shaker at 50 rpm, whereas the dark control is placed in the dark on the 2D shaker at 50 rpm

for 90 min. The dish area is scanned under the Leica DMi8 S laser scanning confocal microscope. At least 15 images from 3 independent experiments were analyzed.

### 4.2.12 DNA-Strand-Displacement cascade

10 µL of iLID functionalized sender proteinosomes, 10 µL of Nano functionalized receiver proteinosomes, and 10 µL of the fuel strand (stock concentration: 2 µM) are mixed in a µ-slide 18 well – flat uncoated polymer dish (Ibidi GmbH, Martinsried, Germany). Then, the samples are moved under the blue light and incubated for 90 min with the light pulsing (120 s ON, 360 s OFF) while shaking on a 2D shaker at 50 rpm, whereas the dark control is placed in the dark on the 2D shaker at 50 rpm for 90 min. Upon the addition of the 2 µL of the input strand (stock concentration: 1 µM), the timelapse imaging is acquired every 5 min for the selected area, for 20 min.

### 4.2.13 Calculating the concentration of the streptavidin in proteinosomes

FITC-labeled streptavidin containing proteinosomes are prepared according to the protocol. 10 µL of the FITC-labeled streptavidin solutions with the following concentrations are fixed between the coverslips: 3.5 µM, 7.5 µM, and 15 µM. The intensity value is measured under the Leica DMi8 S laser scanning confocal microscope. and a calibration curve is obtained. 10 µL of the proteinosomes dispersion in water is placed between the coverslips, the intensity values from proteinosomes are measured under the confocal microscope. The intensity values are fitted to the calibration curve and the streptavidin concentration is calculated.

### 4.2.14 Bead aggregation assay for the self-sorting

50 µL of protein-functionalized beads (5 mg/mL) are diluted to a total volume of 300 µL and the samples are either kept under blue (460 nm) and far-red (730 nm) or red (630 nm) light for 2 h, while being gently agitated in LoBind Eppendorf tubes at 50 rpm in an orbital shaker. For all the experiments the light intensities are 0.71 $mW/cm^2$ blue light, 0.89 $mW/cm^2$ red light and 1.12 $mW/cm^2$ for far-red light. Subsequently, the samples are fixed with 300 µL of 10% (w/v) paraformaldehyde (PFA) for 20 min, 300 µL of the sample is

transferred into an imaging chamber (Lab-Tek®) with a cut pipette tip and allowed to settle for 30 min before acquiring 15 images in the bright field channel for image analysis. All images are acquired using an inverted fluorescent microscope (DMi8, Leica) through the 40× air objective (field of view is $62.3 \times 10^{-5}$ $cm^2$). To study the aggregation dynamics, the samples are prepared and handled as described above but the time under the light illumination was varied. For repeated switching of the assemblies, the samples were handled the same but the samples are alternated between blue and far-red light or red light for 1 h and under far-red light for 30 minu. Experiments with fluorescently labeled $Ni^{2+}$-NTA beads are performed exactly the same way but images are acquired in the FITC and TRITC channels.

### 4.2.15 Preparation of PhyB functionalized *E. coli*

The *E. coli* strain MG1655 was transformed with a plasmid coding for antigen 43 genetically modified with a biotin acceptor peptide (Ag43-BAP) to display biotin on the *E. coli* surface (pOS233, IPTG inducible, T5 promoter, kanamycin-resistant) and an EGFP (enhanced green fluorescent protein) coding plasmid (pOS239, arabinose inducible, $P_{BAD}$ promoter, ampicillin-resistant) as previously described.[102] An overnight culture of the transformed *E. coli* in tryptone broth (TB; 1 w/v % tryptone, 0.5 w/v % NaCl, pH 7.0) containing 50 µg/mL ampicillin and 35 µg/mL kanamycin was diluted 1:100 and cultured at 250 rpm, 34 °C. The expression of Ag43-BAP and EGFP was induced after 2 h with 100 µM IPTG and 0.005 w/v % *L*-arabinose and the bacteria were cultured for 3 h unless stated otherwise. 2 mL of bacteria were harvested at 0.4 *g* for 5 min, resuspended in 500 µL PBS and spun-down again. Then, the bacteria were incubated with 1 µM streptavidin in 200 µL PBS for 10 min at 37 °C, 250 rpm. Excess streptavidin was washed away once with 500 µL PBS and then the suspended bacteria in 200 µL PBS were incubated with 1 µM biotinylated PhyB for 10 min at 37 °C, 250 rpm. For control bacteria, incubation with PhyB was skipped. After washing the excess PhyB away with 500 µL PBS, bacteria were resuspended in PBS with 0.3% BSA to the appropriate concentration.

### 4.2.16 Functionalization of glass substrates with PEG and His-tagged PIF6

The protein functionalization of the glass substrates was described in detail in our previous studies (Appendix Figure A1).[153,244] In short, glass slides (20 x 20 mm) were cleaned in freshly prepared piranha solution (3:1 v/v $H_2SO_4$:$H_2O_2$) for 1 h, and subsequently washed with Milli-Q water and dried in a stream of $N_2$. The glass substrates were immersed into a PEG-azide solution in toluene (10 mg $Si(OEt)_3$-PEG2000-$N_3$) with a drop of trimethylamine under inert $N_2$ atmosphere and the reacted overnight at 79 ºC. The substrates were washed and sonicated first in ethyl acetate, and then in methanol for 5 min each and dried in a stream of $N_2$. PEG-coated surfaces were incubated for 2 h in a moisture chamber at room temperature in contact with 100 µL of a reaction solution containing 100 mM Tris (pH=8.5), 100 mM L-ascorbic acid, 100 µL NTA-alkyne and 1 mM $CuSO_4$. For $Ni^{2+}$ loading, the NTA functionalized surfaces were washed with: 1) 50 mM EDTA (pH 7.4) for 5 min 2) Buffer A (50 mM Tris HCl (pH 7.4), 300 mM NaCl) for 5 min (2 times). 3) 0.1 M $NiCl_2$ for 5 min. 4) Buffer A for 5 min. (2 times). Then, the glass substrates were incubated with 10 µM of PIF6-GFP-TEV-His6-tag in a moisture chamber for 30 min, at 4ºC and washed twice Buffer A and then twice with PBS.

### 4.2.17 Adhesion and detachment of PhyB functionalized bacteria to PIF6 functionalized substrates

PhyB functionalized bacteria resuspended in PBS to $OD_{600}$=1.0 and illuminated with far-red light for 2 min before further use. 2 mL of PhyB functionalized bacteria were seeded on top of each PIF6 functionalized substrate and were incubated either under red light or far-red light for 1 h at room temperature. After 1 h, the substrates were washed with 2 mL PBS three times to remove unattached bacteria and fluorescent images were acquired at on a confocal laser scanning fluorescence microscope (SP5 Leica) through the 20x dry objective (715x 715 µm). To investigate the detachment kinetics, PhyB functionalized bacteria were placed on PIF6 functionalized substrates under red light for 1 h and subsequently illuminated with far-red light. Samples were analyzed at each time point as described above.

### 4.2.18 Quantification of light-dependent attachment and detachment of PhyB functionalized bacteria to PIF6 functionalized PS particles

Non-functionalized and PhyB functionalized bacteria, prepared as described before, were suspended to a final $OD_{600}$ of 3.0. 50 µL of bacteria were mixed with 10 µL (concentration=0.5 mg/mL) PIF6 immobilized magnetic PS particles and incubated under the corresponding light source for the indicated time-periods on an orbital shaker at 70 rpm, at room temperature. The mixture of bacteria and particles were incubated under red light for 10 min for the attachment of cells. For the reversion experiments, the bacteria-particle mixture was first incubated under red light for 10 min, then moved under far-red light or in the dark under the same conditions. After the incubation period under the corresponding light source, particles and the attached bacteria were separated by using a magnet and gently washed twice without disturbing the attached cells with 100 µL PBS. Particles were then resuspended in 100 µL PBS, and the number of bacteria in the solution was quantified by measuring the fluorescent intensity with a fluorescence plate reader (Tecan Spark, $\lambda_{excitation}/\lambda_{emission}$: 488/530 nm). For each culture, a calibration curve of bacteria of known density was used to determine the number of cells in the samples.

Bacteria-particle attachment between eGFP labeled bacteria and far-red labeled PS particles ($\lambda_{excitation}/\lambda_{emission}$: 732/758 nm) was visualized by acquiring fluorescent images on a Leica DMi8 S laser scanning confocal microscope with a 63x water objective (GFP: $\lambda_{excitation}/\lambda_{emission}$: 488/530-600 nm, particles $\lambda_{excitation}/\lambda_{emission}$: 647/720-780 nm)

### 4.2.19 Cell tracking

Bacteriabots were fabricated as described above under 10 min of red light illumination but magnetic PS particles were replaced with far-red labeled PS particles ($\lambda_{excitation}/\lambda_{emission}$: 732/758 nm) as model cargo. The bacteriabot solution was diluted 1:50 and 20 µL of the diluted bacteriabot solution was transferred to a µ-Slide chemotaxis dish (ibiTreat #1.5, ibidi GmbH, Martinsried, Germany). 200 µM α-methyl-*DL*-aspartate was used as the attractant. After 20 min of incubation, fluorescence images of the PS particles were acquired on an

inverted fluorescent microscope at with Cy5 Filter (DMi8, Leica) through a 40x objective. Fluorescent images were acquired every 0.5 s for periods of 5 s. For the reversion experiment, bacteriabot solution was prepared as described above and illuminated first with red light for 10 min and then far-red light for 10 min. The solution was diluted 1:50 and 20 µL of this solution was transferred to the µ-Slide chemotaxis dish and images were acquired as described above. For particle tracking experiments without the bacteria, the addition of bacteria was skipped and the same protocol was followed.

### 4.2.20 Bacterial viability assay

Bacterial viability was measured using the Abcam bacterial viability assay kit, (cat #ab189818). Ag43-BAP transformed MG1655 *E. coli* were grown as described above in 10 mL growth media overnight. The bacteria were harvested by centrifugation at 10000 x *g* for 10 min and were resuspended in 4 mL of wash buffer provided by the kit. 1 mL of bacterial suspension was diluted into 5 mL of wash buffer for each sample. One sample was kept in the dark and used as the live sample (positive control), and the others were incubated either under red or far-red light for 1 h in an Eppendorf tube. For the negative control, 1 mL of bacterial suspension was suspended in 70% isopropanol and incubated for 1 h. The samples were harvested at 10000 x *g* for 10 min and resuspended in 5 mL of wash buffer. The final step was repeated once again but the cells were resuspended in 1 mL of wash buffer. To each sample, 1 µL of Total Cell Stain and 1 µL of Dead Cell Stain were added and then incubated at room temperature in the dark for 1 h. 200 µL from each sample were analyzed for their fluorescence ($\lambda_{excitation}/\lambda_{emission}$: 490/525 nm as reading 1, $\lambda_{excitation}/\lambda_{emission}$: 536/617 nm as reading 2). The percentage of the dead cells was calculated after the blank correction by dividing the reading 2 by reading 1.

### 4.2.21 Cell viability assay

MDA-MB-231 cells were washed with PBS and detached wit 1mL of accutase (Gibco, Catalog # A1110501), and resuspended in 5 mL of DMEM (without phenol red). Subsequently, $5\times10^4$ cells in total volume of 1 mL medium were placed into 1.5 mL Eppendorf tubes and incubated under illumination with red

light, far-red light or in the dark for 1h. After the illumination, 100 µL of medium containing 5000 cells were transferred to a 96-well plate. The viability of the cells was measured using the CellTiter-Glo2.0 Assay (Promega) according to manufacturer's instructions. As blank control, DMEM (without phenol red) containing the bioluminescent reagent used as background control of luminescence.

### 4.2.22 Data aquisition and analysis

**Blue light controlled DNA-based communication:**

All microscopy images and fluorescent data were acquired using the Leica DMi8 S laser scanning confocal microscope, equipped with 488, 552 and 638 nm solid-state lasers and HyD detectors. Imaging was performed with 20x/0.75 NA or 20x/0.75 IMM (field of view: 0.775x0.775 $mm^2$, slice thickness: 2µ) at a resolution of 512x512 pixels. Line correction mode (x4) was used.

All microscopy images were analyzed using the ImageJ software. Images are imported into the software, and an intensity threshold is applied to select particles. The images are converted to binary images and holes are filled using the "Fill holes" tool. Then, the area occupied by beads is quantified using the "Analyze particle tool". First, to quantify the size and the number of the aggregates, the size threshold for a cluster is set to 0.00002 $cm^2$. Then, all proteinosomes in the image are quantified without applying a size limit. By dividing the area occupied with the aggregates to the area occupied by all clusters, the aggregation ratio is calculated.

The intensities of the proteinosomes were analyzed using Image J 1.52b. The mean Alex488 fluorescence intensity inside the randomly picked senders and The mean Cy5 fluorescence intensities inside the randomly picked receivers were measured (n>50) and corrected for the background.

GraphPad Prism Software (La Jolla, CA, USA) was used for statistical analyses. All values in this study were expressed as mean ± SEM, from three biological replicates. Significant differences between groups were analyzed using unpaired

t-test. Differences were considered significant at *p < 0.05, **p < 0.01, and ***p < 0.001.

**Independent blue and red light-triggered narcissistic self-sorting self-assembly of colloidal particles:**

The microscopy images are analyzed using the ImageJ software. After importing the images into the software, an intensity threshold was applied to select particles. The images are made binary and holes were filled using the "Fill holes" tool. Then, the area occupied by beads is quantified using the "Analyze particle tool". First, to quantify the clusters (projected area > 10 beads) a size limit of 30 infinity $\mu m^2$ was applied. Second, all beads in the image are quantified by applying a size limit of 3-infinity $\mu m^2$. From this data, the aggregation ratio occupied by clusters is calculated by dividing the total area occupied by all the clusters by the total area occupied by all the beads in the same image. The sizes of clusters and their number are also quantified.

**Red/Far-Red Light Switchable Cargo Attachment and Release in Bacteria-driven Microswimmers:**

For the study of surface adhesion of the bacteria, fluorescent images were acquired at on a confocal laser scanning fluorescence microscope (SP5 Leica) through the 20x dry objective (715x 715 µm) for quantification, and on a Leica DMi8 S through the 63x water objective ($\lambda_{excitation}/\lambda_{emission}$: 488/530-600 nm). The number of bacteria of each substrate was analyzed using the particle analyzer tool in ImageJ.

For the particle tracking, ImageJ plugin MtrackJ (ibidi GmbH, Martinsried, Germany) was used and then analyzed with the free software Chemotaxis and Migration Tool (ibidi GmbH, Martinsried, Germany) for the velocity and the distance traveled.

GraphPad Prism Software (La Jolla, CA, USA) was used for statistical analyses. All values in this study were expressed as mean ± SEM, from three biological replicates each done in three technical replicates. Significant differences between groups were analyzed using paired t-test was used. Differences were

considered significant at $*p < 0.05$, $**p < 0.01$, and $***p < 0.001$. For cell tracking, the frequency distribution was fitted to a Gaussian distribution.

# Chapter 5: Bibliography


1. Karp, G. Cell and Molecular Biology: Concepts and Experiments. *Wiley; 6th Ed.* **2009**.

2. Dzieciol, A. J.; Mann, S. Designs for Life: Protocell Models in the Laboratory. *Chemical Society Reviews*. **2012**, *41* (1), 79-85.

3. Blain, J. C.; Szostak, J. W. Progress Toward Synthetic Cells. *Annu. Rev. Biochem.* **2014**, *83*, 615–640.

4. Glass, J. I.; Assad-Garcia, N.; Alperovich, N.; Yooseph, S.; Lewis, M. R.; Maruf, M.; Hutchison, C. A.; Smith, H. O.; Venter, J. C. Essential Genes of a Minimal Bacterium. *Proc. Natl. Acad. Sci. U. S. A.* **2006**, *103* (2), 425–430.

5. Roberts, M. A. J.; Cranenburgh, R. M.; Stevens, M. P.; Oyston, P. C. F. Synthetic Biology: Biology by Design. *Microbiol.* **2013**, *159* (Pt 7), 1219.

6. Walde, P. Building Artificial Cells and Protocell Models: Experimental Approaches with Lipid Vesicles. *BioEssays*. **2010**, *32(4)*, 296-303.

7. Joesaar, A.; Yang, S.; Bögels, B.; van der Linden, A.; Pieters, P.; Kumar, B. V. V. S. P.; Dalchau, N.; Phillips, A.; Mann, S.; de Greef, T. F. A. DNA-Based Communication in Populations of Synthetic Protocells. *Nat. Nanotechnol.* **2019**, *14* (4), 369–378.

8. Noireaux, V.; Libchaber, A. A Vesicle Bioreactor as a Step toward an Artificial Cell Assembly. *Proc. Natl. Acad. Sci. U. S. A.* **2004**, *101* (51), 17669–17674.

9. Lee, K. Y.; Park, S. J.; Lee, K. A.; Kim, S. H.; Kim, H.; Meroz, Y.; Mahadevan, L.; Jung, K. H.; Ahn, T. K.; Parker, K. K.; Shin, K. Photosynthetic Artificial Organelles Sustain and Control ATP-Dependent Reactions in a Protocellular System. *Nat. Biotechnol.* **2018**, *36* (6), 530–535.

10. Ma, B. C.; Caire da Silva, L.; Jo, S. M.; Wurm, F. R.; Bannwarth, M. B.; Zhang, K. A. I.; Sundmacher, K.; Landfester, K. Polymer-Based Module for NAD+ Regeneration with Visible Light. *ChemBioChem* **2019**, *20* (20), 2593–2596.

11. Buddingh', B. C.; Van Hest, J. C. M. Artificial Cells: Synthetic Compartments with Life-like Functionality and Adaptivity. *Acc. Chem. Res.* **2017**, *50* (4), 769–777.

12. Kurihara, K.; Tamura, M.; Shohda, K. I.; Toyota, T.; Suzuki, K.; Sugawara, T. Self-Reproduction of Supramolecular Giant Vesicles Combined with the Amplification of Encapsulated DNA. *Nat. Chem.* **2011**, *3* (10), 775.

13. Hindley, J. W.; Zheleva, D. G.; Elani, Y.; Charalambous, K.; Barter, L. M. C.; Booth, P. J.; Bevan, C. L.; Law, R. V.; Ces, O. Building a Synthetic Mechanosensitive Signaling Pathway in Compartmentalized Artificial Cells. *Proc. Natl. Acad. Sci. U. S. A.* **2019**, *116* (34), 16711–16716.

14. Schwille, P.; Spatz, J.; Landfester, K.; Bodenschatz, E.; Herminghaus, S.;

Sourjik, V.; Erb, T. J.; Bastiaens, P.; Lipowsky, R.; Hyman, A.; Dabrock, P.; Baret, J. C.; Vidakovic-Koch, T.; Bieling, P.; Dimova, R.; Mutschler, H.; Robinson, T.; Tang, T. Y. D.; Wegner, S.; Sundmacher, K. MaxSynBio: Avenues Towards Creating Cells from the Bottom Up. *Angewandte Chemie - International Edition*. **2018**, *57* (41), 13382-13392.

15. Mantri, S.; Tanuj Sapra, K. Evolving Protocells to Prototissues: Rational Design of a Missing Link. *Biochem. Soc. Trans.* **2013**, 1159–1165.

16. Morasch, M.; Liu, J.; Dirscherl, C. F.; Ianeselli, A.; Kühnlein, A.; Le Vay, K.; Schwintek, P.; Islam, S.; Corpinot, M. K.; Scheu, B.; Dingwell, D. B.; Schwille, P.; Mutschler, H.; Powner, M. W.; Mast, C. B.; Braun, D. Heated Gas Bubbles Enrich, Crystallize, Dry, Phosphorylate and Encapsulate Prebiotic Molecules. *Nat. Chem.* **2019**, *11* (9), 779–788.

17. Gobbo, P.; Patil, A. J.; Li, M.; Harniman, R.; Briscoe, W. H.; Mann, S. Programmed Assembly of Synthetic Protocells into Thermoresponsive Prototissues. *Nat. Mater.* **2018**, *17* (12), 1145–1153.

18. Martin, N. Dynamic Synthetic Cells Based on Liquid–Liquid Phase Separation. *ChemBioChem*. **2019**, *20* (20), 2553–2568.

19. Merindol, R.; Walther, A. Materials Learning from Life: Concepts for Active, Adaptive and Autonomous Molecular Systems. *Chemical Society Reviews*. **2017**, *46* (18), 5588–5619.

20. Xu, C.; Hu, S.; Chen, X. Artificial Cells: From Basic Science to Applications. *Materials Today*. **2016**, *19* (9), 516-532.

21. Aufinger, L.; Simmel, F. C. Establishing Communication Between Artificial Cells. *Chem. Eur.* **2019**, *25* (55), 12659-12670.

22. Caruso, F.; Caruso, R. A.; Möhwald, H. Nanoengineering of Inorganic and Hybrid Hollow Spheres by Colloidal Templating. *Science.* **1998**, *282* (5391), 1111–1114.

23. Holowka, E. P.; Sun, V. Z.; Kamei, D. T.; Deming, T. J. Polyarginine Segments in Block Copolypeptides Drive Both Vesicular Assembly and Intracellular Delivery. *Nat. Mater.* **2007**, *6* (1), 52–57.

24. Bellomo, E. G.; Wyrsta, M. D.; Pakstis, L.; Pochan, D. J.; Deming, T. J. Stimuli-Responsive Polypeptide Vesicles by Conformation-Specific Assembly. *Nat. Mater.* **2004**, *3* (4), 244–248.

25. Sukhorukov, G.; Fery, A.; Möhwald, H. Intelligent Micro- and Nanocapsules. *Prog. Polym. Sci*. **2005**, *30*(8-9), 885-897.

26. Thompson, K. L.; Armes, S. P.; Howse, J. R.; Ebbens, S.; Ahmad, I.; Zaidi, J. H.; York, D. W.; Burdis, J. A. Covalently Cross-Linked Colloidosomes. *Macromolecules* **2010**, *43* (24), 10466–10474.

27. Dinsmore, A. D.; Hsu, M. F.; Nikolaides, M. G.; Marquez, M.; Bausch, A. R.; Weitz, D. A. Colloidosomes: Selectively Permeable Capsules Composed of Colloidal Particles. *Science.* **2002**, *298* (5595), 1006–1009.

28. Thompson, K. L.; Chambon, P.; Verber, R.; Armes, S. P. Can Polymersomes Form Colloidosomes? *J. Am. Chem. Soc.* **2012**, *134* (30), 12450–12453.

29. Li, M.; Green, D. C.; Anderson, J. L. R.; Binks, B. P.; Mann, S. In Vitro Gene Expression and Enzyme Catalysis in Bio-Inorganic Protocells. *Chem. Sci.* **2011**, *2* (9), 1739–1745.

30. Kumar, R. K.; Li, M.; Olof, S. N.; Patil, A. J.; Mann, S. Artificial Cytoskeletal Structures within Enzymatically Active Bio-Inorganic Protocells. *Small* **2013**, *9* (3), 357–362.

31. Richmond, D. L.; Schmid, E. M.; Martens, S.; Stachowiak, J. C.; Liska, N.; Fletcher, D. A. Forming Giant Vesicles with Controlled Membrane Composition, Asymmetry, and Contents. *Proc. Natl. Acad. Sci. U. S. A.* **2011**, *108* (23), 9431–9436.

32. Weinberger, A.; Tsai, F. C.; Koenderink, G. H.; Schmidt, T. F.; Itri, R.; Meier, W.; Schmatko, T.; Schröder, A.; Marques, C. Gel-Assisted Formation of Giant Unilamellar Vesicles. *Biophys. J.* **2013**, *105* (1), 154–164.

33. Lingwood, D.; Simons, K. Lipid Rafts as a Membrane-Organizing Principle. *Science*. **2010**, *327* (5961), 46-50.

34. Noireaux, V.; Maeda, Y. T.; Libchaber, A. Development of an Artificial Cell, from Self-Organization to Computation and Self-Reproduction. *Proc. Natl. Acad. Sci. U. S. A.* **2011**, *108* (9), 3473-3480.

35. Terasawa, H.; Nishimura, K.; Suzuki, H.; Matsuura, T.; Yomo, T. Coupling of the Fusion and Budding of Giant Phospholipid Vesicles Containing Macromolecules. *Proc. Natl. Acad. Sci. U. S. A.* **2012**, *109* (16), 5942–5947.

36. Gebicki, J. M.; Hicks, M. Ufasomes Are Stable Particles Surrounded by Unsaturated Fatty Acid Membranes. *Nature* **1973**, *243* (5404), 232–234.

37. Shum, H. C.; Lee, D.; Yoon, I.; Kodger, T.; Weitz, D. A. Double Emulsion Templated Monodisperse Phospholipid Vesicles. *Langmuir* **2008**, *24* (15), 7651–7653.

38. Qiao, Y.; Li, M.; Booth, R.; Mann, S. Predatory Behaviour in Synthetic Protocell Communities. *Nat. Chem.* **2017**, *9* (2), 110–119.

39. Li, J.; Liu, X.; Abdelmohsen, L. K. E. A.; Williams, D. S.; Huang, X. Spatial Organization in Proteinaceous Membrane-Stabilized Coacervate Protocells. *Small* **2019**, *15* (36), 1902893.

40. Mason, A. F.; Buddingh, B. C.; Williams, D. S.; Van Hest, J. C. M. Hierarchical Self-Assembly of a Copolymer-Stabilized Coacervate Protocell. *J. Am. Chem. Soc.* **2017**, *139* (48), 17309–17312.

41. Williams, D. S.; Koga, S.; Hak, C. R. C.; Majrekar, A.; Patil, A. J.; Perriman, A. W.; Mann, S. Polymer/Nucleotide Droplets as Bio-Inspired Functional Micro-Compartments. *Soft Matter* **2012**, *8* (22), 6004–6014.

42. Gobbo, P.; Tian, L.; Pavan Kumar, B. V. V. S.; Turvey, S.; Cattelan, M.; Patil,

A. J.; Carraro, M.; Bonchio, M.; Mann, S. Catalytic Processing in Ruthenium-Based Polyoxometalate Coacervate Protocells. *Nat. Commun.* **2020**, *11* (1).

43. Tian, L.; Li, M.; Liu, J.; Patil, A. J.; Drinkwater, B. W.; Mann, S. Nonequilibrium Spatiotemporal Sensing within Acoustically Patterned Two-Dimensional Protocell Arrays. *ACS Cent. Sci.* **2018**, *4* (11), 1551–1558.

44. Li, M.; Huang, X.; Tang, T. Y. D.; Mann, S. Synthetic Cellularity Based on Non-Lipid Micro-Compartments and Protocell Models. *Curr. Opin. Chem. Biol*. **2014**, *22*, 1-11.

45. Rideau, E.; Wurm, F. R.; Landfester, K. Giant Polymersomes from Non-Assisted Film Hydration of Phosphate-Based Block Copolymers. *Polym. Chem.* **2018**, *9* (44), 5385–5394.

46. Rodríguez-Arco, L.; Kumar, B. V. V. S. P.; Li, M.; Patil, A. J.; Mann, S. Modulation of Higher-order Behaviour in Model Protocell Communities by Artificial Phagocytosis. *Angew. Chemie* **2019**, *131* (19), 6399–6403.

47. Discher, D. E.; Eisenberg, A. Polymer Vesicles. *Science*. **2002**, *297* (5583),967-973.

48. Huang, X.; Li, M.; Green, D. C.; Williams, D. S.; Patil, A. J.; Mann, S. Interfacial Assembly of Protein-Polymer Nano-Conjugates into Stimulus-Responsive Biomimetic Protocells. *Nat. Commun.* **2013**, *4* (1), 1–9.

49. Qiao, Y.; Li, M.; Qiu, D.; Mann, S. Response-Retaliation Behavior in Synthetic Protocell Communities. *Angew. Chemie - Int. Ed*. **2019**, *131* (49), 17922-17927.

50. Tang, T. Y. D.; Cecchi, D.; Fracasso, G.; Accardi, D.; Coutable-Pennarun, A.; Mansy, S. S.; Perriman, A. W.; Anderson, J. L. R.; Mann, S. Gene-Mediated Chemical Communication in Synthetic Protocell Communities. *ACS Synth. Biol.* **2018**, *7* (2), 339–346.

51. Dimova, R., and Carlos M., eds. The Giant Vesicle Book*. CRC Press,* **2019**.

52. Huang, X.; Li, M.; Mann, S. Membrane-Mediated Cascade Reactions by Enzyme-Polymer Proteinosomes. *Chem. Commun.* **2014**, *50* (47), 6278–6280.

53. Rodríguez-Arco, L.; Li, M.; Mann, S. Phagocytosis-Inspired Behaviour in Synthetic Protocell Communities of Compartmentalized Colloidal Objects. *Nat. Mater.* **2017**, *16* (8), 857–863.

54. Wolpert, L. Positional Information and the Spatial Pattern of Cellular Differentiation. *J. Theor. Biol.* **1969**, *25* (1), 1–47.

55. Waters, C. M.; Bassler, B. L. Quorum Sensing: Cell-to-Cell Communication in Bacteria. *Annu. Rev. Cell Dev. Biol.* **2005**, *21*, 319–346.

56. Miller, M. B.; Bassler, B. L. Quorum Sensing in Bacteria. *Annu. Rev. Microbiol.* **2001**, *55* (1), 165–199.

57. King, P. J.; Guasti, L.; Laufer, E. Hedgehog Signalling in Endocrine Development and Disease. *Int. J. Endocrinol*. **2008**, *198* (3), 439-450

58. Schwarz-Schilling, M.; Aufinger, L.; Mückl, A.; Simmel, F. C. Chemical Communication between Bacteria and Cell-Free Gene Expression Systems within Linear Chains of Emulsion Droplets. *Integr. Biol.* **2016**, *8* (4), 564–570.

59. Buddingh', B. C.; Elzinga, J.; van Hest, J. C. M. Intercellular Communication between Artificial Cells by Allosteric Amplification of a Molecular Signal. *Nat. Commun.* **2020**, *11* (1), 1652.

60. Booth, R.; Qiao, Y.; Li, M.; Mann, S. Spatial Positioning and Chemical Coupling in Coacervate-in-Proteinosome Protocells. *Angew. Chemie - Int. Ed.* **2019**, *131* (27), 9218–9222.

61. Nakano, T.; Eckford, A. W.; Haraguchi, T. Molecular Communication; *Cambridge University Press*, **2011**.

62. Dittrich, P. S.; Manz, A. Lab-on-a-Chip: Microfluidics in Drug Discovery. *Nat. Rev. Drug Discov*. **2006**, *5* (3), 210-218.

63. Yasui, M.; Hiroshima, M.; Kozuka, J.; Sako, Y.; Ueda, M. Automated Single-Molecule Imaging in Living Cells. *Nat. Commun.* **2018**, *9* (1), 1–11.

64. Gardner, P. M.; Winzer, K.; Davis, B. G. Sugar Synthesis in a Protocellular Model Leads to a Cell Signalling Response in Bacteria. *Nat. Chem.* **2009**, *1* (5), 377–383.

65. Weiss, R.; Knight, T. F. Engineered Communications for Microbial Robotics. In *International Workshop on DNA-based Computers*; Springer, Heidelberg. **2001**, 1-16

66. Wang, X.; Tian, L.; Du, H.; Li, M.; Mu, W.; Drinkwater, B. W.; Han, X.; Mann, S. Chemical Communication in Spatially Organized Protocell Colonies and Protocell/Living Cell Micro-Arrays. *Chem. Sci.* **2019**, *10* (41), 9446–9453.

67. Niederholtmeyer, H.; Chaggan, C.; Devaraj, N. K. Communication and Quorum Sensing in Non-Living Mimics of Eukaryotic Cells. *Nat. Commun.* **2018**, *9* (1), 1–8.

68. Shimizu, Y.; Inoue, A.; Tomari, Y.; Suzuki, T.; Yokogawa, T.; Nishikawa, K.; Ueda, T. Supplemental Material for "Cell-Free Translation Reconstituted with Purified Components. *Nat. Biotechnol.* **2001**, *19* (8), 751–755.

69. Rosier, B. J. H. M.; Markvoort, A. J.; Gumí-Audenis, B.; Roodhuizen, J. A. L.; Hamer, A. den; Brunsveld, L.; Greef, T. F. A. de. A DNA-Based Synthetic Apoptosome. *Nat. Catal.* **2020**, *3* (3), 295-306

70. Baccouche, A.; Montagne, K.; Padirac, A.; Fujii, T.; Rondelez, Y. Dynamic DNA-Toolbox Reaction Circuits: A Walkthrough. *Methods* **2014**, *67* (2), 234–249.

71. Gines, G.; Zadorin, A. S.; Galas, J. C.; Fujii, T.; Estevez-Torres, A.; Rondelez,

Y. Microscopic Agents Programmed by DNA Circuits. *Nat. Nanotechnol.* **2017**, *12* (4), 351–359.

72. Zadorin, A. S.; Rondelez, Y.; Gines, G.; Dilhas, V.; Urtel, G.; Zambrano, A.; Galas, J. C.; Estevez-Torres, A. Synthesis and Materialization of a Reaction-Diffusion French Flag Pattern. *Nat. Chem.* **2017**, *9* (10), 990.

73. Srinivas, N.; Ouldridge, T. E.; Šulc, P.; Schaeffer, J. M.; Yurke, B.; Louis, A. A.; Doye, J. P. K.; Winfree, E. On the Biophysics and Kinetics of Toehold-Mediated DNA Strand Displacement. *Nucleic Acids Res.* **2013**, *41* (22), 10641–10658.

74. Seelig, G.; Soloveichik, D.; Zhang, D. Y.; Winfree, E. Enzyme-Free Nucleic Acid Logic Circuits. *Science.* **2006**, *314* (5805), 1585–1588.

75. Soloveichik, D.; Seelig, G.; Winfree, E. DNA as a Universal Substrate for Chemical Kinetics. *Proc. Natl. Acad. Sci. U. S. A.* **2010**, *107* (12), 5393–5398.

76. Tayar, A. M.; Karzbrun, E.; Noireaux, V.; Bar-Ziv, R. H. Synchrony and Pattern Formation of Coupled Genetic Oscillators on a Chip of Artificial Cells. *Proc. Natl. Acad. Sci. U. S. A.* **2017**, *114* (44), 11609–11614.

77. Srinivas, N.; Parkin, J.; Seelig, G.; Winfree, E.; Soloveichik, D. Enzyme-Free Nucleic Acid Dynamical Systems. *Science.* **2017**, *358* (6369), 2052.

78. Qian, L.; Winfree, E. Scaling up Digital Circuit Computation with DNA Strand Displacement Cascades. *Science.* **2011**, *332* (6034), 1196–1201.

79. Qian, L.; Winfree, E.; Bruck, J. Neural Network Computation with DNA Strand Displacement Cascades. *Nature* **2011**, *475* (7356), 368–372.

80. Green, A. A. Synthetic Bionanotechnology: Synthetic Biology Finds a Toehold in Nanotechnology. *Emerg. Top. Life Sci.* **2019**, *3* (5), 507–516.

81. Hiyama, S.; Moritani, Y. Molecular Communication: Harnessing Biochemical Materials to Engineer Biomimetic Communication Systems. *Nano Commun. Netw.* **2010**, *1* (1), 20–30.

82. Karzbrun, E.; Tayar, A. M.; Noireaux, V.; Bar-Ziv, R. H. Programmable On-Chip DNA Compartments as Artificial Cells. *Science.* **2014**, *345* (6198), 829–832.

83. Nakano, T.; Suda, T.; Koujin, T.; Haraguchi, T.; Hiraoka, Y. Molecular Communication through Gap Junction Channels: System Design, Experiments and Modeling. In *Proceedings of the Bio-Inspired Models of Network, Information, and Computing Systems, Bionetics, IEEE*. **2007**, 139-146.

84. Dupin, A.; Simmel, F. C. Signalling and Differentiation in Emulsion-Based Multi-Compartmentalized in Vitro Gene Circuits. *Nat. Chem.* **2019**, *11* (1), 32–39.

85. Adamala, K. P.; Martin-Alarcon, D. A.; Guthrie-Honea, K. R.; Boyden, E. S. Engineering Genetic Circuit Interactions within and between Synthetic

Minimal Cells. *Nat. Chem.* **2017**, *9* (5), 431–439.

86. Fujii, S.; Matsuura, T.; Sunami, T.; Kazuta, Y.; Yomo, T. In Vitro Evolution of α-Hemolysin Using a Liposome Display. *Proc. Natl. Acad. Sci. U. S. A.* **2013**, *110* (42), 16796–16801.

87. Lentini, R.; Santero, S. P.; Chizzolini, F.; Cecchi, D.; Fontana, J.; Marchioretto, M.; Del Bianco, C.; Terrell, J. L.; Spencer, A. C.; Martini, L.; Forlin, M.; Assfalg, M.; Serra, M. D.; Bentley, W. E.; Mansy, S. S. Integrating Artificial with Natural Cells to Translate Chemical Messages That Direct E. Coli Behaviour. *Nat. Commun.* **2014**, *5* (1), 1–6.

88. Singh, A. V.; Hosseinidoust, Z.; Park, B. W.; Yasa, O.; Sitti, M. Microemulsion-Based Soft Bacteria-Driven Microswimmers for Active Cargo Delivery. *ACS Nano* **2017**, *11* (10), 9759–9769.

89. Alapan, Y.; Yasa, O.; Schauer, O.; Giltinan, J.; Tabak, A. F.; Sourjik, V.; Sitti, M. Soft Erythrocyte-Based Bacterial Microswimmers for Cargo Delivery. *Sci. Robot.* **2018**, *3* (17).

90. Wordinger, R. J.; Clark, A. F. Growth Factors and Neurotrophic Factors as Targets. In *Ocular Therapeutics, Academic Press*; **2008**, 87-116.

91. Bolognesi, G.; Friddin, M. S.; Salehi-Reyhani, A.; Barlow, N. E.; Brooks, N. J.; Ces, O.; Elani, Y. Sculpting and Fusing Biomimetic Vesicle Networks Using Optical Tweezers. *Nat. Commun.* **2018**, *9* (1), 1–11.

92. Bartelt, S. M.; Chervyachkova, E.; Ricken, J.; Wegner, S. V. Mimicking Adhesion in Minimal Synthetic Cells. *Adv. Biosyst*. **2019**, *3* (6), 18000333.

93. Fenz, S. F.; Merkel, R.; Sengupta, K. Diffusion and Intermembrane Distance: Case Study of Avidin and E-Cadherin Mediated Adhesion. *Langmuir* **2009**, *25* (2), 1074–1085.

94. Pontani, L. L.; Jorjadze, I.; Brujic, J. Cis and Trans Cooperativity of E-Cadherin Mediates Adhesion in Biomimetic Lipid Droplets. *Biophys. J.* **2016**, *110* (2), 391–399.

95. Wattenbarger, M. R.; Graves, D. J.; Lauffenburger, D. A. Specific Adhesion of Glycophorin Liposomes to a Lectin Surface in Shear Flow. *Biophys. J.* **1990**, *57* (4), 765–777.

96. Villringer, S.; Madl, J.; Sych, T.; Manner, C.; Imberty, A.; Römer, W. Lectin-Mediated Protocell Crosslinking to Mimic Cell-Cell Junctions and Adhesion. *Sci. Rep.* **2018**, *8* (1), 1–11.

97. Fenz, S. F.; Sengupta, K. Giant Vesicles as Cell Models. *Integrative Biology*. **2012**, *4* (9), 982-995.

98. Fenz, S. F.; Smith, A. S.; Merkel, R.; Sengupta, K. Inter-Membrane Adhesion Mediated by Mobile Linkers: Effect of Receptor Shortage. *Soft Matter.* **2011**, *7* (3), 952–962.

99. Amjad, O. A.; Mognetti, B. M.; Cicuta, P.; Di Michele, L. Membrane Adhesion

through Bridging by Multimeric Ligands. *Langmuir* **2017**, *33* (5), 1139–1146.

100. Chiruvolu, S.; Walker, S.; Israelachvili, J.; Schmitt, F. J.; Leckband, D.; Zasadzinski, J. A. Higher Order Self-Assembly of Vesicles by Site-Specific Binding. *Science.* **1994**, *264* (5166), 1753–1756.

101. Nguyen, V. Du; Han, J. W.; Choi, Y. J.; Cho, S.; Zheng, S.; Ko, S. Y.; Park, J. O.; Park, S. Active Tumor-Therapeutic Liposomal Bacteriobot Combining a Drug (Paclitaxel)-Encapsulated Liposome with Targeting Bacteria (Salmonella Typhimurium). *Sensors Actuators, B Chem.* **2016**, *224*, 217–224.

102. Schauer, O.; Mostaghaci, B.; Colin, R.; Hürtgen, D.; Kraus, D.; Sitti, M.; Sourjik, V. Motility and Chemotaxis of Bacteria-Driven Microswimmers Fabricated Using Antigen 43-Mediated Biotin Display. *Sci. Rep.* **2018**, *8* (1), 1–11.

103. Mostaghaci, B.; Yasa, O.; Zhuang, J.; Sitti, M. Bioadhesive Bacterial Microswimmers for Targeted Drug Delivery in the Urinary and Gastrointestinal Tracts. *Adv. Sci.* **2017**, *4* (6), 1700058.

104. Kojima, M.; Zhang, Z.; Nakajima, M.; Ooe, K.; Fukuda, T. Construction and Evaluation of Bacteria-Driven Liposome. *Sensors Actuators, B Chem.* **2013**, *183*, 395–400.

105. Chakraborty, T.; Bartelt, S. M.; Steinkühler, J.; Dimova, R.; Wegner, S. V. Light Controlled Cell-to-Cell Adhesion and Chemical Communication in Minimal Synthetic Cells. *Chem. Commun.* **2019**, *55* (64), 9448–9451.

106. Bartelt, S. M.; Steinkühler, J.; Dimova, R.; Wegner, S. V. Light-Guided Motility of a Minimal Synthetic Cell. *Nano Lett.* **2018**, *18* (11), 7268–7274.

107. Chervyachkova, E.; Wegner, S. V. Reversible Social Self-Sorting of Colloidal Cell-Mimics with Blue Light Switchable Proteins. *ACS Synth. Biol.* **2018**, *7* (7), 1817–1824.

108. Di Michele, L.; Eiser, E. Developments in Understanding and Controlling Self Assembly of DNA-Functionalized Colloids. *Phys. Chem. Chem. Phys.* **2013**, *15* (9), 3115–3129.

109. Klajn, R.; Bishop, K. J. M.; Grzybowski, B. A. Light-Controlled Self-Assembly of Reversible and Irreversible Nanoparticle Suprastructures. *Proc. Natl. Acad. Sci. U. S. A.* **2007**, *104* (25), 10305–10309.

110. Mirkin, C. A.; Letsinger, R. L.; Mucic, R. C.; Storhoff, J. J. A DNA-Based Method for Rationally Assembling Nanoparticles into Macroscopic Materials. *Nature* **1996**, *382* (6592), 607–609.

111. Di Michele, L.; Varrato, F.; Kotar, J.; Nathan, S. H.; Foffi, G.; Eiser, E. Multistep Kinetic Self-Assembly of DNA-Coated Colloids. *Nat. Commun.* **2013**, *4* (1), 1–7.

112. Valignat, M. P.; Theodoly, O.; Crocker, J. C.; Russel, W. B.; Chaikin, P. M.

Reversible Self-Assembly and Directed Assembly of DNA-Linked Micrometer-Sized Colloids. *Proc. Natl. Acad. Sci. U. S. A.* **2005**, *102* (12), 4225–4229.

113. Van Der Meulen, S. A. J.; Leunissen, M. E. Solid Colloids with Surface-Mobile DNA Linkers. *J. Am. Chem. Soc.* **2013**, *135* (40), 15129–15134.

114. Kundu, P. K.; Samanta, D.; Leizrowice, R.; Margulis, B.; Zhao, H.; Börner, M.; Udayabhaskararao, T.; Manna, D.; Klajn, R. Light-Controlled Self-Assembly of Non-Photoresponsive Nanoparticles. *Nat. Chem.* **2015**, *7* (8), 646–652.

115. Manna, D.; Udayabhaskararao, T.; Zhao, H.; Klajn, R. Orthogonal Light-Induced Self-Assembly of Nanoparticles Using Differently Substituted Azobenzenes. *Angew. Chemie - Int. Ed.* **2015**, *127* (42), 12571–12574.

116. Han, K.; Go, D.; Tigges, T.; Rahimi, K.; Kuehne, A. J. C.; Walther, A. Social Self-Sorting of Colloidal Families in Co-Assembling Microgel Systems. *Angew. Chemie - Int. Ed.* **2017**, *129* (8), 2208–2214.

117. Han, K.; Go, D.; Hoenders, D.; Kuehne, A. J. C.; Walther, A. Switchable Supracolloidal Coassembly of Microgels Mediated by Host/Guest Interactions. *ACS Macro Lett.* **2017**, *6* (3), 310–314.

118. Zhang, L.; Dai, L.; Rong, Y.; Liu, Z.; Tong, D.; Huang, Y.; Chen, T. Light-Triggered Reversible Self-Assembly of Gold Nanoparticle Oligomers for Tunable SERS. *Langmuir* **2015**, *31* (3), 1164–1171.

119. Zhang, Q.; Dong, R.; Chang, X.; Ren, B.; Tong, Z. Spiropyran-Decorated SiO2-Pt Janus Micromotor: Preparation and Light-Induced Dynamic Self-Assembly and Disassembly. *ACS Appl. Mater. Interfaces* **2015**, *7* (44), 24585–24591.

120. He, H.; Feng, M.; Chen, Q.; Zhang, X.; Zhan, H. Light-Induced Reversible Self-Assembly of Gold Nanoparticles Surface-Immobilized with Coumarin Ligands. *Angew. Chemie - Int. Ed.* **2016**, *128* (3), 948–952.

121. Hosseinidoust, Z.; Mostaghaci, B.; Yasa, O.; Park, B. W.; Singh, A. V.; Sitti, M. Bioengineered and Biohybrid Bacteria-Based Systems for Drug Delivery. *Advanced Drug Delivery Reviews*. 2016.

122. Pastrana, E. Optogenetics: Controlling Cell Function with Light. *Nat. Methods* **2011**, *8* (1), 24–25.

123. Motta-Mena, L. B.; Reade, A.; Mallory, M. J.; Glantz, S.; Weiner, O. D.; Lynch, K. W.; Gardner, K. H. An Optogenetic Gene Expression System with Rapid Activation and Deactivation Kinetics. *Nat. Chem. Biol.* **2014**, *10* (3), 196–202.

124. Zita, A.; Hermansson, M. Determination of Bacterial Cell Surface Hydrophobicity of Single Cells in Cultures and in Wastewater in Situ. *FEMS Microbiol. Lett.* **1997**, *152* (2), 299–302.

125. Behkam, B.; Sitti, M. Bacterial Flagella-Based Propulsion and on/off Motion Control of Microscale Objects. *Appl. Phys. Lett.* **2007**, *90* (2), 023902.

126. Taherkhani, S.; Mohammadi, M.; Daoud, J.; Martel, S.; Tabrizian, M. Covalent Binding of Nanoliposomes to the Surface of Magnetotactic Bacteria for the Synthesis of Self-Propelled Therapeutic Agents. *ACS Nano* **2014**, *8* (5), 5049–5060.

127. Traore, M. A.; Damico, C. M.; Behkam, B. Biomanufacturing and Self-Propulsion Dynamics of Nanoscale Bacteria-Enabled Autonomous Delivery Systems. *Appl. Phys. Lett.* **2014**, *105* (17), 173702.

128. Weibel, D. B.; Garstecki, P.; Ryan, D.; DiLuzio, W. R.; Mayer, M.; Seto, J. E.; Whitesides, G. M. Microoxen: Microorganisms to Move Microscale Loads. *Proc. Natl. Acad. Sci. U. S. A.* **2005**, *12* (34), 11963–11967.

129. Akin, D.; Sturgis, J.; Ragheb, K.; Sherman, D.; Burkholder, K.; Robinson, J. P.; Bhunia, A. K.; Mohammed, S.; Bashir, R. Bacteria-Mediated Delivery of Nanoparticles and Cargo into Cells. *Nat. Nanotechnol.* **2007**, *2* (7), 441–449.

130. Fernandes, R.; Zuniga, M.; Sassine, F. R.; Karakoy, M.; Gracias, D. H. Enabling Cargo-Carrying Bacteria via Surface Attachment and Triggered Release. *Small* **2011**, *7* (5), 588–592.

131. Shi, F.; Kawano, F.; Park, S. H. E.; Komazaki, S.; Hirabayashi, Y.; Polleux, F.; Yazawa, M. Optogenetic Control of Endoplasmic Reticulum-Mitochondria Tethering. *ACS Synth. Biol.* **2018**, *7* (1), 2–9.

132. Legris, M.; Klose, C.; Burgie, E. S.; Rojas, C. C.; Neme, M.; Hiltbrunner, A.; Wigge, P. A.; Schäfer, E.; Vierstra, R. D.; Casal, J. J. Phytochrome B Integrates Light and Temperature Signals in Arabidopsis. *Science.* **2016**, *345* (6314), 897–900.

133. Konermann, S.; Brigham, M. D.; Trevino, A. E.; Hsu, P. D.; Heidenreich, M.; Cong, L.; Platt, R. J.; Scott, D. A.; Church, G. M.; Zhang, F. Optical Control of Mammalian Endogenous Transcription and Epigenetic States. *Nature* **2013**, *500* (7463), 472–476.

134. Pathak, G. P.; Spiltoir, J. I.; Höglund, C.; Polstein, L. R.; Heine-Koskinen, S.; Gersbach, C. A.; Rossi, J.; Tucker, C. L. Bidirectional Approaches for Optogenetic Regulation of Gene Expression in Mammalian Cells Using Arabidopsis Cryptochrome 2. *Nucleic Acids Res.* **2017**, *45* (20), 167.

135. Reade, A.; Motta-Mena, L. B.; Gardner, K. H.; Stainier, D. Y.; Weiner, O. D.; Woo, S. TAEL: A Zebrafish-Optimized Optogenetic Gene Expression System with Fine Spatial and Temporal Control. *Dev.* **2017**, *144* (3), 345–355.

136. Graziano, B. R.; Gong, D.; Anderson, K. E.; Pipathsouk, A.; Goldberg, A. R.; Weiner, O. D. A Module for Rac Temporal Signal Integration Revealed with Optogenetics. *J. Cell Biol.* **2017**, *216* (8), 2515–2531.

137. Guglielmi, G.; Barry, J. D.; Huber, W.; De Renzis, S. An Optogenetic Method to Modulate Cell Contractility during Tissue Morphogenesis. *Dev. Cell* **2015**, *35* (5), 646–660.

138. Levskaya, A.; Weiner, O. D.; Lim, W. A.; Voigt, C. A. Spatiotemporal Control of Cell Signalling Using a Light-Switchable Protein Interaction. *Nature* **2009**, *461* (7266), 997–1001.

139. Toettcher, J. E.; Weiner, O. D.; Lim, W. A. Using Optogenetics to Interrogate the Dynamic Control of Signal Transmission by the Ras/Erk Module. *Cell* **2013**, *155* (6), 1422–1434.

140. Guglielmi, G.; Falk, H. J.; De Renzis, S. Optogenetic Control of Protein Function: From Intracellular Processes to Tissue Morphogenesis. *Trends in Cell Biology*. 2016.

141. Guntas, G.; Hallett, R. A.; Zimmerman, S. P.; Williams, T.; Yumerefendi, H.; Bear, J. E.; Kuhlman, B. Engineering an Improved Light-Induced Dimer (ILID) for Controlling the Localization and Activity of Signaling Proteins. *Proc. Natl. Acad. Sci. U. S. A.* **2015**, *112* (1), 112–117.

142. Uda, Y.; Goto, Y.; Oda, S.; Kohchi, T.; Matsuda, M.; Aoki, K. Efficient Synthesis of Phycocyanobilin in Mammalian Cells for Optogenetic Control of Cell Signaling. *Proc. Natl. Acad. Sci. U. S. A.* **2017**, *114* (45), 11962–11967.

143. Ruess, J.; Parise, F.; Milias-Argeitis, A.; Khammash, M.; Lygeros, J. Iterative Experiment Design Guides the Characterization of a Light-Inducible Gene Expression Circuit. *Proc. Natl. Acad. Sci. U. S. A.* **2015**, *112* (26), 8148–8153.

144. Buckley, C. E.; Moore, R. E.; Reade, A.; Goldberg, A. R.; Weiner, O. D.; Clarke, J. D. W. Reversible Optogenetic Control of Subcellular Protein Localization in a Live Vertebrate Embryo. *Dev. Cell* **2016**, *36* (1), 117–126.

145. Liu, Q.; Tucker, C. L. Engineering Genetically-Encoded Tools for Optogenetic Control of Protein Activity. *Curr. Opin. Chem. Biol*. **2017**, *40*, 17-23.

146. Ayling, O. G. S.; Harrison, T. C.; Boyd, J. D.; Goroshkov, A.; Murphy, T. H. Automated Light-Based Mapping of Motor Cortex by Photoactivation of Channelrhodopsin-2 Transgenic Mice. *Nat. Methods* **2009**, *6* (3), 219–224.

147. Nagel, G.; Szellas, T.; Huhn, W.; Kateriya, S.; Adeishvili, N.; Berthold, P.; Ollig, D.; Hegemann, P.; Bamberg, E. Channelrhodopsin-2, a Directly Light-Gated Cation-Selective Membrane Channel. *Proc. Natl. Acad. Sci. U. S. A.* **2003**, *100* (24), 13940–13945.

148. Lagali, P. S.; Balya, D.; Awatramani, G. B.; Münch, T. A.; Kim, D. S.; Busskamp, V.; Cepko, C. L.; Roska, B. Light-Activated Channels Targeted to ON Bipolar Cells Restore Visual Function in Retinal Degeneration. *Nat. Neurosci.* **2008**, *11* (6), 667–675.

149. Gradinaru, V.; Mogri, M.; Thompson, K. R.; Henderson, J. M.; Deisseroth, K. Optical Deconstruction of Parkinsonian Neural Circuitry. *Science.* **2009**, *324* (5925), 354–359.

150. Hörner, M.; Gerhardt, K.; Salavei, P.; Hoess, P.; Härrer, D.; Kaiser, J.; Tabor, J. J.; Weber, W. Production of Phytochromes by High-Cell-Density E. Coli

Fermentation. *ACS Synth. Biol.* **2019**, *8* (10), 2442–2450.

151. Kawano, F.; Suzuki, H.; Furuya, A.; Sato, M. Engineered Pairs of Distinct Photoswitches for Optogenetic Control of Cellular Proteins. *Nat. Commun.* **2015**, *6* (1), 1–8.

152. Yu, G.; Onodera, H.; Aono, Y.; Kawano, F.; Ueda, Y.; Furuya, A.; Suzuki, H.; Sato, M. Optical Manipulation of the Alpha Subunits of Heterotrimeric G Proteins Using Photoswitchable Dimerization Systems. *Sci. Rep.* **2016**, *6*, 35777.

153. Yüz, S. G.; Ricken, J.; Wegner, S. V. Independent Control over Multiple Cell Types in Space and Time Using Orthogonal Blue and Red Light Switchable Cell Interactions. *Adv. Sci.* **2018**, *5* (8), 18000446.

154. Wiltbank, L. B.; Kehoe, D. M. Diverse Light Responses of Cyanobacteria Mediated by Phytochrome Superfamily Photoreceptors. *Nat. Rev. Microbiol*. **2019**, *17* (1), 37-50.

155. Pham, V. N.; Kathare, P. K.; Huq, E. Phytochromes and Phytochrome Interacting Factors. *Plant Physiol.* **2018**, *176* (2), 1025–1038.

156. Weber, P. C.; Ohlendorf, D. H.; Wendoloski, J. J.; Salemme, F. R. Structural Origins of High-Affinity Biotin Binding to Streptavidin. *Science.* **1989**, 243 (4887), 85–88.

157. García-Domínguez, M.; Muro-Pastor, M. I.; Reyes, J. C.; Florencio, F. J. Light-Dependent Regulation of Cyanobacterial Phytochrome Expression. *J. Bacteriol.* **2000**, *182* (1), 38–44.

158. Burgie, E. S.; Vierstra, R. D. Phytochromes: An Atomic Perspective on Photoactivation and Signaling. *Plant Cell*. **2014**, *26* (12), 4568-4583.

159. Takala, H.; Björling, A.; Berntsson, O.; Lehtivuori, H.; Niebling, S.; Hoernke, M.; Kosheleva, I.; Henning, R.; Menzel, A.; Ihalainen, J. A.; Westenhoff, S. Signal Amplification and Transduction in Phytochrome Photosensors. *Nature* **2014**, *509* (7499), 245–248.

160. Quail, P. H.; Boylan, M. T.; Parks, B. M.; Short, T. W.; Xu, Y.; Wagner, D. Phytochromes: Photosensory Perception and Signal Transduction. *Science.* **1995**, *268* (5211), 675–680.

161. Shimizu-Sato, S.; Huq, E.; Tepperman, J. M.; Quail, P. H. A Light-Switchable Gene Promoter System. *Nat. Biotechnol.* **2002**, *20* (10), 1041–1044.

162. Beyer, H. M.; Juillot, S.; Herbst, K.; Samodelov, S. L.; Müller, K.; Schamel, W. W.; Römer, W.; Schäfer, E.; Nagy, F.; Strähle, U.; Weber, W.; Zurbriggen, M. D. Red Light-Regulated Reversible Nuclear Localization of Proteins in Mammalian Cells and Zebrafish. *ACS Synth. Biol.* **2015**, *4* (9), 951–958.

163. Müller, K.; Engesser, R.; Metzger, S.; Schulz, S.; Kämpf, M. M.; Busacker, M.; Steinberg, T.; Tomakidi, P.; Ehrbar, M.; Nagy, F.; Timmer, J.; Zubriggen, M. D.; Weber, W. A Red/Far-Red Light-Responsive Bi-Stable Toggle Switch to Control Gene Expression in Mammalian Cells. *Nucleic Acids Res.* **2013**, *41*

(7), 77.

164. Müller, K.; Zurbriggen, M. D.; Weber, W. Control of Gene Expression Using a Red- and Far-Red Light-Responsive Bi-Stable Toggle Switch. *Nat. Protoc.* **2014**.

165. Hughes, R. M.; Bolger, S.; Tapadia, H.; Tucker, C. L. Light-Mediated Control of DNA Transcription in Yeast. *Methods* **2012**, *58* (4), 385–391.

166. Hochrein, L.; Mitchell, L. A.; Schulz, K.; Messerschmidt, K.; Mueller-Roeber, B. L-SCRaMbLE as a Tool for Light-Controlled Cre-Mediated Recombination in Yeast. *Nat. Commun.* **2018**, *9* (1), 1–10.

167. Reichhart, E.; Ingles-Prieto, A.; Tichy, A. M.; McKenzie, C.; Janovjak, H. A Phytochrome Sensory Domain Permits Receptor Activation by Red Light. *Angew. Chemie - Int. Ed.* **2016**, *55* (21), 6339–6342.

168. Schmidl, S. R.; Sheth, R. U.; Wu, A.; Tabor, J. J. Refactoring and Optimization of Light-Switchable Escherichia Coli Two-Component Systems. *ACS Synth. Biol.* **2014**, *3* (11), 820–831.

169. Tabor, J. J.; Levskaya, A.; Voigt, C. A. Multichromatic Control of Gene Expression in Escherichia Coli. *J. Mol. Biol.* **2011**, *405* (2), 315–324.

170. Levskaya, A.; Chevalier, A. A.; Tabor, J. J.; Simpson, Z. B.; Lavery, L. A.; Levy, M.; Davidson, E. A.; Scouras, A.; Ellington, A. D.; Marcotte, E. M.; Voigt, C. A. Engineering Escherichia Coli to See Light. *Nature* **2005**, *438* (7067), 441–442.

171. Fernandez-Rodriguez, J.; Moser, F.; Song, M.; Voigt, C. A. Engineering RGB Color Vision into Escherichia Coli. *Nat. Chem. Biol.* **2017**, *13* (7), 706–708.

172. Ma, S.; Luo, S.; Wu, L.; Liang, Z.; Wu, J. R. Re-Engineering the Two-Component Systems as Light-Regulated in Escherichia Coli. *J. Biosci.* **2017**, *42* (4), 565–573.

173. Lemmon, M. A.; Schlessinger, J. Cell Signaling by Receptor Tyrosine Kinases. *Cell*. **2010**, *103* (2), 211-225.

174. Christie, J. M.; Salomon, M.; Nozue, K.; Wada, M.; Briggs, W. R. LOV (Light, Oxygen, or Voltage) Domains of the Blue-Light Photoreceptor Phototropin (Nph1): Binding Sites for the Chromophore Flavin Mononucleotide. *Proc. Natl. Acad. Sci. U. S. A.* **1999**, *96* (15), 8779–8783.

175. Swartz, T. E.; Corchnoy, S. B.; Christie, J. M.; Lewis, J. W.; Szundi, I.; Briggs, W. R.; Bogomolni, R. A. The Photocycle of a Flavin-Binding Domain of the Blue Light Photoreceptor Phototropin. *J. Biol. Chem.* **2001**, *276* (39), 36493–36500.

176. Zoltowski, B. D.; Crane, B. R. Light Activation of the LOV Protein Vivid Generates a Rapidly Exchanging Dimer. *Biochemistry* **2008**, *47* (27), 7012–7019.

177. Lungu, O. I.; Hallett, R. A.; Choi, E. J.; Aiken, M. J.; Hahn, K. M.; Kuhlman, B.

Designing Photoswitchable Peptides Using the AsLOV2 Domain. *Chem. Biol.* **2012**, *19* (4), 507–517.

178. Nihongaki, Y.; Suzuki, H.; Kawano, F.; Sato, M. Genetically Engineered Photoinducible Homodimerization System with Improved Dimer-Forming Efficiency. *ACS Chem. Biol.* **2014**, *9* (3), 617–621.

179. Zhu, J.; Mathes, T.; Hontani, Y.; Alexandre, M. T. A.; Toh, K. C.; Hegemann, P.; Kennis, J. T. M. Photoadduct Formation from the FMN Singlet Excited State in the LOV2 Domain of Chlamydomonas Reinhardtii Phototropin. *J. Phys. Chem. Lett.* **2016**, *7* (21), 4380–4384.

180. Konold, P. E.; Mathes, T.; Weienborn, J.; Groot, M. L.; Hegemann, P.; Kennis, J. T. M. Unfolding of the C-Terminal Jα Helix in the LOV2 Photoreceptor Domain Observed by Time-Resolved Vibrational Spectroscopy. *J. Phys. Chem. Lett.* **2016**, *7* (17), 3472–3476.

181. Zimmerman, S. P.; Hallett, R. A.; Bourke, A. M.; Bear, J. E.; Kennedy, M. J.; Kuhlman, B. Tuning the Binding Affinities and Reversion Kinetics of a Light Inducible Dimer Allows Control of Transmembrane Protein Localization. *Biochemistry* **2016**, *55* (37), 5264–5271.

182. Yumerefendi, H.; Lerner, A. M.; Zimmerman, S. P.; Hahn, K.; Bear, J. E.; Strahl, B. D.; Kuhlman, B. Light-Induced Nuclear Export Reveals Rapid Dynamics of Epigenetic Modifications. *Nat. Chem. Biol.* **2016**, *12* (6), 399–401.

183. Hallett, R. A.; Zimmerman, S. P.; Yumerefendi, H.; Bear, J. E.; Kuhlman, B. Correlating in Vitro and in Vivo Activities of Light-Inducible Dimers: A Cellular Optogenetics Guide. *ACS Synth. Biol.* **2016**, *5* (1), 53–64.

184. Yu, Q.; Wang, Y.; Zhao, S.; Ren, Y. Photocontrolled Reversible Self-Assembly of Dodecamer Nitrilase. *Bioresour. Bioprocess.* **2017**, *4* (1), 1–8.

185. Johnson, H. E.; Goyal, Y.; Pannucci, N. L.; Schüpbach, T.; Shvartsman, S. Y.; Toettcher, J. E. The Spatiotemporal Limits of Developmental Erk Signaling. *Dev. Cell* **2017**, *40* (2), 185–192.

186. O'Neill, P. R.; Kalyanaraman, V.; Gautam, N. Subcellular Optogenetic Activation of Cdc42 Controls Local and Distal Signaling to Drive Immune Cell Migration. *Mol. Biol. Cell* **2016**, *29* (9), 1442–1450.

187. O'Neill, P. R.; Castillo-Badillo, J. A.; Meshik, X.; Kalyanaraman, V.; Melgarejo, K.; Gautam, N. Membrane Flow Drives an Adhesion-Independent Amoeboid Cell Migration Mode. *Dev. Cell* **2018**, *46* (1), 9–22.

188. Vaidya, A. T.; Chen, C. H.; Dunlap, J. C.; Loros, J. J.; Crane, B. R. Structure of a Light-Activated LOV Protein Dimer That Regulates Transcription. *Sci. Signal.* **2011**, *4* (184), ra50.

189. Müller, K.; Engesser, R.; Schulz, S.; Steinberg, T.; Tomakidi, P.; Weber, C. C.; Ulm, R.; Timmer, J.; Zurbriggen, M. D.; Weber, W. Multi-Chromatic Control of Mammalian Gene Expression and Signaling. *Nucleic Acids Res.* **2013**, *41*

(12), 124.

190. Müller, K.; Engesser, R.; Timmer, J.; Zurbriggen, M. D.; Weber, W. Orthogonal Optogenetic Triple-Gene Control in Mammalian Cells. *ACS Synth. Biol.* **2014**, *3* (11), 796–801.

191. Han, T.; Chen, Q.; Liu, H. Engineered Photoactivatable Genetic Switches Based on the Bacterium Phage T7 RNA Polymerase. *ACS Synth. Biol.* **2017**, *6* (2), 357–366.

192. Zhang, G.; Liu, P.; Wei, W.; Wang, X.; Wei, D.; Wang, W. A Light-Switchable Bidirectional Expression System in Filamentous Fungus Trichoderma Reesei. *J. Biotechnol.* **2016**, *240*, 85–93.

193. Wang, X.; Chen, X.; Yang, Y. Spatiotemporal Control of Gene Expression by a Light-Switchable Transgene System. *Nat. Methods* **2012**, *9* (3), 266.

194. Wang, W.; Shi, X. Y.; Wei, D. Z. Light-Mediated Control of Gene Expression in Filamentous Fungus Trichoderma Reesei. *J. Microbiol. Methods* **2014**, *103*, 37–39.

195. Sheets, M. B.; Wong, W. W.; Dunlop, M. J. Light-Inducible Recombinases for Bacterial Optogenetics. *ACS Synth. Biol.* **2020**, *9* (2), 227–235.

196. Yao, S.; Yuan, P.; Ouellette, B.; Zhou, T.; Mortrud, M.; Balaram, P.; Chatterjee, S.; Wang, Y.; Daigle, T. L.; Tasic, B.; Kuang, X.; Gong, H.; Luo, Q.; Zeng, S.; Curtright, A.; Dhaka, A.; Kahan, A.; Gradinaru, V.; Chrapkiewicz, R.; Schnitzer, M.; Zeng, H.; Cetin, A. RecV Recombinase System for in Vivo Targeted Optogenomic Modifications of Single Cells or Cell Populations. *Nat. Methods* **2020**, *17* (4), 422–429.

197. Bonner, J. T. The Origins of Multicellularity. *Integr. Biol. Issues, News, Rev.* **1998**, *1* (1), 27–36.

198. Vella, F. The Cell. A Molecular Approach. *Biochem. Educ.* **1998**.

199. Moritani, Y.; Hiyama, S.; Suda, T. Molecular Communication - A Biochemically-Engineered Communication System -. In *Proceedings of the Frontiers in the Convergence of Bioscience and Information Technologies, IEEE.* **2007**, 839-844

200. Lentini, R.; Martín, N. Y.; Forlin, M.; Belmonte, L.; Fontana, J.; Cornella, M.; Martini, L.; Tamburini, S.; Bentley, W. E.; Jousson, O.; Mansy, S. S. Two-Way Chemical Communication between Artificial and Natural Cells. *ACS Cent. Sci.* **2017**, *3* (2), 117–123.

201. Hilburger, C. E.; Jacobs, M. L.; Lewis, K. R.; Peruzzi, J. A.; Kamat, N. P. Controlling Secretion in Artificial Cells with a Membrane and Gate. *ACS Synth. Biol.* **2019**, *8* (6), 1224–1230.

202. Sun, S.; Li, M.; Dong, F.; Wang, S.; Tian, L.; Mann, S. Chemical Signaling and Functional Activation in Colloidosome-Based Protocells. *Small* **2016**, *12* (14), 1920–1927.

203. Möller, N.; Hellwig, T.; Stricker, L.; Engel, S.; Fallnich, C.; Ravoo, B. J. Near-Infrared Photoswitching of Cyclodextrin-Guest Complexes Using Lanthanide-Doped LiYF4 Upconversion Nanoparticles. *Chem. Commun.* **2017**, *53* (1), 240–243.

204. Tayar, A. M.; Karzbrun, E.; Noireaux, V.; Bar-Ziv, R. H. Propagating Gene Expression Fronts in a One-Dimensional Coupled System of Artificial Cells. *Nat. Phys.* **2015**, *11* (12), 1037–1041.

205. Aufinger, L.; Simmel, F. C. Artificial Gel-Based Organelles for Spatial Organization of Cell-Free Gene Expression Reactions. *Angew. Chemie - Int. Ed.* **2018**, *57* (52), 17245–17248.

206. Grosberg, R. K.; Strathmann, R. R. The Evolution of Multicellularity: A Minor Major Transition? *Annu. Rev. Ecol. Evol. Syst.* **2007**, *38*, 621–654.

207. Steinberg, M. S. Differential Adhesion in Morphogenesis: A Modern View. *Curr.Opin. Gen. Dev*. **2007**, *17* (4), 281-286.

208. Toda, S.; Blauch, L. R.; Tang, S. K. Y.; Morsut, L.; Lim, W. A. Programming Self-Organizing Multicellular Structures with Synthetic Cell-Cell Signaling. *Science.* **2018**, *361* (6398), 156–162.

209. Hibbing, M. E.; Fuqua, C.; Parsek, M. R.; Peterson, S. B. Bacterial Competition: Surviving and Thriving in the Microbial Jungle. *Nat. Rev. Microbiol.***2010.**

210. Li, F.; Josephson, D. P.; Stein, A. Colloidal Assembly: The Road from Particles to Colloidal Molecules and Crystals. *Angew. Chemie - Int. Ed.* **2011**, *50* (2), 360-388.

211. Weiss, M.; Frohnmayer, J. P.; Benk, L. T.; Haller, B.; Janiesch, J. W.; Heitkamp, T.; Börsch, M.; Lira, R. B.; Dimova, R.; Lipowsky, R.; Bodenschatz, E.; Baret, J. C.; Vidakovic-Koch, T.; Sundmacher, K.; Platzman, I.; Spatz, J. P. Sequential Bottom-up Assembly of Mechanically Stabilized Synthetic Cells by Microfluidics. *Nat. Mater.* **2018**, *17* (1), 89–96.

212. Liu, X.; Zhou, P.; Huang, Y.; Li, M.; Huang, X.; Mann, S. Hierarchical Proteinosomes for Programmed Release of Multiple Components. *Angew. Chemie - Int. Ed.* **2016**, *128* (25), 7211–7216.

213. Elani, Y.; Law, R. V.; Ces, O. Vesicle-Based Artificial Cells as Chemical Microreactors with Spatially Segregated Reaction Pathways. *Nat. Commun.* **2014**, *5*, 5305.

214. Elbert, D. L. Bottom-up Tissue Engineering. *Cur. Opin. Biotechn*. **2011**, *22* (5). 374-680.

215. Go, D.; Kodger, T. E.; Sprakel, J.; Kuehne, A. J. C. Programmable Co-Assembly of Oppositely Charged Microgels. *Soft Matter* **2014**, *10* (40), 8060–8065.

216. Wang, B.; Jacquet, M.; Wang, K.; Xiong, K.; Yan, M.; Courtois, J.; Royal, G. PH-Induced Fragmentation of Colloids Based on Responsive Self-Assembled Copper(Ii) Metallopolymers. *New J. Chem.* **2018**, *42* (10), 7823–7829.

217. Zhou, Y.; Wang, D.; Huang, S.; Auernhammer, G.; He, Y.; Butt, H. J.; Wu, S. Reversible Janus Particle Assembly via Responsive Host-Guest Interactions. *Chem. Commun.* **2015**, *51* (13), 2725–2727.

218. Vilanova, N.; De Feijter, I.; Teunissen, A. J. P.; Voets, I. K. Light Induced Assembly and Self-Sorting of Silica Microparticles. *Sci. Rep.* **2018**, *8* (1), 1–9.

219. Li, S.; Moosa, B. A.; Croissant, J. G.; Khashab, N. M. Electrostatic Assembly/Disassembly of Nanoscaled Colloidosomes for Light-Triggered Cargo Release. *Angew. Chemie - Int. Ed.* **2015**, *127* (23), 6908–6912.

220. Zhang, Q.; Qu, D. H.; Wang, Q. C.; Tian, H. Dual-Mode Controlled Self-Assembly of TiO2 Nanoparticles Through a Cucurbit[8]Uril-Enhanced Radical Cation Dimerization Interaction. *Angew. Chemie - Int. Ed.* **2015**, *127* (52), 16015–16019.

221. Stoffelen, C.; Voskuhl, J.; Jonkheijm, P.; Huskens, J. Dual Stimuli-Responsive Self-Assembled Supramolecular Nanoparticles. *Angew. Chemie - Int. Ed.* **2014**, *53* (13), 3400–3404.

222. Lan, Y.; Wu, Y.; Karas, A.; Scherman, O. A. Photoresponsive Hybrid Raspberry-like Colloids Based on Cucurbit[8]Uril Host-Guest Interactions. *Angew. Chemie - Int. Ed.* **2014**, *53* (13), 3400–3404.

223. Zoltowski, B. D.; Vaccaro, B.; Crane, B. R. Mechanism-Based Tuning of a LOV Domain Photoreceptor. *Nat. Chem. Biol.* **2009**, *5* (11), 827–834.

224. Schwerdtfeger, C.; Linden, H. VIVID Is a Flavoprotein and Serves as a Fungal Blue Light Photoreceptor for Photoadaptation. *EMBO J.* **2003**, *22* (18), 4846–4855.

225. Lamparter, T.; Esteban, B.; Hughes, J. Phytochrome Cph1 from the Cyanobacterium Synechocystis PCC6803 Purification, Assembly, and Quaternary Structure. *Eur. J. Biochem.* **2001**, *268* (17), 4720–4730.

226. Xi, J.; Schmidt, J. J.; Montemagno, C. D. Self-Assembled Microdevices Driven by Muscle. *Nat. Mater.* **2005**, *4* (2), 180–184.

227. Feinberg, A. W. Biological Soft Robotics. *Annu. Rev. Biomed. Eng.* **2015**, *17*, 243–265.

228. Park, B. W.; Zhuang, J.; Yasa, O.; Sitti, M. Multifunctional Bacteria-Driven Microswimmers for Targeted Active Drug Delivery. *ACS Nano* **2017**, *11* (9), 8910–8923.

229. Felfoul, O.; Mohammadi, M.; Taherkhani, S.; De Lanauze, D.; Zhong Xu, Y.; Loghin, D.; Essa, S.; Jancik, S.; Houle, D.; Lafleur, M.; Gaboury, L.; Tabrizian, M.; Kaou, N.; Atkin, M.; Vuong, T.; Batist, G.; Beauchemin, N.; Radzioch, D.; Martel, S. Magneto-Aerotactic Bacteria Deliver Drug-Containing Nanoliposomes to Tumour Hypoxic Regions. *Nat. Nanotechnol.* **2016**, *11* (11), 941–947.

230. Stanton, M. M.; Park, B. W.; Miguel-López, A.; Ma, X.; Sitti, M.; Sánchez, S.

Biohybrid Microtube Swimmers Driven by Single Captured Bacteria. *Small* **2017**, *13* (19), 1603679.

231. Martel, S.; Tremblay, C. C.; Ngakeng, S.; Langlois, G. Controlled Manipulation and Actuation of Micro-Objects with Magnetotactic Bacteria. *Appl. Phys. Lett.* **2006**, *89* (23), 233904.

232. Edwards, M. R.; Wright Carlsen, R.; Sitti, M. Near and Far-Wall Effects on the Three-Dimensional Motion of Bacteria-Driven Microbeads. *Appl. Phys. Lett.* **2013**, *102* (14), 143701.

233. Sitti, M. Voyage of the Microrobots. *Nature* **2009**, *458* (7242), 1121–1122.

234. Angelani, L.; Di Leonardo, R.; Ruocco, G. Self-Starting Micromotors in a Bacterial Bath. *Phys. Rev. Lett.* **2009**, *102* (4), 048104.

235. Schwarz, L.; Medina-Sánchez, M.; Schmidt, O. G. Hybrid BioMicromotors. *Appl. Phys. Rev*. **2017**, *4* (3), 031301

236. Magdanz, V.; Medina-Sánchez, M.; Schwarz, L.; Xu, H.; Elgeti, J.; Schmidt, O. G. Spermatozoa as Functional Components of Robotic Microswimmers. *Adv. Mat.* **2017**, *29* (24), 1606301.

237. Kim, D.; Liu, A.; Diller, E.; Sitti, M. Chemotactic Steering of Bacteria Propelled Microbeads. *Biomed. Microdevices* **2012**, *14* (6), 1009–1017.

238. Zhuang, J.; Sitti, M. Chemotaxis of Bio-Hybrid Multiple Bacteria-Driven Microswimmers. *Sci. Rep.* **2016**, *6*, 32135.

239. Steager, E.; Kim, C. B.; Patel, J.; Bith, S.; Naik, C.; Reber, L.; Kim, M. J. Control of Microfabricated Structures Powered by Flagellated Bacteria Using Phototaxis. *Appl. Phys. Lett.* **2007**, *90* (26), 263901.

240. Zhuang, J.; Carlsen, R. W.; Sitti, M. PH-Taxis of Biohybrid Microsystems. *Sci. Rep.* **2015**, *5*, 11403.

241. Paulick, A.; Jakovljevic, V.; Zhang, S.; Erickstad, M.; Groisman, A.; Meir, Y.; Ryu, W. S.; Wingreen, N. S.; Sourjik, V. Mechanism of Bidirectional Thermotaxis in Escherichia Coli. *Elife* **2017**, *6*, 26607.

242. Chen, F.; Wegner, S. V. Blue Light Switchable Bacterial Adhesion as a Key Step toward the Design of Biofilms. *ACS Synth. Biol.* **2017**, *6* (12), 2170–2174.

243. Beyer, H. M.; Engesser, R.; Hörner, M.; Koschmieder, J.; Beyer, P.; Timmer, J.; Zurbriggen, M. D.; Weber, W. Synthetic Biology Makes Polymer Materials Count. *Adv. Mater.* **2018**, *30* (21), 1800472.

244. Schenk, F. C.; Boehm, H.; Spatz, J. P.; Wegner, S. V. Dual-Functionalized Nanostructured Biointerfaces by Click Chemistry. *Langmuir* **2014**, *30* (23), 6897–6905.

# Chapter 6: Appendix

## 6.1 Nucleotide and amino acid sequences of the optogenetic proteins

### 6.1.1 iLID

Nucleotide sequence:

ATGAGAGGATCGCATCACCATCACCATCACGGATCCGGGGAGTTTCTGGCAACCAC
ACTGGAACGGATCGAGAAAAATTTCGTGATTACTGATCCGAGACTGCCTGACAACC
CAATCATTTTTGCGAGCGATTCCTTCCTGCAGCTGACAGAATATTCTCGGGAAGAG
ATCCTGGGGCGCAATTGCCGTTTTCTGCAGGGACCCGAGACAGACCGTGCCACTGT
TCGGAAAATCAGAGATGCTATTGACAACCAGACTGAAGTGACCGTTCAGCTGATCA
ATTATACCAAGAGCGGCAAGAAGTTCTGGAACGTGTTCCACCTGCAGCCGATGCGC
GATTATAAGGGCGACGTCCAGTACTTCATTGGCGTGCAGCTGGATGGCACCGAACG
TCTTCATGGCGCCGCTGAGCGTGAGGCGGTCATGCTGATCAAAAAGACAGCCTTTC
AGATTGCTGAGGCAGCGAACGACGAAAATTACTTTTAA

Amino acid sequence:

MRGSHHHHHHGSGEFLATTLERIEKNFVITDPRLPDNPIIFASDSFLQLTEYSREE
ILGRNCRFLQGPETDRATVRKIRDAIDNQTEVTVQLINYTKSGKKFWNVFHLQPMR
DYKGDVQYFIGVQLDGTERLHGAAEREAVMLIKKTAFQIAEAANDENYF-

### 6.1.2 MBP-SspB-Nano

Nucleotide sequence:

ATGAGAGGATCGCATCACCATCACCATCACGGATCTAAAATCGAAGAAGGTAAACT
GGTAATCTGGATTAACGGCGATAAAGGCTATAACGGTCTCGCTGAAGTCGGTAAGA
AATTCGAGAAAGATACCGGAATTAAAGTCACCGTTGAGCATCCGGATAAACTGGAA
GAGAAATTCCCACAGGTTGCGGCAACTGGCGATGGCCCTGACATTATCTTCTGGGC
ACACGACCGCTTTGGTGGCTACGCTCAATCTGGCCTGTTGGCTGAAATCACCCCGG
ACAAAGCGTTCCAGGACAAGCTGTATCCGTTTACCTGGGATGCCGTACGTTACAAC
GGCAAGCTGATTGCTTACCCGATCGCTGTTGAAGCGTTATCGCTGATTTATAACAA
AGACCTGCTGCCGAACCCGCCAAAAACCTGGGAAGAGATCCCGGCGCTGGATAAAG
AACTGAAAGCGAAAGGTAAGAGCGCGCTGATGTTCAACCTGCAAGAACCGTACTTC
ACCTGGCCGCTGATTGCTGCTGACGGGGGTTATGCGTTCAAGTATGAAAACGGCAA

GTACGACATTAAAGACGTGGGCGTGGATAACGCTGGCGCGAAAGCGGGTCTGACCT
TCCTGGTTGACCTGATTAAAAACAAACACATGAATGCAGACACCGATTACTCCATC
GCAGAAGCTGCCTTTAATAAAGGCGAAACAGCGATGACCATCAACGGCCCGTGGGC
ATGGTCCAACATCGACACCAGCAAAGTGAATTATGGTGTAACGGTACTGCCGACCT
TCAAGGGTCAACCATCCAAACCGTTCGTTGGCGTGCTGAGCGCAGGTATTAACGCC
GCCAGTCCGAACAAAGAGCTGGCAAAAGAGTTCCTCGAAAACTATCTGCTGACTGA
TGAAGGTCTGGAAGCGGTTAATAAAGACAAACCGCTGGGTGCCGTAGCGCTGAAGT
CTTACGAGGAAGAGTTGGCGAAAGATCCACGTATTGCCGCCACTATGGAAAACGCC
CAGAAAGGTGAAATCATGCCGAACATCCCGCAGATGTCCGCTTTCTGGTATGCCGT
GCGTACTGCGGTGATCAACGCCGCCAGCGGTCGTCAGACTGTCGATGAAGCCCTGA
AAGACGCGCAGACTAATTCGAGCTCGAACAACAACAACAATAACAATAACAACAAC
CTCGGGATCGAGGGAACGACCGAAAACCTGTATTTTCAGGGATCCAGCTCCCCGAA
ACGCCCTAAGCTGCTGCGTGAATATTACGATTGGCTGGTTGATAACAGCTTTACCC
CATATCTGGTGGTGGATGCCACATACCTGGGCGTGAACGTGCCCGTGGAGTATGTG
AAAGACGGTCAGATCGTGCTGAATCTGTCTGCAAGTGCGACCGGCAACCTGCAACT
GACAAATGATTTTATCCAGTTCAACGCCCGCTTTAAGGGCGTGTCTCGTGAACTGT
ATATCCCGATGGGTGCCGCTCTGGCCATTTACGCTCGCGAGAACGGCGATGGTGTG
ATGTTCGAACCAGAAGAAATCTATGACGAGCTGAATATTGGTTAA

Amino acid sequence:

MRGSHHHHHHGSKIEEGKLVIWINGDKGYNGLAEVGKKFEKDTGIKVTVEHPDKLE
EKFPQVAATGDGPDIIFWAHDRFGGYAQSGLLAEITPDKAFQDKLYPFTWDAVRYN
GKLIAYPIAVEALSLIYNKDLLPNPPKTWEEIPALDKELKAKGKSALMFNLQEPYF
TWPLIAADGGYAFKYENGKYDIKDVGVDNAGAKAGLTFLVDLIKNKHMNADTDYSI
AEAAFNKGETAMTINGPWAWSNIDTSKVNYGVTVLPTFKGQPSKPFVGVLSAGINA
ASPNKELAKEFLENYLLTDEGLEAVNKDKPLGAVALKSYEEELAKDPRIAATMENA
QKGEIMPNIPQMSAFWYAVRTAVINAASGRQTVDEALKDAQTNSSSNNNNNNNNNN
LGIEGTTENLYFQGSSSPKRPKLREYYDWLVDNSFTPYLVVDATYLGVNVPVEYVK
DGQIVLNLSASATGNLQLTNDFIQFNARFKGVSRELYIPMGAALAIYARENGDGVM
FEPEEIYDELNIG-

### 6.1.3 VVDHigh

Nucleotide sequence:

ATGCACACACTATATGCTCCCGGAGGGTATGATATAATGGGATACCTAATTCAAAT
AATGAACCGTCCGAACCCGCAAGTGGAGCTGGGCCCGGTGGACACCAGCTGCGCGC
TGATCCTGTGCGACCTGAAGCAGAAAGATACCCCGATTGTGTACGCGAGCGAGGCG
TTCCTGTACATGACCGGTTATAGCAACGCGGAAGTTCTGGGCCGTAACTGCCGTTT
TCTGCAAAGCCCGGATGGTATGGTGAAGCCGAAAAGCACCCGTAAGTATGTTGACA
GCAACACCATCAACACCATTCGTAAAGCGATCGATCGTAACGCGGAAGTGCAGGTT
GAAGTGGTTAACTTCAAGAAAAACGGCCAACGTTTCGTGAACTTTCTGACCATCAT
TCCGGTTCGTGATGAGACCGGCGAATATCGTTATAGCATGGGTTTTCAATGCGAGA
CCGAAGGCGGTAGCCACCACCACCACCACTGA

Amino acid sequence:

MHTLYAPGGYDIMGYLIQIMNRPNPQVELGPVDTSCALILCDLKQKDTPIVYASEA
FLYMTGYSNAEVLGRNCRFLQSPDGMVKPKSTRKYVDSNTINTIRKAIDRNAEVQV
EVVNFKKNGQRFVNFLTIIPVRDETGEYRYSMGFQCETEGGSHHHHHH-

### 6.1.4 Cph1

Nucleotide sequence:

ATGCACCATCACCACCACCACGAGAATCTGTACTTTCAAGGCGGATCCGAATTCGA
GCTCGCAACCACCGTTCAACTGAGCGACCAAAGCCTGCGTCAGCTGGAAACCCTGG
CTATCCACACCGCTCACCTGATTCAGCCGCATGGCCTGGTGGTGGTGCTGCAGGAA
CCGGACCTGACCATCAGCCAGATTAGCGCCAACTGCACCGGCATCCTGGGTCGTAG
CCCGGAGGATCTGCTGGGTCGCACCCTGGGCGAAGTGTTCGACAGCTTTCAGATCG
ATCCAATCCAGAGCCGCCTGACCGCCGGTCAGATCAGCAGCCTGAACCCGAGCAAG
CTGTGGGCTCGTGTGATGGGTGACGATTTCGTGATTTTTGACGGCGTGTTCCACCG
CAACAGCGATGGTCTGCTGGTGTGCGAGCTGGAACCGGCGTACACCAGCGACAACC
TGCCGTTCCTGGGTTTTTATCACATGGCTAATGCCGCGCTGAACCGTCTGCGTCAG
CAGGCGAACCTGCGTGACTTTTACGATGTGATCGTGGAGGAAGTGCGTCGCATGAC
CGGCTTCGACCGTGTGATGCTGTATCGCTTTGATGAGAACAACCACGGTGACGTGA
TTGCGGAGGATAAACGTGACGATATGGAACCGTACCTGGGCCTGCACTATCCGGAA
AGCGACATCCCACAGCCAGCTCGTCGCCTGTTCATTCACAACCCGATCCGCGTGAT
TCCGGACGTGTACGGTGTGGCTGTGCCACTGACCCCGGCTGTGAACCCGAGCACCA
ACCGTGCTGTGGACCTGACCGAGAGCATCCTGCGCAGCGCCTACCACTGCCACCTG

ACCTATCTGAAGAACATGGGCGTGGGTGCTAGCCTGACCATCAGCCTGATCAAGGA
TGGTCACCTGTGGGGCCTGATTGCTTGCCACCACCAGACCCCGAAAGTGATCCCGT
TTGAGCTGCGTAAAGCCTGCGAGTTCTTCGGCCGCGTGGTGTTCAGCAACATCAGC
GCGCAGGAAGACACCGAAACCTTTGATTATCGTGTGCAGCTGGCGGAGCACGAAGC
TGTGCTGCTGGACAAGATGACCACCGCTGCCGATTTCGTGGAGGGTCTGACCAATC
ATCCAGACCGTCTGCTGGGCCTGACCGGTAGCCAGGGCGCGGCTATCTGCTTTGGT
GAAAAGCTGATTCTGGTGGGCGAAACCCCGGATGAAAAAGCCGTGCAGTACCTGCT
GCAGTGGCTGGAGAACCGTGAAGTGCAGGACGTGTTCTTTACCAGCAGCCTGAGCC
AGATCTATCCGGATGCGGTGAACTTCAAAAGCGTGGCTAGCGGCCTGCTGGCTATC
CCAATTGCCCGTCACAACTTCCTGCTGTGGTTTCGCCCGGAAGTGCTGCAGACCGT
GAACTGGGGCGGTGACCCGAACCATGCCTACGAGGCGACCCAGGAAGATGGCAAGA
TTGAGCTGCACCCGCGTCAGAGCTTTGACCTGTGGAAAGAAATCGTGCGCCTGCAG
AGCCTGCCATGGCAGAGCGTGGAGATTCAATCCGCGCTGGCACTGAAAAAGGCTAT
CGTGAACCTGATTCTGCGTCAAGCTGAGTAA

Amino acid sequence:

MHHHHHHENLYFQGGSEFELATTVQLSDQSLRQLETLAIHTAHLIQPHGLVVVLQE
PDLTISQISANCTGILGRSPEDLLGRTLGEVFDSFQIDPIQSRLTAGQISSLNPSK
LWARVMGDDFVIFDGVFHRNSDGLLVCELEPAYTSDNLPFLGFYHMANAALNRLRQ
QANLRDFYDVIVEEVRRMTGFDRVMLYRFDENNHGDVIAEDKRDDMEPYLGLHYPE
SDIPQPARRLFIHNPIRVIPDVYGVAVPLTPAVNPSTNRAVDLTESILRSAYHCHL
TYLKNMGVGASLTISLIKDGHLWGLIACHHQTPKVIPFELRKACEFFGRVVFSNIS
AQEDTETFDYRVQLAEHEAVLLDKMTTAADFVEGLTNHPDRLLGLTGSQGAAICFG
EKLILVGETPDEKAVQYLLQWLENREVQDVFFTSSLSQIYPDAVNFKSVASGLLAI
PIARHNFLLWFRPEVLQTVNWGGDPNHAYEATQEDGKIELHPRQSFDLWKEIVRLQ
SLPWQSVEIQSALALKKAIVNLILRQAE-

### 6.1.5 PhyB

Nucleotide sequence:

ATGGTTAGCGGTGTTGGTGGTAGCGGTGGTGGTCGTGGTGGCGGTCGCGGAGGTGA
AGAAGAACCGAGCAGCAGCCATACCCCGAATAATCGCCGTGGTGGTGAACAGGCAC
AGAGCAGCGGCACCAAAAGCCTGCGTCCGCGTAGCAATACCGAAAGCATGAGCAAA
GCAATTCAGCAGTATACCGTTGATGCACGTCTGCATGCCGTTTTCGAACAGAGCGG

TGAAAGCGGTAAAAGCTTTGATTATAGCCAGAGCCTGAAAACCACCACCTATGGTA
GCAGCGTGCCGGAACAGCAGATTACCGCATATCTGAGCCGTATTCAGCGTGGTGGC
TACATTCAGCCGTTTGGCTGCATGATCGCAGTTGATGAAAGCAGCTTTCGCATTAT
TGGCTACAGCGAAAATGCACGTGAAATGCTGGGCATTATGCCGCAGAGCGTTCCGA
CCCTGGAAAAACCGGAAATTCTGGCAATGGGCACCGATGTTCGTAGCCTGTTTACC
AGCAGCAGCTCCATTCTGCTGGAACGTGCCTTTGTTGCCCGTGAAATTACCCTGCT
GAATCCGGTTTGGATTCATAGCAAAAACACCGGCAAACCGTTTTATGCAATTCTGC
ATCGTATTGATGTTGGCGTGGTTATTGATCTGGAACCGGCACGTACCGAAGATCCG
GCACTGAGCATTGCCGGTGCAGTTCAGAGCCAGAAACTGGCAGTTCGTGCAATTAG
CCAGCTGCAGGCACTGCCTGGTGGTGATATCAAACTGCTGTGTGATACCGTTGTTG
AAAGCGTTCGTGATCTGACCGGCTACGACCGTGTTATGGTGTATAAATTCCACGAA
GATGAACATGGTGAAGTTGTTGCAGAAAGCAAACGTGATGACCTGGAACCGTATAT
TGGTCTGCATTATCCAGCAACCGATATTCCGCAGGCAAGCCGTTTCCTGTTCAAAC
AGAATCGTGTGCGCATGATTGTTGATTGTAATGCAACACCGGTTCTGGTTGTTCAG
GATGATCGTCTGACCCAGAGCATGTGTCTGGTTGGTAGCACCCTGCGTGCACCGCA
TGGTTGTCATAGCCAGTATATGGCAAATATGGGTAGCATCGCAAGCCTGGCCATGG
CGGTGATCATCAATGGTAATGAAGATGATGGTAGCAATGTTGCAAGCGGTCGTAGC
AGCATGCGTCTGTGGGGTCTGGTTGTGTGTCATCATACCAGCAGTCGCTGCATTCC
GTTTCCGCTGCGTTATGCATGTGAATTTCTGATGCAGGCATTTGGACTGCAGCTGA
ATATGGAACTGCAACTGGCACTGCAGATGAGCGAAAAACGTGTTCTGCGTACCCAG
ACCCTGCTGTGCGATATGCTGCTGCGTGATAGTCCGGCAGGCATTGTTACCCAGAG
CCCGAGCATTATGGATCTGGTGAAATGCGATGGTGCAGCCTTTCTGTATCACGGTA
AATACTATCCGCTGGGTGTTGCACCGAGCGAAGTTCAGATTAAAGATGTTGTTGAG
TGGCTGCTGGCAAATCATGCAGATAGCACCGGTCTGAGCACCGATAGCCTGGGTGA
TGCAGGTTATCCGGGTGCAGCAGCACTGGGAGATGCAGTTTGTGGTATGGCAGTTG
CATACATTACCAAACGCGATTTTCTGTTTTGGTTTCGTAGCCATACCGCCAAAGAA
ATCAAATGGGGTGGTGCAAAACATCACCCGGAAGATAAAGATGACGGTCAGCGTAT
GCATCCGCGTAGTAGCTTTCAGGCATTTCTGGAAGTGGTGAAAAGCCGTAGCCAGC
CGTGGGAAACCGCAGAAATGGATGCAATTCATAGCCTGCAACTGATTCTGCGCGAT
AGCTTCAAAGAAAGCGAAGCAGCAATGAATAGCAAAGTTGTTGATGGTGTTGTTCA
GCCGTGTCGTGATATGGCAGGCGAACAGGGTATTGATGAACTGGGTGCAGGTTCTG
GTAGCGGTCTGAACGACATCTTCGAAGCTCAGAAAATCGAATGGCACGAACATCAT
CACCATCACCATTAA

Amino acid sequence:

MVSGVGGSGGGRGGGRGGEEEPSSSHTPNNRRGGEQAQSSGTKSLRPRSNTESMSK
AIQQYTVDARLHAVFEQSGESGKSFDYSQSLKTTTYGSSVPEQQITAYLSRIQRGG
YIQPFGCMIAVDESSFRIIGYSENAREMLGIMPQSVPTLEKPEILAMGTDVRSLFT
SSSSILLERAFVAREITLLNPVWIHSKNTGKPFYAILHRIDVGVVIDLEPARTEDP
ALSIAGAVQSQKLAVRAISQLQALPGGDIKLLCDTVVESVRDLTGYDRVMVYKFHE
DEHGEVVAESKRDDLEPYIGLHYPATDIPQASRFLFKQNRVRMIVDCNATPVLVVQ
DDRLTQSMCLVGSTLRAPHGCHSQYMANMGSIASLAMAVIINGNEDDGSNVASGRS
SMRLWGLVVCHHTSSRCIPFPLRYACEFLMQAFGLQLNMELQLALQMSEKRVLRTQ
TLLCDMLLRDSPAGIVTQSPSIMDLVKCDGAAFLYHGKYYPLGVAPSEVQIKDVVE
WLLANHADSTGLSTDSLGDAGYPGAAALGDAVCGMAVAYITKRDFLFWFRSHTAKE
IKWGGAKHHPEDKDDGQRMHPRSSFQAFLEVVKSRSQPWETAEMDAIHSLQLILRD
SFKESEAAMNSKVVDGVVQPCRDMAGEQGIDELGAGSGSGLNDIFEAQKIEWHEHH
HHHH-

## 6.2 Appendix figures

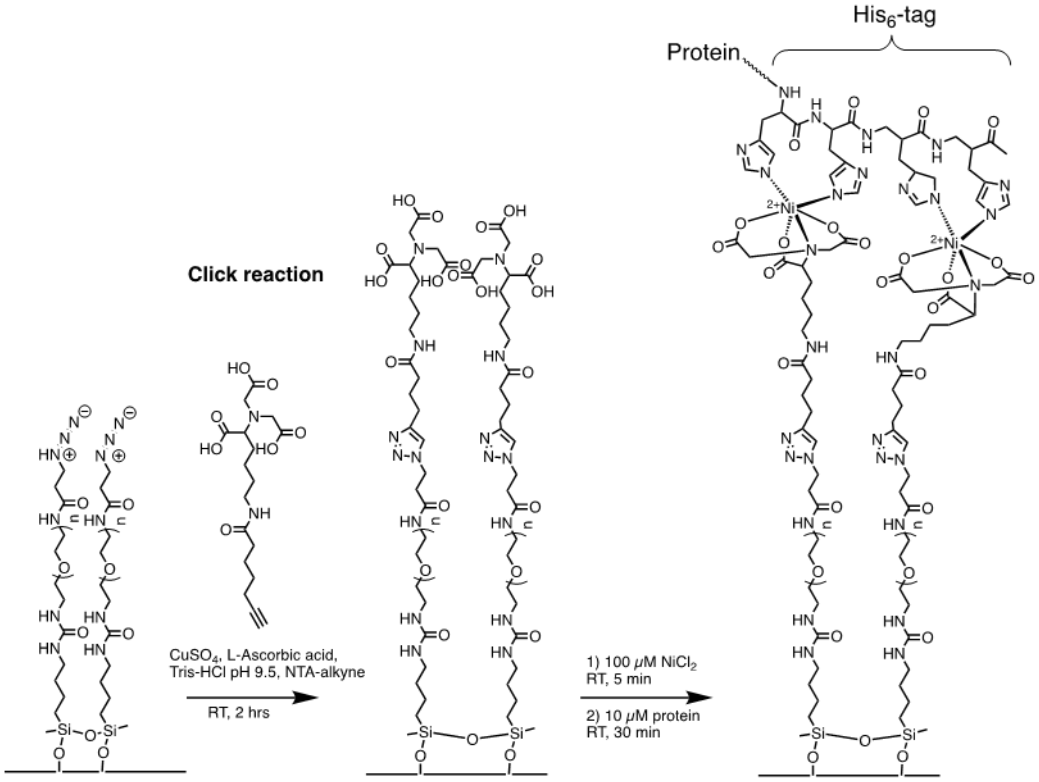


**Figure A1** Click Reaction for PEG-azide functionalization

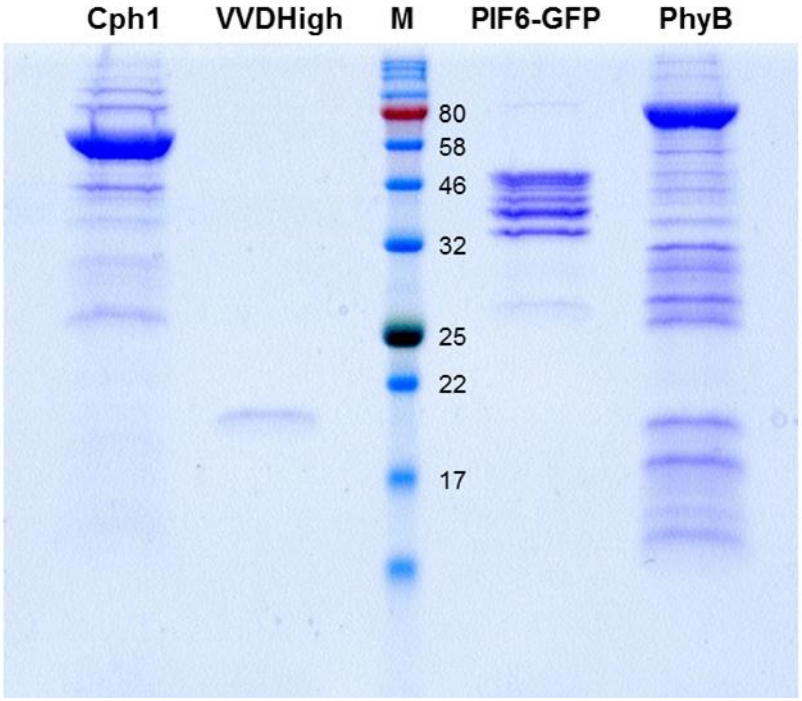


**Figure A2** SDS-PAGE of purified proteins: Cph1, VVDHigh, PIF6-GFP and PhyB

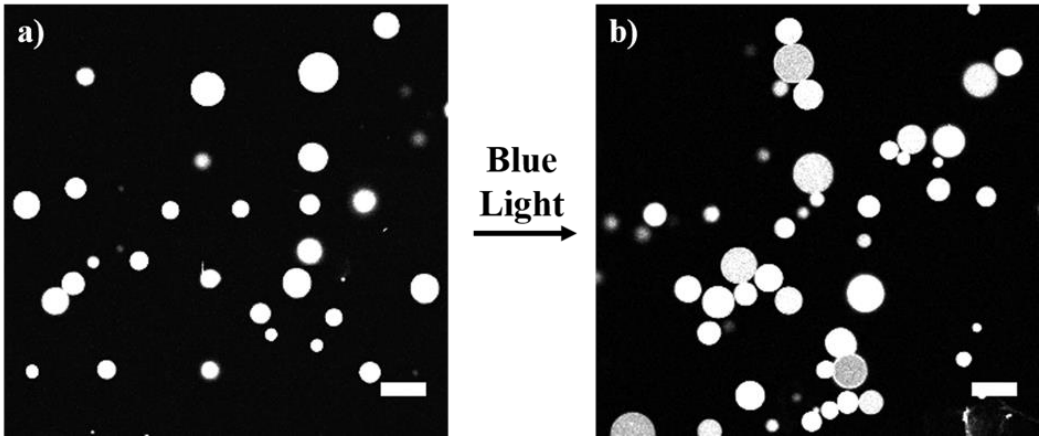


**Figure A3** Photoswitchable proteinosome adhesions showing the microscopy images of iLID and Nano functionalized proteinosomes, a) in the dark, proteinosomes do not stick together and remain dispersed in the solution, b) after 90 min of blue light illumination induces the heterodimerization of iLID and Nano proteins, results in the aggregation of the proteinosomes. The scale bars are 50 μm.

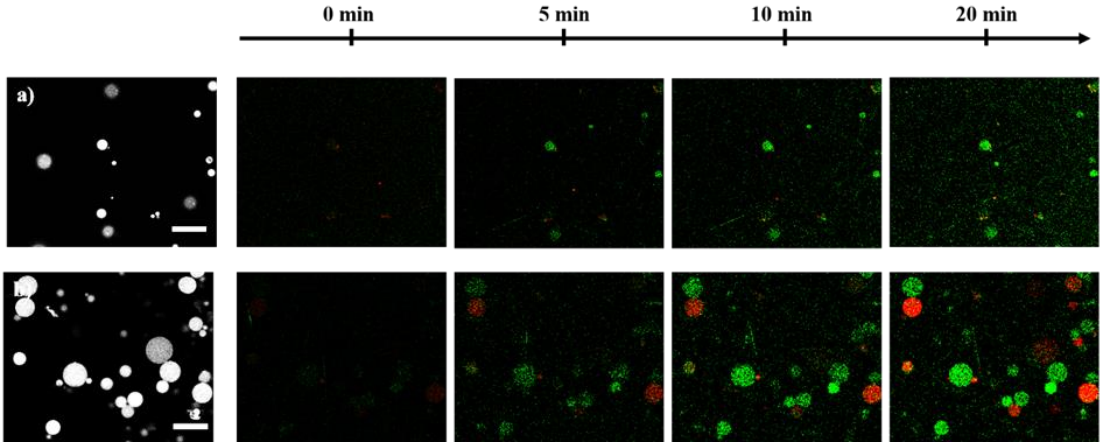


**Figure A4** Confocal images of the adhesion-dependent signaling cascade between the sender cells (green), and the receiver cells (red). t=0 is the time point when the input strand was added. a) In the dark, the proteinosomes are dispersed in the buffer. Upon the addition of the input strand, the sender cell secretes the signal and Alexa488 is activated, which can be observed as the generation of the green fluorescence. However, the receiver cells do not receive the signal and the communication is impaired. b) Under blue light, proteinosomes are aggregated and upon the input strand, the sender cells secrete the signal and Alexa488 is activated. The secreted signal is received by the neighboring receiver cell, activating the Cy5 signal, observed as the generation of the fluorescence signal (represented in red color). The scale bars are 100 μm.